ERDC/CHL TR-00-18

Coastal and Hydraulics Laboratory

US Army Corps
of Engineers®
Engineer Research and
Development Center

Cape Fear-Northeast Cape Fear River, North Carolina

Numerical Model Study

Robert T. McAdory, Jr.

August 2000

The contents of this report are not to be used for advertising, publication, or promotional purposes. Citation of trade names does not constitute an official endorsement or approval of the use of such commercial products.

The findings of this report are not to be construed as an official Department of the Army position, unless so designated by other authorized documents.

PRINTED ON RECYCLED PAPER

ERDC/CHL TR-00-18
August 2000

Cape Fear-Northeast Cape Fear River, North Carolina

Numerical Model Study

by Robert T. McAdory, Jr.

Coastal and Hydraulics Laboratory
U.S. Army Engineer Research and Development Center
3909 Halls Ferry Road
Vicksburg, MS 39180-6199

Final report

Prepared for U.S. Army Engineer District, Wilmington
P.O. Box 1890
Wilmington, NC 28402-1890

Engineer Research and Development Center Cataloging-in-Publication Data

McAdory, Robert T.

Cape Fear-Northeast Cape Fear River, North Carolina : numerical model study / by Robert T. McAdory, Jr. ; prepared for U.S. Army Engineer District, Wilmington.

93 p. : ill. ; 28 cm. -- (ERDC/CHL ; TR-00-18)

Includes bibliographic references.

1. Navigation -- North Carolina -- Cape Fear River. 2. Cape Fear River (N.C.) 3. Salinity -- North Carolina -- Cape Fear River -- Mathematical models. 4. Tides -- North Carolina -- Cape Fear River -- Mathematical models. 5. Saltwater encroachment -- North Carolina -- Cape Fear River. I. United States. Army. Corps of Engineers. Wilmington District. II. Engineer Research and Development Center (U.S.) III. Coastal and Hydraulics Laboratory (U.S.) IV. Title. V. Series: ERDC/CHL TR ; 00-18.

TA7 E8 no.ERDC/CHL TR-00-18

Contents

List of Figures

List of Tables

Preface

The three-dimensional numerical modeling testing of hydrodynamic and salinity conditions for the Cape Fear River Navigation Channels, NC Project, as documented in this report, was performed for the U. S. Army Engineer District, Wilmington (SAW) by personnel of the Coastal and Hydraulics Laboratory (CHL) of the U. S. Army Engineer and Research Development Center (ERDC).

The study was conducted under the general supervision of Dr. James R. Houston, former Director, CHL; Mr. Charles C. Calhoun, Jr., former Assistant Director, CHL; and Dr. W. H. McAnally, Jr., Chief, Estuaries and Hydrosciences Division (EHD). The work was performed and the report was prepared by Dr. R. T. McAdory, Jr., EHD.

At the time of publication of this report, Dr. James R. Houston was Director of ERDC, and COL James S. Weller, EN, was Commander.

1 Introduction

Background

Location and description of system

The Cape Fear River (CFR) estuarine system is located in the southeastern quadrant of North Carolina, rising in the Piedmont region and draining 23,581 sq km (9,140 square miles) (Giese, Wilder, and Parker 1985) (see Figure 1). This report concerns a three-dimensional (3-D) hydrodynamic and salinity intrusion study of the CFR and its two largest lower tributaries, the Black River (BR) and the Northeast Cape Fear River (NECFR). The study area includes the CFR to Lock and Dam No. 1 (LD1), the BR up to the U.S. Geological Survey (USGS) gauge at Tomahawk, NC, and the NECFR up to the USGS gauge at Chinquapin, NC.

Wilmington, NC, is located approximately 45 km (28 miles) upstream of the mouth of the CFR near the confluence of the CFR and the NECFR. The BR joins the CFR about 22.5 km (14 miles) up the CRF from Market Street in Wilmington. Approximately 4.8 km (3 miles) up the CFR from Market Street the Brunswick River (BWR) distributary flows around the western side of Eagle Island and rejoins the CFR at the southern tip of Eagle Island near the Exxon Pier, about 6.5 km (4 miles) down river of Market Street. North of the Exxon Pier the river system has a characteristic riverine appearance with widths on the order of a few hundred feet, but tidal influence extends to LD1 on the CFR, 59.5 km (37 miles) upriver from Market Street and 104.5 km (65 miles) from the mouth of the CFR near Southport, NC, to near the south edge of Sampson County on the BR, about 61 km (38 miles) upriver from the confluence of the BR with the CFR, and to 77 km (48 miles) up the NECFR, above Holly Shelter Creek (Giese, Wilder, and Parker 1985). At Wilmington the CFR gradually widens and, south of the Exxon Pier, it rapidly attains widths of approximately 1.6 to 3 km (1 to 2 miles). This lower reach of the river is characterized by numerous islands along the deep-dredged channel and by shallow off-channel areas, nominally 11.6 m (38 ft) and 0.3 to 1.8 m (1 to 6 ft) respectively.

The Cape Fear River estuary is unique among North Carolina estuaries in its comparatively free and direct access to the Atlantic Ocean (Giese, Wilder, and Parker 1985). The outlet between Oak and Smith islands was defined as the primary connection to the ocean by the construction of the Rocks breakwater near

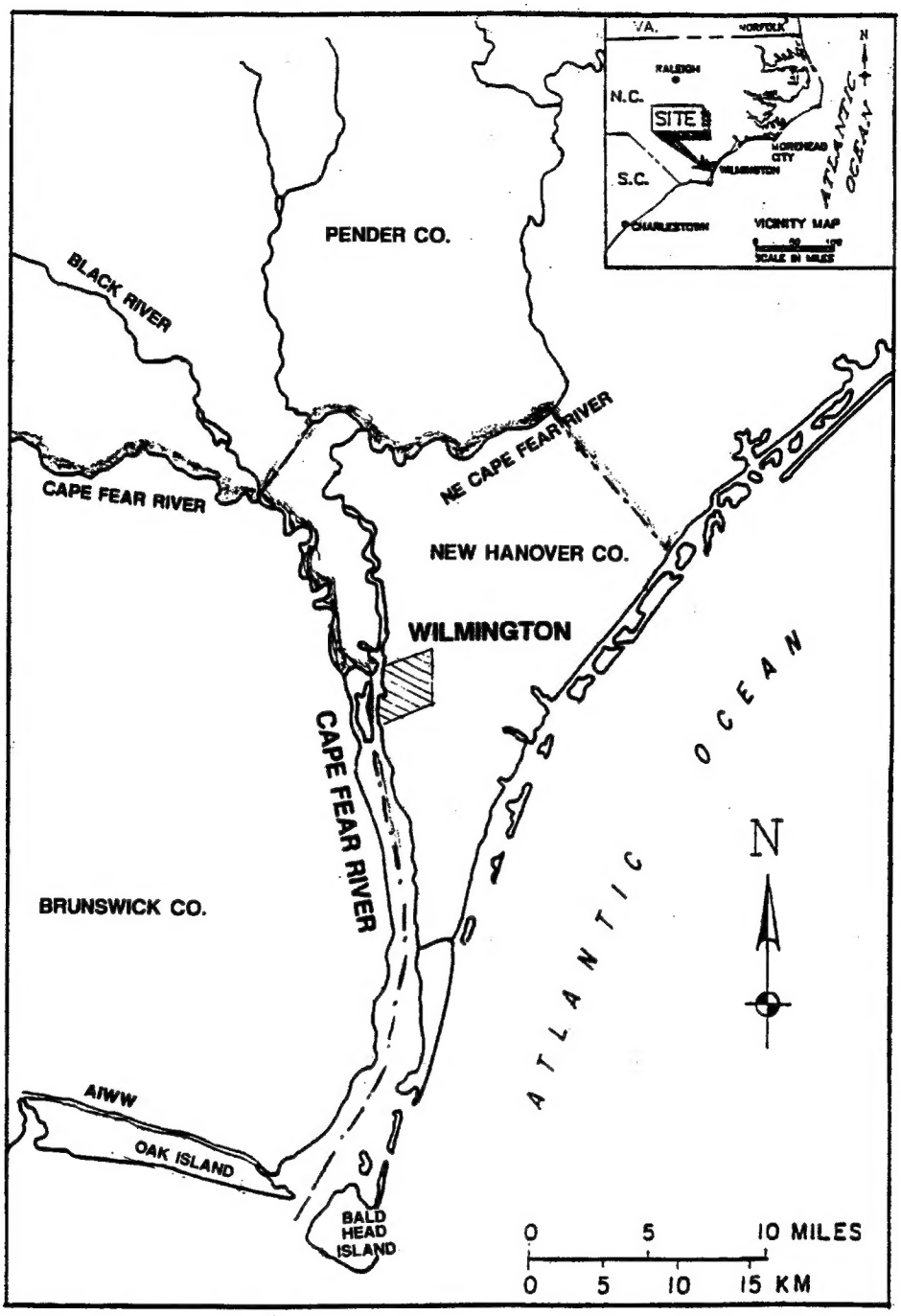

Figure 1. Location map of Cape Fear River

Zekes Island in the 19th century which, effectively, cut off New Inlet. Construction of Snow's Cut in 1930 and, in 1952, Carolina Beach Inlet, enhanced and complicated the connection of the river with the Atlantic. Snow's Cut is approximately 16 km (10 miles) downriver from Wilmington, and Carolina Beach Inlet, about 1.6 km (one mile) north of the eastern opening of Snow's Cut, is the most direct connection of Snow's Cut with the Atlantic. Snow's Cut, with its almost direct connection to the Atlantic Ocean and its position midway between

Wilmington and Southport, has a major impact on the salinity regime of the Cape Fear River estuary. A "Chronology of Navigation-Related Developments" for the Cape Fear River to 1971 is given in Table 1 (USAED, Wilmington, 1960, 1976; Welch 1979).

The mean tide range in the CFR varies from 1.31 m (4.3 ft) at Baldhead to 1.25 m (4.1 ft) at Wilmington (National Ocean Service 1991). Tide ranges at intermediate locations are lower, for example, 1.25 m (4.1 ft) at Southport, 1.19 m (3.9 ft) at Reeves Point, 1.22 m (4.0 ft) at Orton Point, 1.16 m (3.8 ft) at Campbell Island, and indicate resonance behavior in the estuary to some extent. Tide range at LD1 is about 0.3 m (1 ft) (Trawle 1980).[1] Channel depth plays a significant role in determining the tide range at Wilmington as witnessed by a 1960 U.S. Army Engineer report (USAED, Wilmington, 1960) giving tide ranges of 1.28 m (4.2 ft) at Southport and 1.24 m (3.4 ft) at Wilmington. In a 1911 USAE report by E. I. Brown, District Engineer, Wilmington District (USAED, Wilmington, 1976)[2] the tide range at Wilmington and the mouth of the Cape Fear River are reported as 0.82 m (2.7 ft) and 1.37 m (4.5 ft), respectively. In 1960 the main CFR ship channel had a project depth of 10.4 m (34 ft) to Castle Street at Wilmington and 9.1 m (30 ft) to the Hilton Bridge over the NECFR; in 1907 the depth to Wilmington was 6.1 m (20 ft). This contrasts with the current project depth of, essentially, 11.6 m (38 ft) to the Hilton Bridge and 8.2 m (27 ft) for a mile or so farther up the NECFR. Bar channel depths also differed.

Freshwater flows through the CFR system average 311 cu m/sec (11,000 cfs) with seasonal high flows (winter and spring) averaging about 509 cu m/sec (18,000 cfs) and seasonal low flows (summer and fall) averaging about 28 cu m/sec (1,000 cfs) (Giese, Wilder, and Parker 1985; USAED, Wilmington, 1992). Peak flows can exceed 1,132 cu m/sec (40,000 cfs). For example, the discharge from LD1 was 1,633 cu m/sec (57,700 cfs) on 3 March 1979, according to USGS water discharge record (USGS 1998). The presence of significant tides and a wide range of freshwater discharge values means the estuary varies from well mixed to partially mixed depending on the exact flow and tide regime and depending on the location in the system. Generally, the system is more likely to be partially mixed when freshwater flows are large, at which time the largest top to bottom salinity gradients occur in the lower half of the portion of the river below Wilmington, also referred to as Wilmington Harbor.

The dredged shipping channels maintained in the CFR system include the main, deep-draft channel along the natural channel of the CFR up to the confluence of the NECFR and continuing a few miles up the NECFR, the CFR above the NECFR junction, the Military Ocean Terminal Sunny Point (MOTSU) harbor channels, and the Intracoastal Waterway (which includes Snow's Cut). This study is concerned primarily with the main shipping channel, including the

---

[1] Trawle, M. J., Banchetti, A. J., and Berger, R. C. (1980). "Military ocean terminal at Sunny Point (MOTSU), North Carolina hybrid model study, Report 1: hydraulic and salinity verification of the Cape Fear River physical model," unpublished report, U.S. Army Engineer Waterways Experiment Station, Vicksburg, MS.

[2] U.S. Army Engineer District, Wilmington. (1976). "A feasibility study on reducing maintenance dredging costs at the Military Ocean Terminal, Sunny Point," unpublished manuscript.

Table 1
Chronology of Navigation-Related Developments, Cape Fear River (USAED, Wilmington, 1960, 1976; Welch 1979)

Date (Work Completed)	Description of Work Lower Cape Fear River	Ocean Entrance and River Channel, Depth and Width[1] (Low Water Datum)
1829-1889	During this period, a number of engineering works were undertaken for the purpose of increasing the depths of the lower Cape Fear River in the interest of navigation. The improvements included: (a) construction of contraction jetties in the eight-mile river reach immediately below Wilmington; (b) closure of New Inlet through the construction of New Inlet Dam; and (c) dredging of the river channel shoals. By 1889, the river's navigation channel between the ocean entrance and Wilmington had been developed to a depth of 16 feet and a width of 270 feet.	16' x 270' River Channel (By 1889)
1907	River channel dimensions increased to a depth of 20 feet and width of 270 feet by dredging. Mooring basin excavated at Wilmington.	20' x 270' River Channel
1913	Ocean entrance channel dredged to a depth of 26 feet and width of 400 feet. River channel dredged to a depth of 26 feet and width of 300 feet to Wilmington.	26' x 400' Ocean Entrance 26' x 300' River Channel
1916	Anchorage basin was dredged at Wilmington having a length of approximately 2,000 feet, a width of about 1,000 feet, and a depth of 26 feet.	26' x 400' Ocean Entrance 26' x 300' River Channel
1926	The ocean entrance channel was dredged to a depth of 30 feet and a bottom width of 400 feet.	30' x 400' Ocean Entrance 26' x 300' River Channel
1930	Excavation of Snows Cut effecting connection of Atlantic Intracoastal Waterway (AIWW) with Cape Fear River.	30' x 400' Ocean Entrance 26' x 300' River Channel
1932	River channel dimensions increased by dredging to a depth of 30 feet and bottom width of 300 feet. A turning basin having a width of approximately 600 feet was also excavated at Wilmington. Work accomplished between 1931 and 1932.	30' x 400' Ocean Entrance 30' x 300' River Channel
1948	The river channel was extended 1.25 miles north of Wilmington for the Hilton railroad bridge to an upstream point in the Northeast (Cape Fear) River. This extension had a channel depth of 25 feet and a bottom width of 200 feet. Work accomplished in winter 1948.	30' x 400' Ocean Entrance 30' x 300' River Channel to Hilton Bridge 25' x 200' River Channel above Hilton Bridge
1949	Ocean entrance and river channel dimensions increased to a depth of 32 feet and bottom width of 400 feet. Work accomplished between 1947 and 1949.	32' x 400' Ocean Entrance 32' x 400' River Channel to Wilmington
1952	Carolina Beach Inlet was opened through barrier beach by earth-moving equipment and explosives. Work accomplished in summer of 1952.	32' x 400' Ocean Entrance 32' x 400' River Channel to Wilmington
1955	Navigation facilities dredged at Military Ocean Terminal Sunny Point (MOTSU). Basins were dredged to a width of 800 feet and depth of 34 feet. Entrance channels dredged to a width of 300 feet and depth of 34 feet. Work accomplished between 1953 and 1955.	32' x 400' Ocean Entrance 32' x 400' River Channel to Wilmington
1958	Ocean entrance dimensions increased to depth of 35 feet and bottom width of 400 feet. River channel dimensions to Wilmington increased to a depth of 34 feet and bottom width of 400 feet. Work accomplished between 1956-1958.	35' x 400' Ocean Entrance 34' x 400' River Channel to Wilmington
1970	River channel dimension increased to a depth of 38 feet and bottom width of 400 feet. Work accomplished between 1965 and 1970.	35' x 400' Ocean Entrance 38' x 300' River Channel to Wilmington
1971	Ocean entrance channel dimensions increased to a depth of 40 feet and width of 500 feet. Work accomplished between 1970 and 1973.	40' x 500' Ocean Entrance 38' x 400' River Channel

[1] All depth and width are in feet. To convert to meters multiply by 0.3048.

bar channel and 19 channel or subchannel reaches up to Wilmington, proper and numerous other reaches to the Chemserve/Arcadian area 1.6 km (1 mile) north of the Hilton Railroad Bridge on the NECFR.

The Cape Fear River is an important commercial and recreational waterway, providing an important link to the ocean for North Carolina industry. Commercial fishermen, shippers, and recreational vessels use the river and harbor extensively. The presence of MOTSU on the west side of the river about 13.7 km (8.5 miles) upstream from the mouth of the CFR means the CFR is an important military port as well. The existing depth of the ship channel has been cited as the most limiting aspect of Wilmington Harbor. Shippers, pilots, and the State Port Authority have requested deeper channel depths to improve overall efficiency of port operations. With presently authorized and maintained channel depths of 11.6 m (38 ft), pilots can bring in ships on high tide with drafts of 11.6 m (38 ft) and leave on high tide with drafts of 11.3 m (37 ft). This practice requires careful scheduling with associated time delays to take advantage of the additional high-water levels. Shipping interests have expressed a need for an optimum channel configuration which would reduce vessel delays, decrease transportation costs, and allow the port to keep up with the trend toward larger vessels.

Study objectives

To address the navigation concerns previously mentioned, the U.S. Army Engineer District, Wilmington, NC, (SAW), has proposed deepening and, in certain critical areas, widening the CFR deep-draft ship channel. Since such changes in channel geometry may affect the hydrodynamic and salinity regimes of the CFR system, SAW proposed that the U.S. Army Research and Development Center (ERDC) conduct a comprehensive 3-D numerical modeling effort of the CFR system for the purpose of determining the effects of various proposed channel alterations on the hydrodynamic and salinity behavior of the estuary. This modeling effort, detailed in this report, is intended to help in the formulation of project alternatives and in the assessment of potential impacts to interior CFR/Wilmington Harbor estuarine processes due to project construction in the areas of water level and salinity intrusion and distribution. As part of the modeling investigation, a field data collection effort was conducted by ERDC (Benson 1995).

Approach

The general modeling approach used in this numerical effort was to develop a computational grid, establish appropriate boundary conditions, and employ a digital computer code, all of which constitute the model proper. This model was then used to compute numerical results that were compared to field data for verification and, once verified as a useful tool for investigating the response of the system to channel alternatives, various numerical experiments of detailed channel alteration alternatives were defined and performed. Analysis and interpretation of the model results followed.

2 Study Description

Model Description

Grid

The computational grid is a discrete collection of points defined with x, y, and z coordinates in such a way as to approximate the physical system, i.e., the CFR estuarine system. The grid used in the CFR work is one suitable for use in finite element method (FEM) computation. A FEM grid is unstructured, lending itself to quick alterations that aid in the verification process as the grid is being developed and in making grid changes to accommodate plan alternatives.

A plan view of the CFR grid is shown in Figure 2. The Wilmington to Campbell Island reach grid is shown in Figure 3. Each vertex and each point half way between vertex pairs connected by a line segment represent a calculational point, or node, for which a solution for the system dynamical equations is sought. Nodes are grouped into elements that are the polygons seen in the plan views of Figures 2 and 3, and 3-D elements are one of four simple solids (brick, prism, pyramid, tetrahedron) bounded by the allowed triangular and quadrilateral polygons. A plan view polygon is, in the 3-D regions, the two-dimensional (2-D) element bounding the top of a 3-D, or solid, element.

The grid is a combination of 2-D and 3-D elements that enable the physical system to be modeled to capture complicated boundary features and to provide for depth-averaged calculations where adequate (2-D regions) and calculations of variables at various depths (3-D regions) where vertical gradients in salinity or velocity are suspected to be important in the dynamics of the estuary. Though some regions are modeled in 2-D, the local system bathymetry is nevertheless included in the calculation; the calculated values of velocity and salinity are simply not resolved vertically (i.e., depth-averaged values, only, are calculated in the 2-D regions).

The grid shown in Figures 2 and 3 represents the existing condition and was used in the verification process. Except for widening of the deep-draft ship channel in particular turns and reaches, all grids in the tests have a similar appearance in plan view. Aside from the widening, the various testing scenarios differ in depth and bottom topography. The existing condition grid has in it channel bottom depths as reported in the Wilmington District survey of August

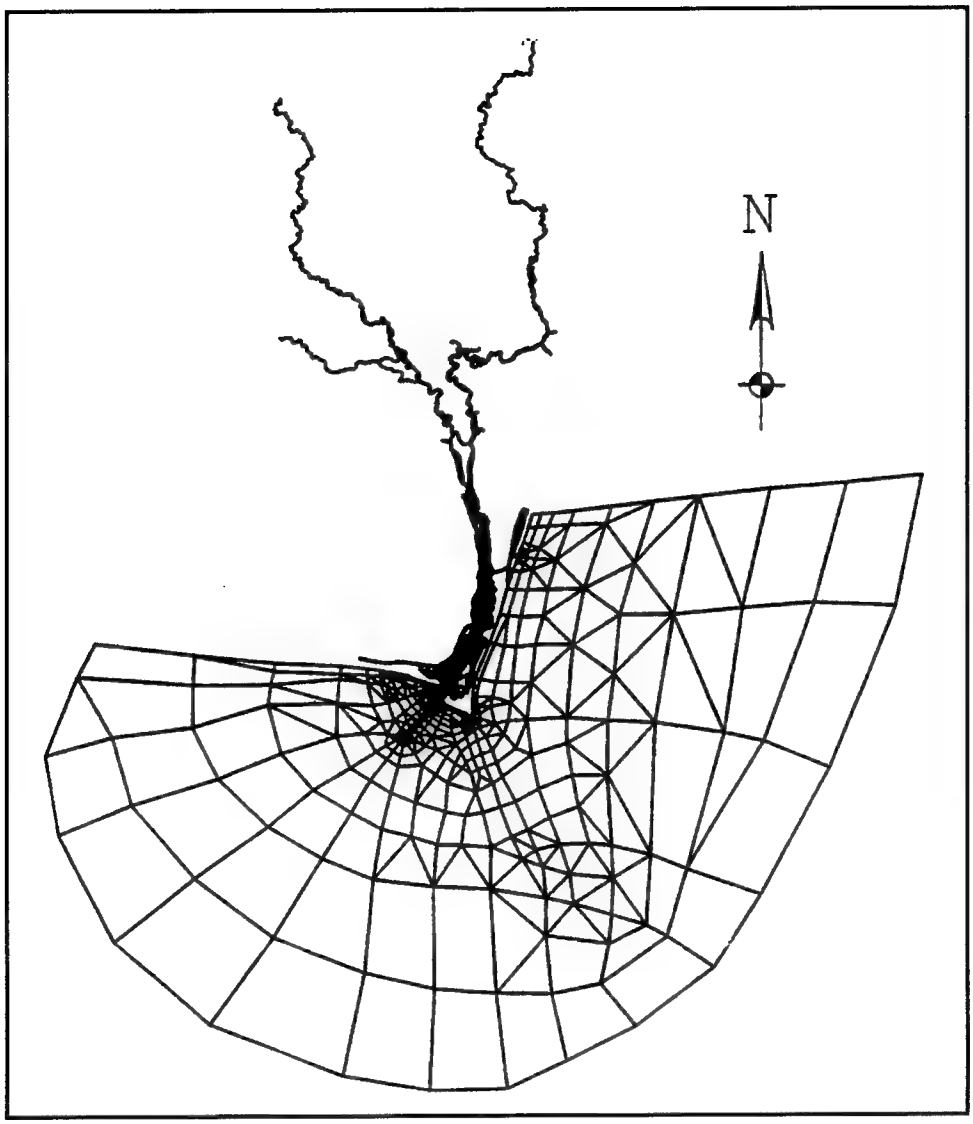

Figure 2. Numerical grid

1993 (USAED, Wilmington, 1993), and the bathymetry of the existing grid is thus irregular and reflects the scouring and shoaling in the channel as it was during the survey. Channel depths range from shoals less than project depths to scours greater than project depths, a range of approximately 11.3 m (37 ft) to 16.2 m (53 ft) below mlw.

Unless otherwise noted, all grids have the same number of nodes and elements: 48,889 total nodes, 31,459 surface nodes; 17,487 total elements; and 8,855 surface elements. The grid is primarily 3-D from just below the junction of the BR on the CFR and from approximately Long Creek on the NECFR to a delta region at the river ocean outlet with a radius approximately equal to the bar channel. Snow's Cut, Carolina Beach Inlet, and environs are also 3-D. At approximately the latitude of Wilmington and points farther north, creeks and marshes adjacent to the 3-D river channels are modeled with 2-D elements.

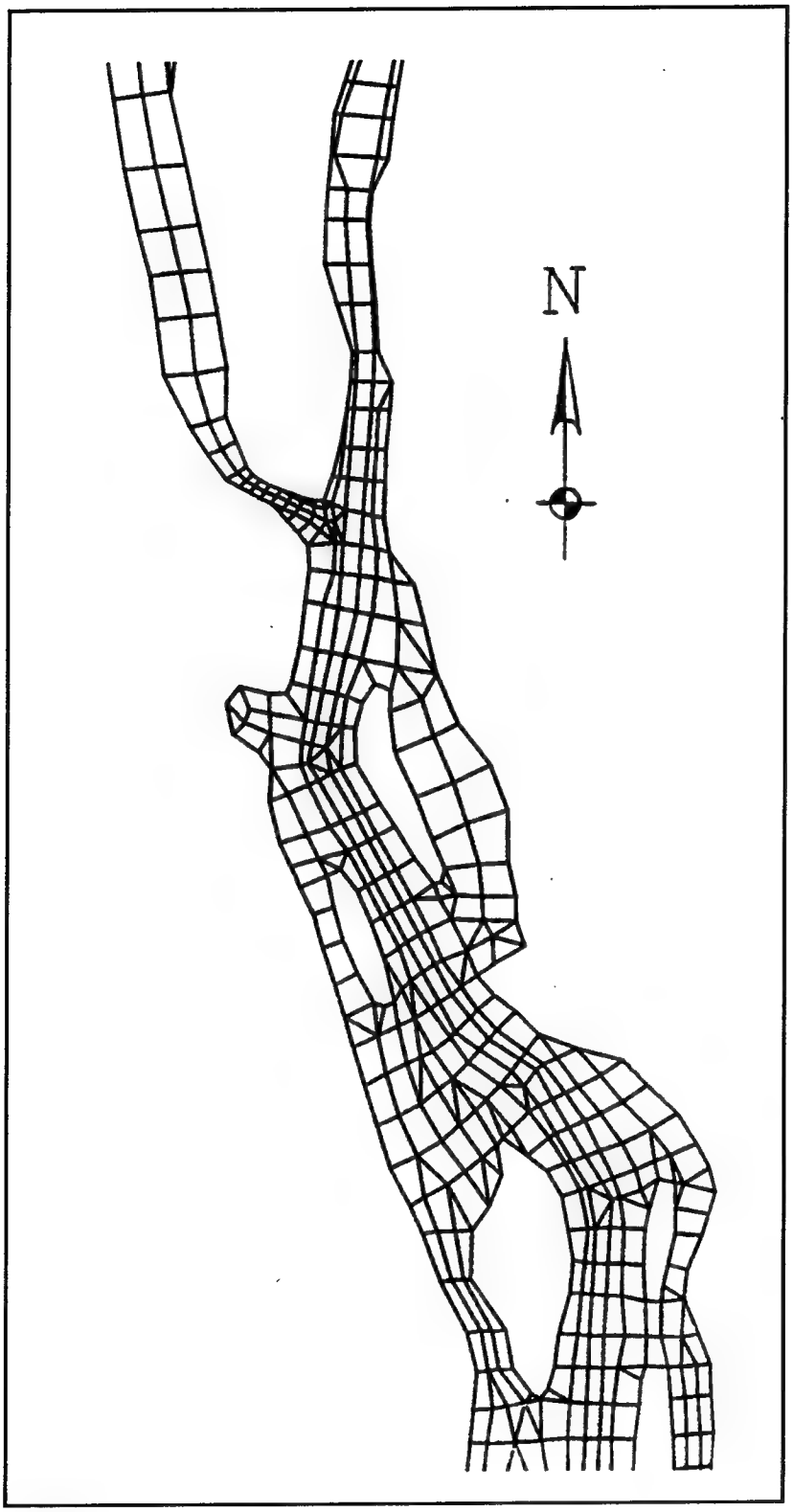

Figure 3. Wilmington to Campbell Island portion of numerical grid

Farther up the CFR, BR, and NECFR the river channels are modeled in 2-D and side channels and adjacent marshes are modeled, generally, as shallow 2-D elements. The river below Wilmington has numerous grass marshes modeled in 3-D.

All 3-D regions, except the main deep-draft ship channel, are modeled one layer deep; the channel is modeled three-layers deep. Element corner nodes in 3-D regions thus have three (one-layer regions) or seven (three-layer regions) calculational nodes at and below the surface. In the channel, with depths of approximately 12.2 m (40 ft), a vertical resolution on the order of 1.8 m (6 ft) is given. Off channel resolution, where depths in the large shallow regions are about 3 m (10 ft) or fewer, is about 1 m (3 ft) or smaller in the vertical dimension.

Boundary conditions

Boundary conditions are the driving forces of ocean salinity, tide, wind, and freshwater inflow that interact with the topography and topology of the estuary, as represented in the grid, through the computer code to produce values for the variables of the system at each node. Ocean salinity, tide, wind, and freshwater inflow data are generally taken from a combination of field data reports and synthetically generated data for the system and are incorporated into a file read by the computer code and used as part of the initial conditions for the calculation of nodal variable values at each time-step.

The tidal boundary was based on a combination of data taken in the ERDC field effort at Fort Caswell and synthetic tides generated by the software TIDES (NOS 1993). The synthetic tide was used to extend the field data into the past so that the model could be spun up prior to the field collection effort beginning time; the synthetic and field tides joined smoothly. This combined tide time series was then reduced in amplitude by 10 percent using a fast Fourier transform (FFT) and placed at the ocean boundary. This reduction resulted, due to amplification of the tide wave amplitude as it moves into the shallow environs of the CFR, in a good amplitude match between the calculated and observed tides at Fort Caswell. Tides used as boundary conditions are shown in Figure 4. Tidal verification will be discussed more in the model verification section.

Wind data used are those hourly values of wind speed and direction recorded by the National Weather Service at the Wilmington airport for 27 July to 31 October 1993. (NWS Station 723013.) These wind data were used to calculate the shear stress, $_s$, at the water surface in terms of the air density, $_a$ and speed, W, using the expression

$$t_s = C r_a W^2 \tag{1}$$

C is described in Wu (1980) as

$$C = \left(0.8 + 0.0656W\right) \times 10^{-3}$$

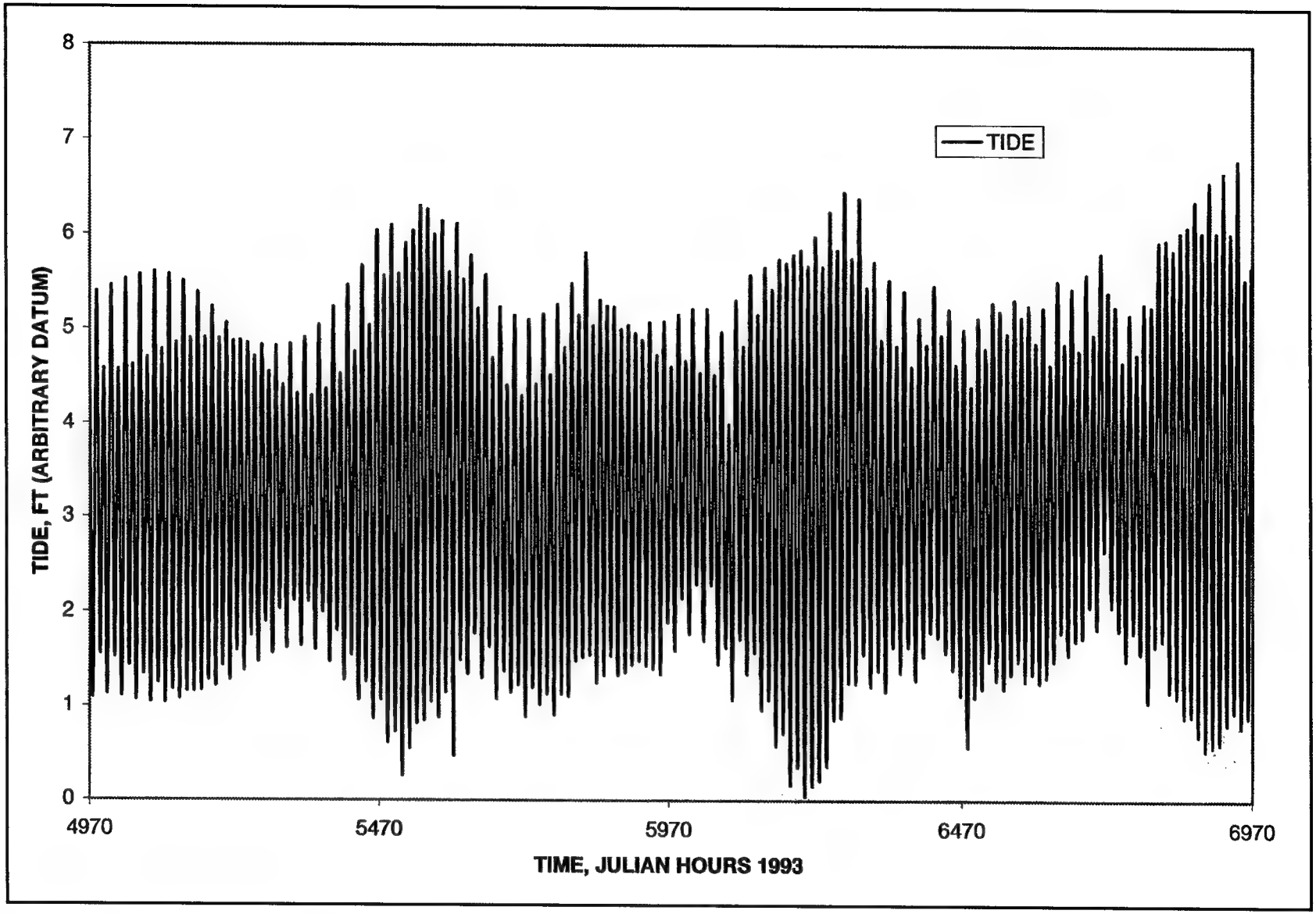

Figure 4. Tide signal used for boundary conditions (To convert tide to meters, multiply by 0.3048)

The wind field is applied over the CFR system from its outlet between Smith Island and Oak Island to points north.

Three freshwater inflows are employed at LD1 (on the CFR), Tomahawk (on the BR), and Chinquapin (on the NECFR). Hourly discharge data from USGS gauges 02105769, 2106500, and 02108000, respectively, were used along with the Concurrent Discharge Relation from Giese (1985) for an estimate of the ungauged flows to obtain hourly flows for the three gauge sites for use as a boundary condition. The total flow is plotted in Figure 5. These inflows were used for the verification process and some of the experiments. Other experiments used modified inflows and will be discussed later.

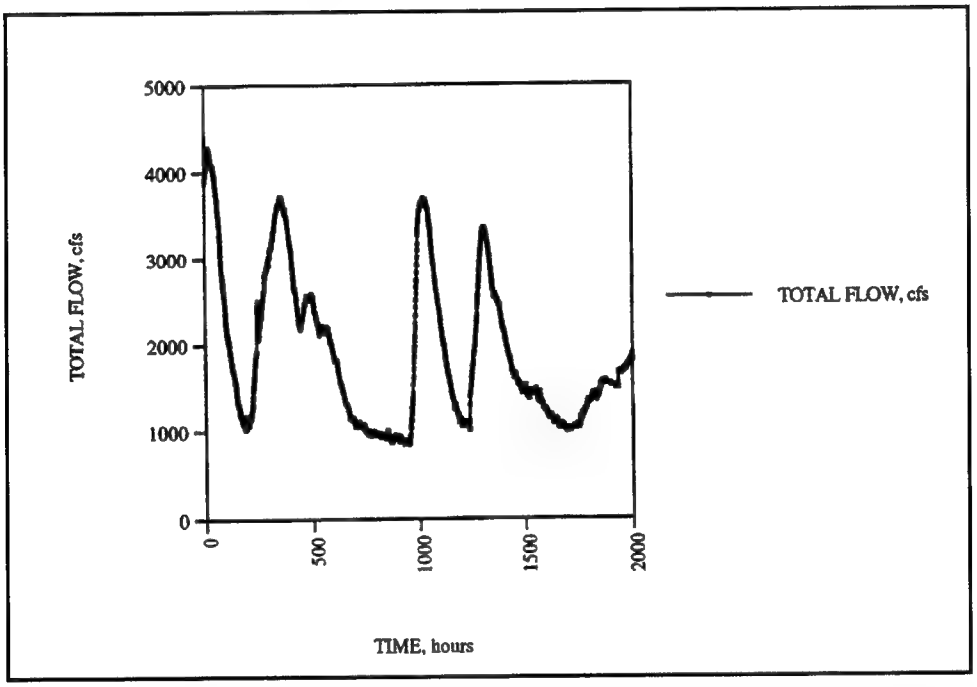

Figure 5. Total freshwater inflow, including gauged and ungauged flows for the Cape Fear River, the Black River, and the Northeast Cape Fear River (To convert total flow to cubic meters per second, multiply by 0.3048)

To begin calculations, the model needs initial conditions. The ocean salinity was constant, 36 ppt, and the initial tide value was the first water level in the tidal boundary condition sequence. The velocities were set to an initially very small magnitude and common direction, and the initial wind speed and direction were the values corresponding to the simulation start time. Salinities were chosen by assigning reasonable salinity values to a few selected locations in the system, guided by field data, and then assigning all other nodal salinities as a distance weighted average of these few selected location salinities.

$$salt(i) = \frac{\sum [salt(j)/d^4(j)]}{\sum [1/d^4(j)]} \qquad (2)$$

The interpolation formula was where i refers to an arbitrary node in the grid to which a salinity value is to be assigned, and d(j) is the distance from i to the j^{th} location for which salinities are specified. The sum is over all the selected locations, 47 in this case. This formula was used in a previous study (Berger 1995a,b).

The initial conditions take a finite time to wash out of the system. After a few tidal cycles the tides and velocities are past the transient stage and have settled down to their long-term behavior. Unlike the tide and velocity, whose disturbances travel with the wave speed of the system (i.e., essentially with the tide), the salinity travels at the much slower particle speed of the system, and thus requires hundreds of hours, or dozens of tidal cycles or longer, for the initially chosen values to be removed. Hence the system must be run for period of time, a spin-up time, before its values, particularly salinity, can be considered to represent the system.

Computer code

The computer code used was RMA10-WES. This FEM code encapsulates the basic physics of hydrodynamics and salt movement, which includes the laws of conservation of water and salt mass and the momentum equations (Newton's 2nd Law). RMA10-WES has been used successfully to study the hydrodynamic and salinity characteristics of many estuarine systems, including Galveston Bay, San Francisco Bay, the St. Johns River, the Lake Ponchartrain area, the Columbia River, and Charleston Harbor, among others.

The Reynolds form of the basic Navier-Stokes equations for the momentum and the continuity equation, and the advection-diffusion equation for salinity are the starting points of the discretized description of the basic physics into the RMA10-WES code. In the derivation of the exact equations coded, various assumptions are made consistent with the realities of the system modeled and the constraints of modern computation. For example, the most important simplification made is the hydrostatic assumption, meaning that vertical accelerations are assumed to be negligible. This assumption eliminates the need to calculate the vertical velocity as part of the primary dynamical calculation yielding faster, but accurate, values for a system, such as CFR, for which this assumption pertains. This code includes representations to utilize the boundary condition forcing functions described previously as well as the bed friction shear, a turbulence model, and an equation of state for the water density/salinity relationship. Appendix A contains a more detailed description of the RMA10-WES code and references.

Model Verification

Verification approach

Verification is the process of establishing to what extent the model behaves similarly to the prototype, whether the model reproduces that behavior without

continual adjustment, and whether the model is suitable for use in gauging system impacts caused by proposed alterations and for use in gaining insight into prototype response to change. Verification involves comparison of model data with field, or prototype, data through direct comparison of particular data sets and through the development of statistical comparisons of data sets. These statistical comparisons can also be used for comparison with other studies to gain perspective on what is possible with modeling of estuarine systems. Verification also involves sensitivity checks and qualitative assessments to see if previous qualitative behavior is represented in the use of the model for historical conditions. Verification is, then, an iterative process whereby the model is adjusted within the limits allowed by uncertainties in the various aspects of the physical system, such as bed roughness, or by taking into account better knowledge of the system as it becomes available, such as bathymetry, and then rechecking model results, after these adjustments, against the prototype data. This iterative procedure is continued until the model is judged capable of fulfilling the objectives set out in the particular study.

The verification process begins with comparisons between a model data set and a particular, usually short in time, prototype data set. This process is iterated until an adequate match is found. Data taken with the tide and current meters during the first few days of the data collection effort, 16 to 19 August 1993, were used for this adjustment phase of the verification process.

Estuarine model adjustments proceed in order from tides, to velocity, and then salinity. The adjustment parameter was the bed roughness as this is the parameter about which the uncertainty is the greatest. In the tidal adjustment phase the roughness for fairly large general regions and bed types is set to allow model results to compare well with the prototype observations. The further adjustments for velocity consist of some additional finer scale roughness changes in order that the distribution of velocity may be slightly improved, but the overall roughness is the same as that from the tidal adjustment phase. If the salinity values then do not match, the usual problems are inaccurate freshwater inflow or the initial startup error since the salinity in and of itself is only indirectly affected by roughness.

After the initial adjustment is finished, the model is allowed to run for longer times and model-prototype comparisons are made to determine the extent to which the model reproduces the behavior of the prototype without further adjustments. At this point, the extent to which the model behaves similarly to the prototype is dependent on, essentially, the physics inherent in the computer code and the limitations of the modeling abstraction process, and the model's value as a tool to make comparisons, wherein model-prototype differences can be thought to cancel out in plan tests, is enhanced. Since models are not and cannot be reproductions of complex systems such as estuaries, an appreciation of the use of a model to gain insight into the workings of such a complex system and, also, to make comparisons and thus measure the relative response of the modeled system to change, is essential.

Qualitative model-prototype comparisons

Plates 1 through 33 show direct comparisons of the prototype and model calculation for the existing conditions during portions of the prototype data collection period from August through October 1993. Most of the plates show data taken from 14 August to 3 September 1993 (Julian hours 5400 to 5900, approximately). This 500-hr period is used because it contains a neap-spring sequence during which most of the long-term tide, velocity, and salinity meters collected data that were not obviously marred by fouling or malfunction. The data collection effort is described in a separate report (Benson 1995).

Tides. Plates 1 through 4 show the comparison of 11 tide gauge locations maintained for this study and the NOAA gauge at Wilmington for the 14 August to 3 September 1993 period. Gauge locations are shown in Figure 6. The plot of data for the gauge at Ft. Caswell, sta 1_3B, includes the synthetically generated tide for that location that preceded the meter installation at Julian hr 5462 (1400 hr, 16 August). Aside from the NOAA gauge, the gauges are not surveyed in and so comparisons between model and prototype are made after their means are removed. The NOAA comparison, however, is between actual calculated and measured values.

All of the gauges show good agreement between prototype and model water surface levels, with the best agreement being between stations nearer the outlets, as is typical in complex estuarine modeling. The large-scale response of the tide to both neap-spring forcing and the short-term mean tide level changes evident in the plates are reproduced well. Tide range and phase comparisons are, again, best for stations near the openings, but remain good through the Wilmington vicinity. The poorest comparisons are for the gauges near the extreme upper end of the model at Castle Hayne on the NECFR, the upper BR, and at LD1 on the CFR. Even these, however, show good agreement between the larger-scale phenomena as well as adequate agreement in the details of range and phase.

One major difference between model and prototype is the shape of the tide curves. For gauges progressively farther away from the outlets, the shape of the curves deviates from that of the prototype data, the model tide curves typically being steeper in the second half of the rising portion of the tide curve and more symmetrical than the prototype curves. Plates 5 to 8 show enlargements of the first few title cycles for all of the tide gauges. These differences account in part for differences in tide range and phase seen in the model and prototype comparison and are due to local topographic and physical details beyond the scope of this study to model. More quantitative comparisons between model and prototype tides are given later.

Velocities. Twelve of the deployed long-term current gauges provided data for comparison with model calculations. Ten of the 12 were deployed in pairs, with one at approximately middepth and the other located 1.5 m (5 ft) above the bottom. Gauge locations are shown in Figure 6. The data for the 14 August to 3 September 1993 period are displayed in Plates 9 to 12. Positive values indicate flood flow, and negative values indicate ebb flow. Most of the instruments took

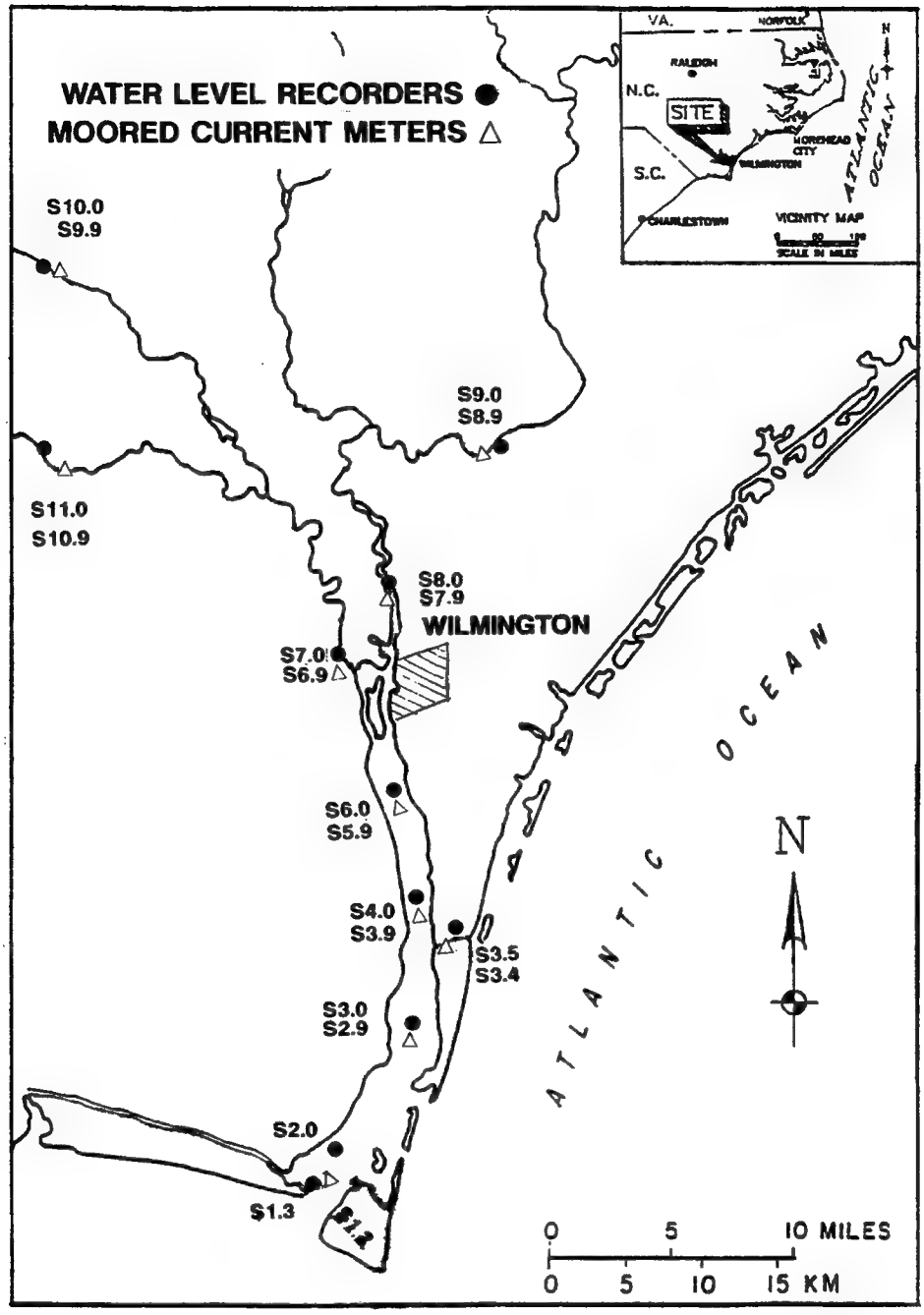

Figure 6. Meter locations for the prototype data collection effort (Benson 1995)

data that were not obviously affected by fouling or some other outside perturbation. Exceptions include the near bottom meter at sta 3.9 (Orton Point, sta 3.9b on Plate 10), which appears to have been fouled or otherwise influenced, especially with regard to ebb currents, and the near bottom meter at sta 5.9 (Exxon Pier, sta 5.9b on Plate11), which failed soon after deployment. Other meters originally deployed, such as those at Castle Hayne and LD1, either failed almost immediately or were never recovered.

The model results are in good general agreement with the prototype data. The general characteristics of ebb and flow, including the neap-spring sequence, are evident. Model results are sometimes a little larger (usually below Exxon Pier) and other times a little smaller (usually at and above Exxon Pier) than prototype. Where the meters are paired, both the prototype and the model data show stratification. More quantitative comparisons between model and prototype velocities are given later.

Salinities. Time series comparisons of salinity prototype data and model results are shown in Plates 13 through 33. Salinity data were taken in conjunction with most of the tide and current velocity stations, including near surface values associated with the tide gauges, middepth and near bottom values taken with the paired current meters, and values taken with the unpaired current meters. Meter locations are shown in Figure 6. The calculation actually began approximately 300 hr, or about 24 tidal cycles, before the field data start time to spin-up the model system's salinity values.

Plates 13 through 15 show the comparison of model and prototype salinities for the 14 August to 3 September 1993 period for the salinity concentration gauges deployed with the tide gauges near and south of Wilmington. Plates 16 through 19 show the comparison for the same time period for the gauges deployed with the current meters. This approximately 500-hr period is emphasized for the salinity gauges due to the fouling experienced by many of the gauges. As appropriate, other periods of time will be discussed for some of the meters, shown in Plates 20 through 26.

Plates 27 through 33 are shown to place the salinity meter results and the biological fouling that occurred in context. Biological fouling is most serious in warm, summer temperatures and for salinities above the 10 to 15 ppt range. A meter left in these conditions will often show fouling caused by barnacle growth in the small orifice of the conductivity probe after a few hundred hours of exposure unless protected by anti-fouling coatings. Barnacle growth blocks the free flow of water through the meter aperture and thus produces an incorrect result for the conductivity results that go into the salinity calculation. As barnacle growth proceeds, the tidal averaged values and the tidal range values of the salinity reported by the meter decrease from the actual values and, in some cases, the values become noisier. Anti-fouling coatings, developed to prevent barnacle growth on the meter surfaces, are available and were used in this deployment. When coatings are not available, periodic meter cleaning will mitigate fouling (Fagerburg et al. 1994). The anti-fouling coatings applied to many of the meters deployed in this study unexpectedly failed. However, sufficient data are available to verify the model. The original data collection effort was scheduled for six weeks, however, leading any additional data beyond hr 6400 as a bonus.

Generally, meters in salinities above the 15 ppt level begin to deviate due to fouling between 400 and 600 hr after deployment. This is seen most dramatically in surface meters at Fort Caswell, Southport, and Reeves Point, where the water is warmest and saltiest (as shown in Plate 27), and the trend is also evident in the surface meters at Snow's Cut, Orton Point, and Exxon Pier (Plate 28), and the non-surface meters at Fort Caswell, Snow's Cut, Orton Point, and the mid-depth

meter at Exxon Pier (Plates 30 and 31). Meters deployed in lower ambient salinities or those deployed deeper in lower temperature waters generally show a slower drift.

These meters deployed in generally lower salinity or temperature regimes yield longer data series without significant deviation. The near bottom meter at Exxon Pier, paired meters at Navassa and Hilton Bridge, the surface meters at Navassa and Hilton Bridge (shown in Plates 32, 33, 29 respectively), do not exhibit the sharp change in salinity values seen in many of the meters deployed elsewhere, and the monotonic deviations that appear attributable to fouling do not appear as early as other meters. These longest records, such as seen in the Navassa, Hilton Bridge, and (near bottom) Exxon Pier meters, can be attributed to a combination of low salinity or low temperature that is not conducive to biological fouling. Some of these upper estuary meters, such as the near bottom meter at Exxon Pier, the paired meters at Navassa and Hilton Bridge, and the Hilton Bridge surface meters appear to show a fouling related meter failure at the end of the deployment as ambient salinities rise to or above the 10 to 15 ppt range, as expected. Biological fouling, especially from barnacle growth, can be episodic and time varying, especially in regions such as in the upper estuary where conditions favorable to barnacle growth are likely to change rapidly.

The data not obviously affected by the fouling problems detailed above are, however, substantial, and show good agreement between the prototype and model predictions. The surface meter results in the 14 August to 3 September period (hr 5400 to 5900) (shown in Plates 13, 14, and 15) and, for the Navassa and Hilton Bridge deployments in the 4-24 September (hr 5900 to 6400) and 24 September to 15 October (hr 6400 to 6900) periods (shown in Plates 20 and 21), show that the model reproduces the general ebb and flow oscillations of the salinity values and follows the longer-term variations correlated with the neap spring cycles of the tides and the variations of the river hydrograph.

The near bottom and middepth meter results in the 14 August to 3 September period (shown in Plates 16, 17, 18, and 19) and the results for the Exxon Pier, Navassa, and Hilton Bridge meters for all or part of the 4-24 September and 25 September to 15 October periods (shown in Plates 22, 23, 24, 25, and 26) also show that the model reproduces the general ebb and flow oscillations of the salinity values and follow the longer-term variations correlated with the neap spring cycles of the tides and the variations of the river hydrograph. The meters in and around the Wilmington area that have the longest reliable times series, *viz.* the near bottom Exxon Pier meter and the meters deployed near Navassa and Hilton Bridge are, in fact, remarkable for the faithfulness with which the trends are reproduced over the 1500 hr, approximately, comparison time period. Since the numerical model takes account of only the grossest features of the system, particularly with regard to the local nature of freshwater sources such as inflows and rainfall, variations between model and field data are inevitable. Field data itself must also be considered carefully since they, too, are limited representations of the prototype that are subject to error. Similar long-term data set comparisons can be found in studies detailed in references Berger et al. (1995a) and Johnson et al. (1993).

Quantitative model-prototype comparisons

Tides. The quantitative comparison between model and prototype tide values is shown in Figure 7. The approximately 500-hr period from 16 August to 6 September 1993 (hr 5462 to 5966.5) was analyzed using the ERDC program Harmony for M2, S2, K1, O1, M4, and M6 tidal components. This time period was chosen because it has the longest continuous signal with the maximum number of stations available for the prototype values for salinity, with a few exceptions which will be noted where appropriate. The tide and velocity values also have long continuous data sets for this period. The vector resultant of the amplitude components and the average phase in hours were computed for both the field data and model data sets. The tidal amplitudes were normalized to their respective values at the most seaward tide station, Fort Caswell; the phases are presented by giving the respective phases relative to the Fort Caswell values. The plots are presented by referring to the meter station (shown in Figure 7), which is for the most part a north to south progression up the estuary.

The comparison of tidal amplitudes is good in terms of the normalized values, showing the model reproduces the relative change in the tidal amplitude signal from the outlet of the estuary in to its upper reaches. Stations for the Cape Fear River proper and for Galveston Bay are shown in Figure 8 for comparison purposes (Berger et al. 1995a). The relative tidal phasings also compare well, with the largest differences occurring at a boundary, in the upper reaches at LD1, where a strong reflection is expected. The prototype displays a generally smaller relative phase lag than the model, except at LD1.

Velocities. The quantitative comparison between model and prototype values is shown in Figure 9. The time period used was the same as for the tides, except for sta 5.9b, the near bottom meter at Exxon Pier, where the meter failed after a few days, and these few days of data are used to compute the root mean square (RMS) values for that meter. RMS values of the velocities were computed for both prototype and model results for use in the comparisons.

The velocity RMS values compare very well, with two notable exceptions. At sta 3.9b, which is the Orton Point near bottom meter, the meter suffered an obvious fouling problem for ebb currents, and this skews the prototype RMS velocity to a lower value. At sta 5.9a, the Exxon Pier middepth station, the model underpredicts the prototype by 18 percent. A similar RMS velocity comparison, for Galveston Bay, is shown in Figure 9 for comparison purposes (Berger et al. 1995a).

Salinities. The quantitative comparison between model and prototype salinity values is shown in Tables 2 and 3. Two time periods were chosen for use in the analysis because the salinity meters became fouled. To obtain comparisons for as many synoptic data sets for as many meters as possible, the 338 hr of data (677 data points) from hr 5462 to hr 5800 were chosen. Since some of the meters had longer usable data sets, 1327.5 hr of data (2656 data points) from hr 5462 to hr 6789.5 were also used where appropriate. Since field data were taken at 15-min intervals and model data were calculated at 30-min intervals; the data selected for the comparison are thus those at the 30-min interval.

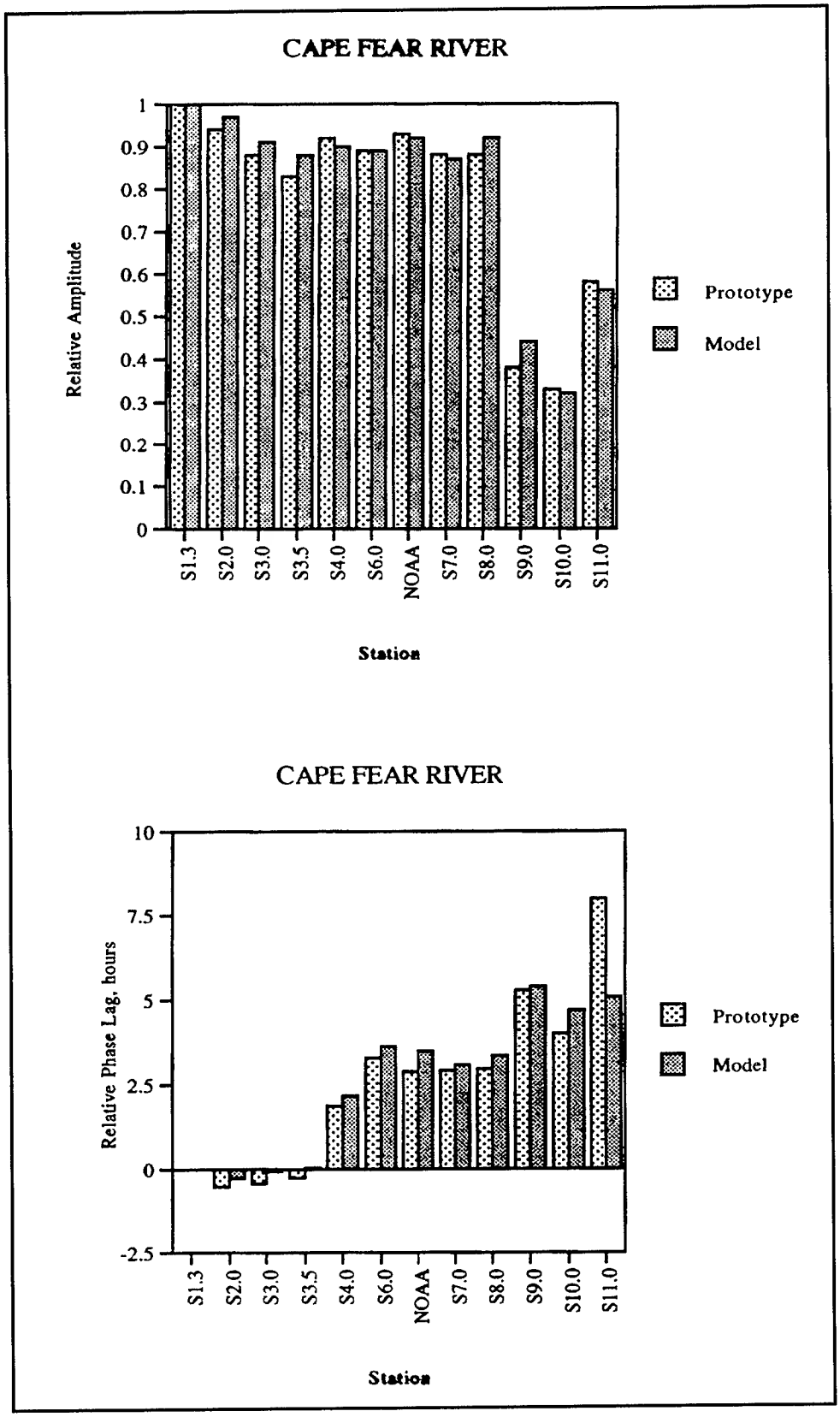

Figure 7. Tidal amplitude and phase comparison, prototype and model, for 12 stations

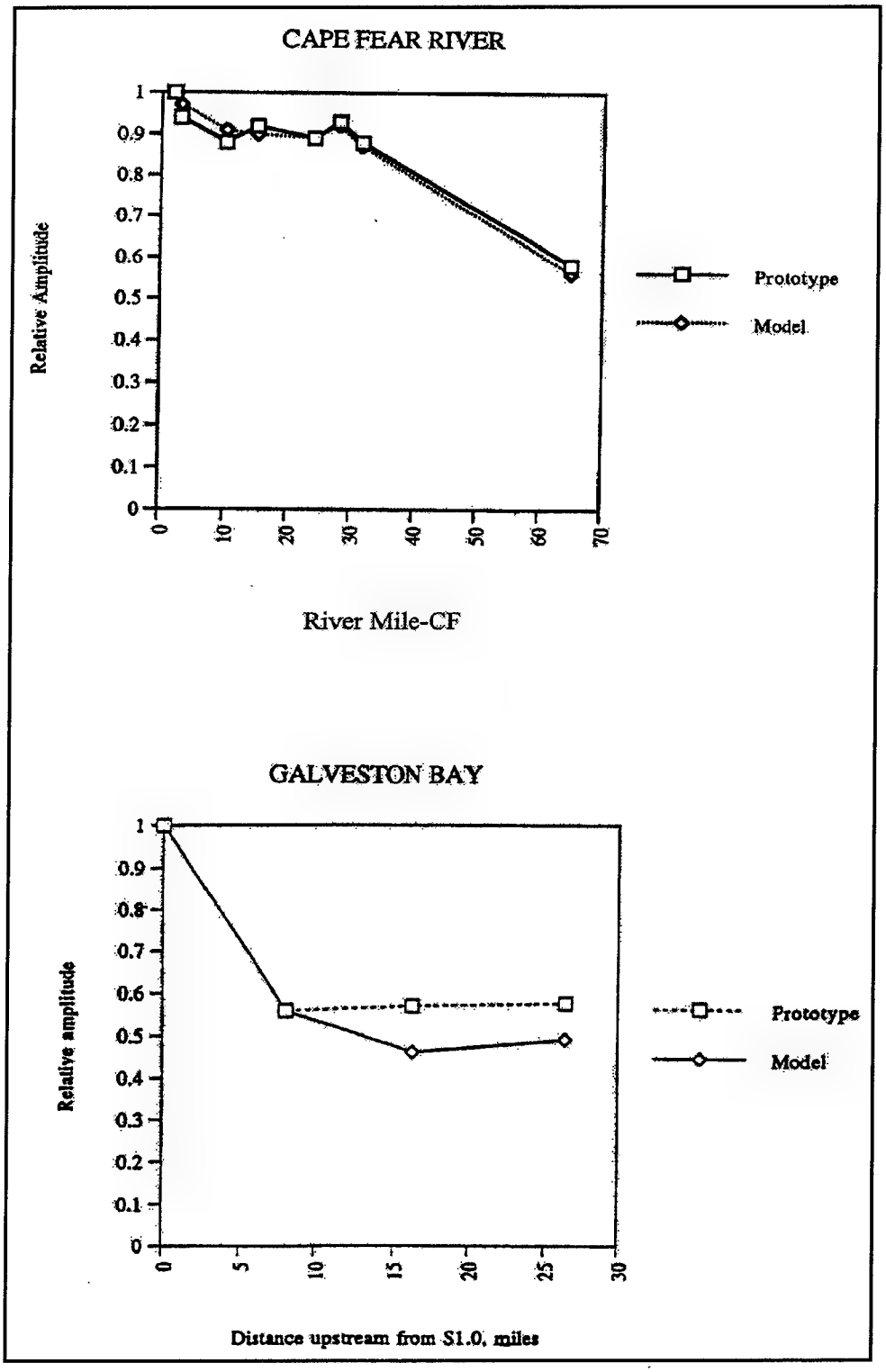

Figure 8. Tidal amplitude comparisons, prototype and model, for the Cape Fear River and for Galveston Bay

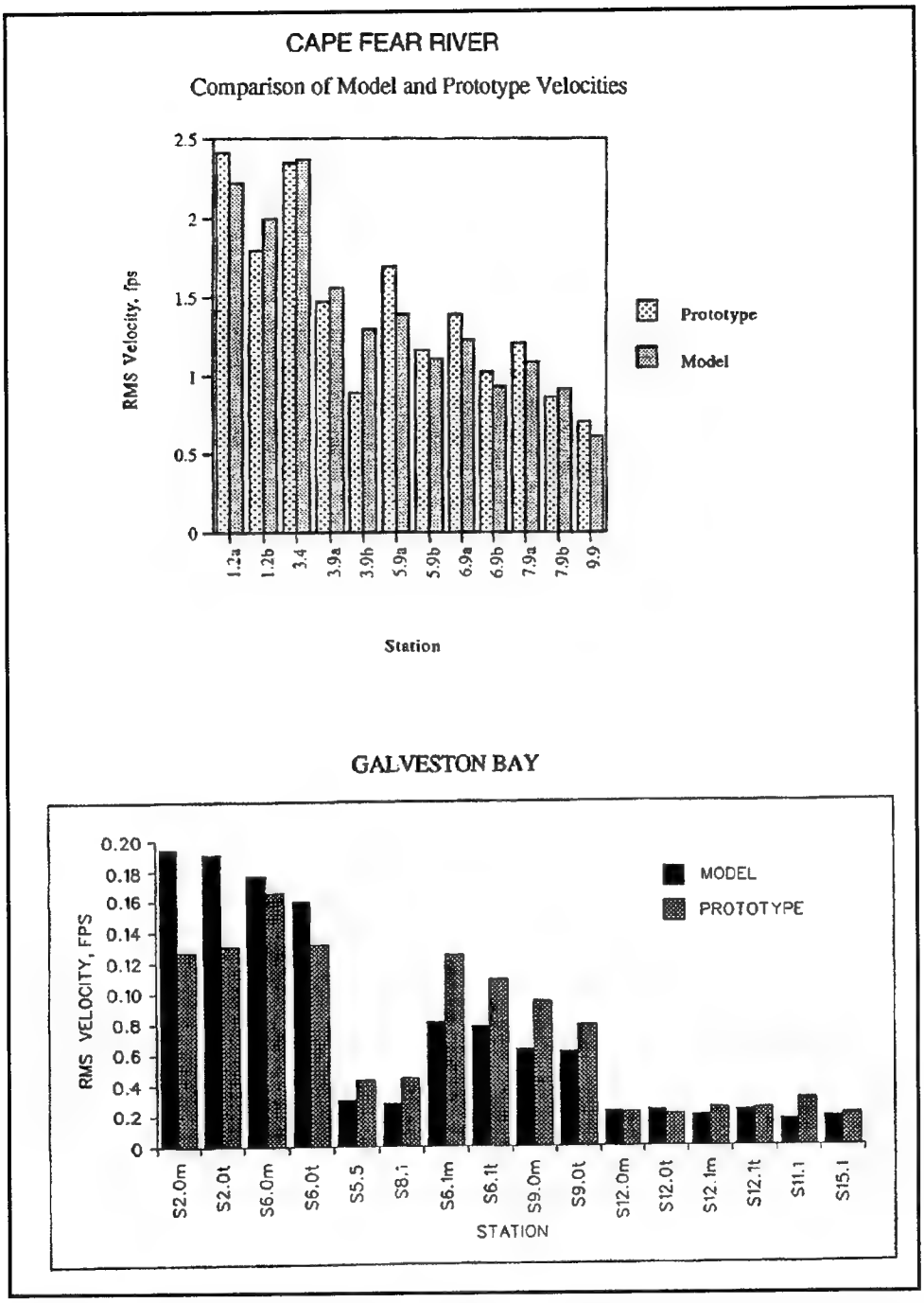

Figure 9. Velocity comparison, prototype and model, for the Cape Fear River and for Galveston Bay (To convert velocities to meters per second, multiply by 0.3048)

Table 2
Table of Short Time Period Salinity Statistics

Station	Mean Difference (model-prototype)	MAE (|model-prototype|)	Correlation	d	Standard Deviation	95% Confidence Interval
1.3	0.92	0.92	0.95	0.83	0.56	0.92±0.04
1.2a	0.80	0.80	0.95	0.88	0.49	0.80±0.04
1.2b	0.74	0.75	0.95	0.89	0.46	0.74±0.03
2.0	1.42	1.46	0.71	0.68	1.16	1.42±0.09
3.0	1.53	1.58	0.91	0.83	1.09	1.53±0.08
3.5	1.97	2.11	0.93	0.90	1.68	1.97±0.13
3.4	2.01	2.23	0.92	0.89	1.86	2.01±0.14
4.0	2.76	2.76	0.94	0.79	1.02	2.76±0.08
3.9a	0.98	1.28	0.88	0.91	1.31	0.98±0.10
3.9b	0.09	1.02	0.91	0.93	1.18	0.09"0.09
6.0	-0.32	0.82	0.91	0.93	0.96	-0.32±0.07
5.9a	-0.68	0.96	0.90	0.92	0.97	-0.68"0.07
5.9b	-1.82	1.93	0.85	0.77	1.13	-1.82±0.09
7.0	1.55	1.68	0.89	0.85	1.21	1.55±0.09
6.9a	-1.47	2.15	0.93	0.84	2.04	-1.47±0.15
6.9b	-1.77	2.39	0.93	0.82	2.13	-1.77±0.16
8.0	-2.10	2.10	0.84	0.55	0.65	-2.10±0.05
7.9a	-2.48	2.48	0.89	0.55	0.60	2.48±0.05
7.9b	-2.61	2.61	0.92	0.58	0.64	-2.61±0.05
338 hours 677 data points	<MD> = 0.08	<MAE> = 1.69	<r> = 0.90			

Table 3
Table of Long Time Period Salinity Statistics

Station	Mean Difference (model-prototype)	MAE (|model-prototype|)	Correlation	d	Standard Deviation	95% Confidence Interval
5.9b	-0.49	1.66	0.77	0.85	1.92	-0.49±0.07
7.0	2.87	2.96	0.75	0.71	2.15	2.87±0.08
6.9a	-1.78	1.90	0.88	0.90	2.06	-1.78±0.08
6.9b	-1.98	2.49	0.89	0.87	2.17	-1.98±0.08
8.0	-0.22	1.63	0.58	0.75	1.94	-0.22±0.07
7.9a	-0.81	1.45	0.73	0.81	0.60	-0.81±0.02
7.9b	-1.37	1.58	0.82	0.83	1.43	-1.37±0.05
1327.5 hours 2656 data points	<MD> = -0.54	<MAE> = 1.95	<r> = 0.77			

Various statistics are displayed in Tables 2 and 3 similar to those in other salinity studies to allow comparisons across studies (Berger et al. 1995a; Johnson et al. 1993). Calculation of some of these statistics assumes that the data represent a random sample of salinity differences at specific estuarine locations which, of course, they do not in every sense. The samples follow one another temporally at the regular 30-min interval and are strongly affected by the regularities of the tide, for example, and any slight phasing differences can also introduce large apparent differences. The samples are also not from exactly the same location because of the limits of resolution in the model and the uncertainties of meter location. The vagaries of local wind, rain, detailed bathymetry, and other localized and hard to model events do, however, contribute to the randomness of the sample differences.

Table 2 gives the statistics for the short period of record. These show that the model is representing the salinity response of the system well. The mean differences (MD) between model and prototype range, in magnitude, from 0.09 ppt at sta 3.9b (near bottom near Orton point) to 2.61 ppt at sta 7.9b (near bottom near the Hilton Railroad Bridge). Salinity readings are generally accurate to 0.1 ppt. Extra significant figures are included here to illustrate differences. The mean absolute error (MAE), or average of the absolute values of the model and prototype differences, range from 0.75 ppt at sta 1.2b (near bottom near Ft. Caswell) to 2.76 ppt at sta 4.0 (near surface near Orton Point). These values are similar to those from other studies, as shown in Tables 4 and 5. The average MD for all stations is 0.08 ppt; the average MD for stations below Exxon Pier (sta 6.0) is 1.32 ppt and for Exxon Pier stations and above it is -1.30 ppt. The average of all MAE values is 1.69 ppt. Thus, in this particular model-prototype comparison sample, the model underpredicts the salinity in the upper reaches of the estuary and overpredicts it in the lower reaches although, as at sta 7 (near surface near Navassa), the differences for some samples are reversed or are very small.

Table 4
Chesapeake Bay Model Salinity Statistics (Johnson 1993)

Year	Main Bay				Tributaries			
	Mean Bias Error, ppt	MAE, ppt	RMS Error ppt	Absolute Relative Error, %	Mean Bias Error, ppt	MAE, ppt	RMS Error ppt	Absolute Relative Error, %
(a) Near Surface								
1984	-0.05	1.21	1.45	10.13	-0.20	1.54	1.85	17.25
1985	0.90	1.49	1.93	11.43	1.09	1.66	2.04	16.32
1986	0.25	1.52	1.87	12.29	0.32	1.60	2.04	15.02
(b) Near Bottom								
1984	-0.64	1.72	2.12	10.44	-0.09	2.36	2.83	19.94
1985	1.12	1.78	2.34	12.11	1.27	2.31	2.99	18.30
1986	-0.16	1.35	1.68	8.74	0.24	2.23	2.65	13.40

As referred to above, slight phasing differences between the model and prototype data set can contribute to average differences, as in sta 5.9b (near bottom near Exxon Pier) in Plate 18. Also, the model and prototype curve shapes generally differ, contributing to differences. Such shape differences are caused by the practical limits of model resolution and local uncertainties in forcings and field data. In some cases, the range of values do not match as well as the average. This is due to meter problems that restrict the short-term tidal variations from being registered, and to the previously discussed modeling limitations that limit the resolution of very sharp and fast-moving gradients.

For the long period of record (shown in Table 3), the MD ranges, in magnitude, from 0.22 ppt (near surface near the Hilton Railroad Bridge) to 2.87 ppt (near surface near Navassa), and the MAE ranges from 1.45 ppt (near middepth near the Hilton Railroad Bridge) to 2.96 ppt (near surface near Navassa). The average MD for all stations is -0.54 ppt; the average MAE for all stations is 1.95 ppt. For all but one of these seven meters with long records, the MAE is smaller or approximately the same than their short record values. The MD is significantly smaller for the Exxon Pier near bottom station (sta 5.9b) and the Hilton Railroad Bridge stations (sta 8.0, 7.9a, and 7.9b). The longer data sets generally indicate that, within the uncertainties of the modeling process and the prototype data, the model continues reproducing the prototype salinity well. The Navassa stations (sta 7.0, 6.9a, and 6.9b), though representing well the long-term response of the system to the river hydrograph and the qualitative tidal behavior, do not capture perfectly the extremely sharp salinity gradient in this branch of the estuary.

Table 5
Galveston Bay Model Salinity Statistics (Berger 1995b)

Station	Hours	Mean Difference (model-prototype)	MAE (|model-prototype|)	Correlation	d
Trinity Bay					
S11.0	3389	-0.3	1.3	0.85	0.91
S11.2	1060	-1.8	2.0	---	---
S14.0[1]	3694.5	-0.4	1.1	0.97	0.98
S15.0	4137	-0.8	1.8	0.89	0.94
Upper West Bay					
S12.0m	883	0.0	2.2	---	---
S12.0t	883	-2.2	2.4	---	---
S12.1t	382	-0.6	1.4	---	---
S12.1t	1940	0.5	2.0	---	---
S13.0[1]	3459.5	-3.3	3.3	0.98	0.74
Mid-Bay					
S6.1m	1269	-0.4	2.4	---	---
S9.0m	1419	-1.2	2.4	---	---
S9.0t	1419	-1.6	3.1	---	---
East Bay					
S7.0[1]	3454.5	-0.3	0.8	0.97	0.98
S8.0	3692	-1.4	1.9	0.81	0.85
West Bay					
S4.0	4155	-1.5	3.0	-0.45	0.10
S5.0	2318	-3.7	3.7	0.78	0.56
S5.5	1090	0.6	0.8	---	---

[1] Based on hand-held meter readings taken during servicing.

Table 2 also contains the correlation coefficient, *r*, between the model and prototype data. Given the large number of points in the sample and the large values of *r*, the model and prototype data are seen to be highly correlated. The average of all stations for the short period of record is $r = 0.90$. Table 3 has the *r* values for the longer data sets. These values, calculated on the basis of four times as many data points as those in Table 2, also indicate a strong correlation. The average of all of these stations is $r = 0.77$. Though indicating a high correlation, *r* is nevertheless smaller for the seven longer data set meters. For the Hilton Railroad Bridge stations (sta 8.0, 7.9a, and 7.9b) and the Navassa stations (sta 7.0, 6.9a, and 6.9b), the surface meters at each location show the weakest correlation. Since the surface meters are most affected by subtidal and local disturbances that are modeled imperfectly or not at all, such effects may be the origin of some of the differences between model and prototype. Visual inspection of the Hilton Railroad Bridge and Navassa stations in Plates 29, 32, and 33 for the long-term

comparison demonstrates this phenomenon well. Even though the general long-term and short-term trends are similar, intermediate time scale behaviors differ.

Tables 2 and 3 also show the standard deviations of the two data sets for each station represented. Using the standard deviations and the number of data points in each of the short and long data sets, a 95 percent confidence interval can be calculated for each station for the short and the long data set periods. These confidence intervals suggest that a MD calculated for the same time period with another randomly selected data set would have a 95 percent chance of being in the interval.

Another statistic, denoted *d*, was proposed by Willmott (1982; Willmott et al. 1985) and used by Berger et al. (1995a) to indicate trends as well as shifts in data set comparisons. The quantity *d* is defined as follows:

$$d = 1 - \left[\frac{\sum_i (M_i - P_i)}{\sum_j \left(|M_j^D| - |P_j^D| \right)^2} \right] \quad , \quad 0 \le d \le 1 \tag{3}$$

where

M_i = model reading i

P_I = prototype reading i

M_j^D = model reading j minus average prototype value

P_j^D = prototype reading j minus average prototype value, and the sums are over the number of data points in the sample

The worst comparison is for the Hilton Railroad Bridge meters for the short time period. When the longer time period data set is examined, the *d* values rise to values comparable to those of other meters. The model compares well with this statistic, indicating an overall faithfulness to the trends and salinity behaviors of the prototype.

The main channel alteration in each proposal involves deepening. To assess the qualitative behavior of the model for historical conditions, calculations were made with a flat channel bottom and historical depths characteristic of those historical channel depth conditions. In these calculations the model predicted that in the upper reaches of the system salinity and tide range increase as depth increase, as has been the case in fact (see Chapter 1). Specific values of tide and salinity will be presented in the plan experimentation discussions.

Conclusions

The objective of this modeling effort is to help in the formulation of project alternatives and in the assessment of potential impacts to interior CFR/ Wilmington Harbor estuarine processes caused by project construction in the areas of water level and of salinity intrusion and distribution. The model verification described previously indicates that the model adequately describes the hydrodynamic and salinity behavior of the CFR estuary for use in base and plan comparisons of project alternatives. The hindcasting of historical relationships between channel depth change and tide range and salinity also supports the use of the model in plan comparisons.

Experiments

The testing program consisted of creating alternative numerical grids representing the Cape Fear system under differing assumptions of navigation channel configuration, performing experiments with these grids, and comparing the results of the experiments. The grids differed in respect to the controlling depths in the channel reaches, the topography of the bottom, and the degree of widening. The experiments involved calculations with these grids and boundary condition files that included the conditions of tide, wind, and freshwater inflow as used in the verification period and variations on these verification conditions that included constant inflows. Table 6 summarizes the cases for which calculations are reported.

Originally, two plans were to be tested, representing interior channel depths of 12.8 m (42 ft) and 13.4 m (44 ft), respectively (these depths include 0.6 m (2 ft) of overdepth). In Table 6, these original plans are the 42-ir and 44-ir grids ("ir" means "irregular bottom topography"). Calculations with these grids were to be compared with the 40-ir grid calculations, which represents the existing project conditions and overdepth. The 40-ir, 42-ir, and 44-ir grids were created from the existing grid by increasing the depth in each range so that no depth in a given range was less than the given control depth. As the shoals are progressively flattened out for deeper and deeper channel alternatives, then, the channel depths become more uniform. The irregular topography of the existing channel is thus retained, though less sharply.

The "flat" grids use the given depth throughout the respective reaches. The 34-fl (flat bottom topography) grid represents the 1949 channel project conditions; the 36-fl grid represents the 1958 channel project conditions. Both sets of conditions include 0.6 m (2 ft) of overdepth below the Hilton Railroad Bridge. The 38-fl grid represents the project conditions as reported on NOAA chart 11537, 24th edition, September, 1985, with no overdepth. The 40-fl is the flat version of the existing project conditions with overdepth. The 42-fl and 44-fl are the flat versions of 42-ir and 44-ir.

Table 6
Characteristics of Grids Used in Calculations

Grid Name	Bottom Topography	Controlling Depths (MLW) x Width					Widening
		Ocean Bar	Entrance	To Cape Fear Memorial Bridge	To Hilton Railroad Bridge	To Arcadian	
Existing[1]	irregular	36.5'[2] x 500'	40' x 500'	36' x 400'	32' x 300'	25' x 200'	no
40-ir	irregular	43' x 500'	42' x 500'	40' x 400'	40' x 300'	27' x 200'	no
42-ir	irregular	45' x 500'	44' x 500'	42' x 500'	42' x 400'	32' x 250'	yes
44-ir	irregular	47' x 500'	46' x 500'	44' x 500'	44' x 400'	40' x 250'	yes
34-fl	flat	34' x 400'	34' x 400'	34' x 400'	32' x 300'	25' x 200'	no
36-fl	flat	37' x 400'	36' x 400'	36' x 400'	32' x 300'	25' x 200'	no
38-fl	flat	40' x 500'	40' x 500'	38' x 400'	32' x 300'	25' x 200'	no
40-fl	flat	43' x 500'	42' x 500'	40' x 400'	40' x 300'	27' x 200'	no
42-fl	flat	45' x 500'	44' x 500'	42' x 500'	42' x 400'	32' x 250'	yes
44-fl	flat	47' x 500'	46' x 500'	44' x 500'	44' x 400'	40' x 250'	yes

[1] These depths for the existing conditions are the minimum depths near the channel center of the respective reach. The channel is generally deeper than these shoal values from the 1992 survey.
[2] All depth and width are in feet. To convert to meters multiply by 0.3048.

All grids representing plans, 42-ir, 44-ir, 42-fl, and 44-fl, have some widening. The widening is in the Lower Midnight and Lower Lilliput Channels, the 10-km (6.2-mile) passing lane to 183 m (600 ft), in the Hilton Railroad Bridge to Arcadian reaches to 76 m (250 ft), and in some of the turns. The widened turns include the Upper Brunswick-Lower Brunswick Channels turn, the Upper Big Island Channel turns, the Lower Big Island-Keg Island Channels turn, the turns in and on either side of the passing lane, and the Horseshoe Shoal-Snow's Marsh Channel turn. Finally, the Anchorage Basin at the North Carolina Port Authority is widened to 427 m (1,400 ft), and the turning basin at Arcadian is widened to 244 m (800 ft).

3 Analysis

Introduction

The comparison of results from the calculations made with the grids from Table 6 will consist of comparisons of salinity and water level changes. In particular, average salinity results and results for the averaged tidal quantities, such as tide range and tide level changes for periods of neap-spring and longer time periods will be presented.

Salinity Changes

Table 7 contains calculated salinities for the three controlling depths and the two bathymetry types, namely flat and irregular. Middepth stations at Ft. Caswell (1.2a), Orton Point (3.9a), Exxon Pier (5.9a), Hilton RR (7.9a), and Navassa (6.9a) are plotted in Figure 10. The salinity decreases with increasing controlling depth. Figures 11 and 12, respectively, show plots of these salinities up the Northeast Cape Fear River (to Hilton RR) and up the Cape Fear River (to Navassa) for the flat bathymetry case. The salinity values range in difference from about 0.8 ppt to 1.5 ppt. These results were calculated with the verification tides and inflows and represent averages over approximately 1300 hr. Calculations for depths in the 12.2 to 13.4 m (40 to 44 ft) depth range but with constant low or average flows yielded similar results. These results were not expected since, generally, increased depth often implies increased salinity intrusion, all other things being equal.

To check these results, a series of additional experiments were carried out. Historical channel configurations from 1949 [10.4-m (34-ft) deep] and 1958 [11-m (36-ft) deep] were put into the numerical grid and calculated with the verification tides and a low constant inflow of 27 cu m/sec (950 cfs). Table 8 contains the results of the constant low-flow salinity calculations. The salinity values are averaged over a 385-hr period. Figure 13 shows middepth salinities. The historical channel dimension calculations show a general increase in salinity with deepening from the 10.4-m- (34-ft-) to 12.2-m- (40-ft-) deep condition. The 13.4-m- (44-ft-) deep channel example, however, shows the lower salinity value. Figure 14 shows the salinity versus controlling depth for the four locations indicated. Though the salinity calculated in the model generally increases as depth increases from 10.4 to 12.2 m (34 to 40 ft), the increase is not monotonic, as can

Table 7
Averaged Calculated Middepth Salinities from 1300 Hour Time Series for Flat and Irregular Bathymetries Using Real Tides and Inflows

Station	40 Flat ppt	42 Flat ppt	44 Flat ppt	40 Irreg ppt	42 Irreg ppt	44 Irreg ppt
1.3	34.1	33.6	33.4	33.8	33.5	33.0
1.2a	34.2	33.7	33.5	33.9	33.7	33.2
1.2b	34.2	33.8	33.5	33.9	33.7	33.2
2	33.6	33.0	32.7	33.2	32.9	32.3
3	30.6	29.5	28.9	29.8	29.3	28.3
3.5	30.6	29.8	29.4	30.0	29.7	28.9
3.4	24.9	29.6	29.1	29.8	29.5	28.6
4	25.0	23.7	23.0	24.0	23.5	22.3
3.9a	24.9	23.7	23.1	23.9	23.5	22.4
3.9b	25.1	23.9	23.3	24.1	23.7	22.6
6A	15.1	14.2	13.6	14.2	14.0	13.0
5.9a	16.3	15.4	14.8	15.4	15.3	14.3
5.9b	17.0	16.0	15.4	16.1	15.9	14.8
NOAA	11.7	10.9	10.3	10.9	10.7	9.7
7	6.4	6.0	5.6	5.9	5.8	5.3
6.9a	6.5	6.0	5.7	5.9	5.9	5.3
6.9b	6.6	6.1	5.7	6.0	5.9	5.3
8	10.5	9.8	9.2	9.7	9.6	8.7
7.9a	10.9	10.2	9.7	10.1	10.0	9.2
7.9b	11.4	10.7	10.3	10.6	10.5	9.7

be seen in the flat portion of the curve between 10.4 and 11 m (34 and 36 ft). The model, therefore, reproduces the general trend of salinity increases with depths that have occurred historically, and the irregular way in which the salinity increases indicates that salinity increases may not be monotonic. Near surface and bottom salinities showed the same trends.

Additional experiments were carried out to explore the decreasing salinity result. The model results reported thus far were calculated with three vertical layers (7 nodes) in the channel. To see the qualitative dependence of the calculations on the vertical resolution, additional experiments were carried out using four and five layers (9 and 11 nodes) in the channel. The results were similar to those previously reported. Channels that were 12.2-m (40-ft) and 13.4-m (44-ft) deep were used in the calculations, and the results differed mainly in the timing of the salinity values, with the salinities taking longer to reach quasi-equilibrium in the higher resolution cases. Calculations were also made without Snow's Cut, and the qualitative results were similar.

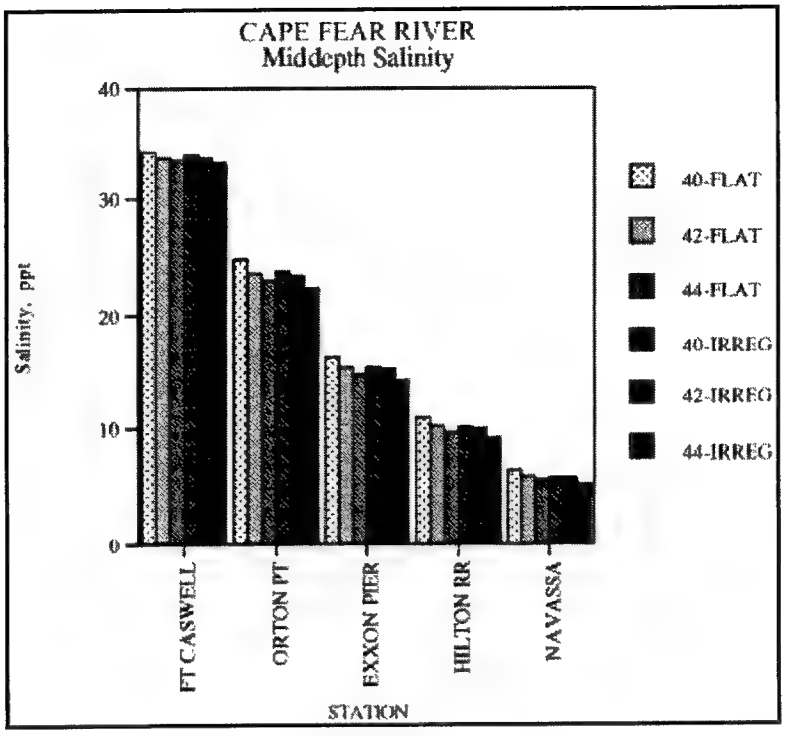

Figure 10. Plan salinity comparisons for three depths and two bottom topographies at selected locations

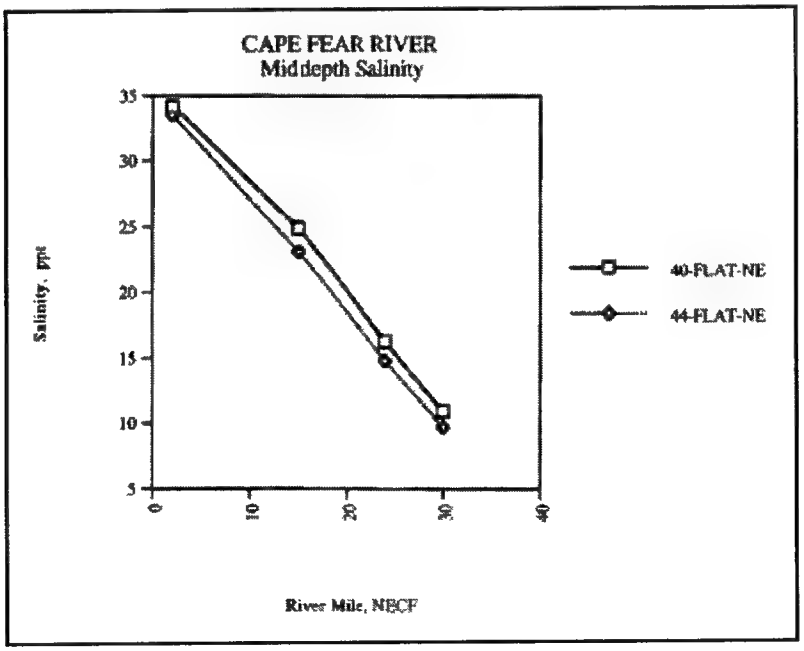

Figure 11. Plan salinity comparisons from Ft. Caswell upriver to the Hilton Railroad Bridge on the NECFR

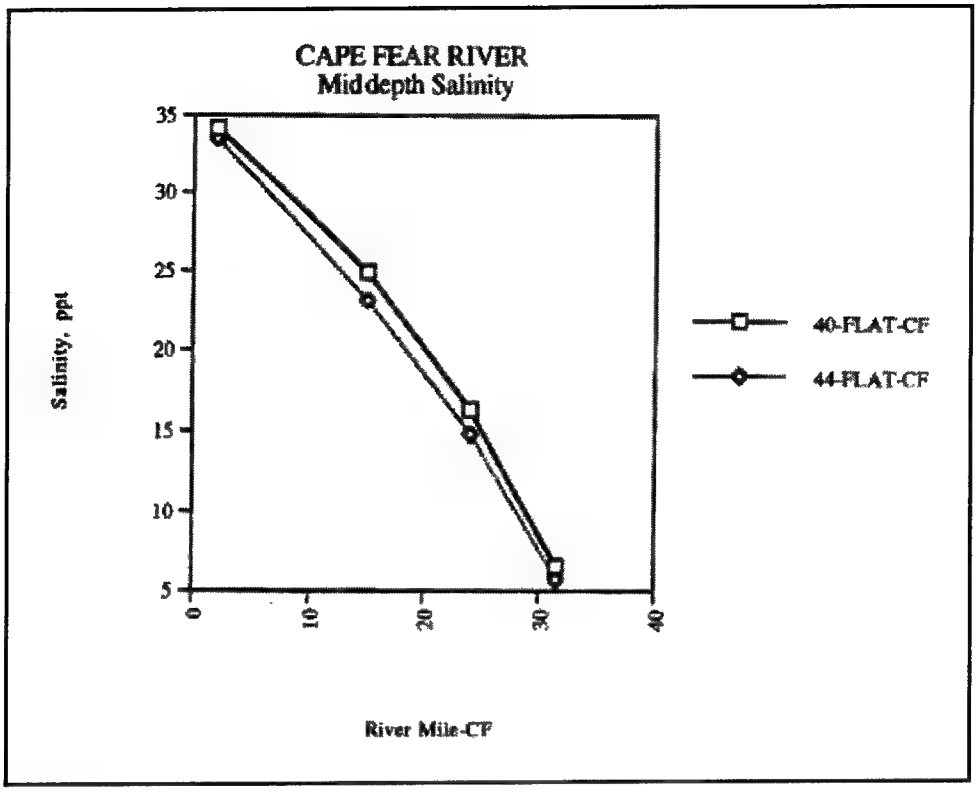

Figure 12. Plan salinity comparisons from Ft. Caswell upriver to Navassa on the CFR

The only instance in which the deeper 13.4-m (44-ft) channel calculations resulted in higher salinities than the 11.6-m- (38-ft-) deep case was when the realistic tides were replaced with a repeating, sinusoidal, semidiurnal tide. This case indicates that complex phasings of the tidal signal, particularly in the lower portion of the estuary in the entrance channels, may play a role in the salinity results. The channel reaches near the entrance make large, near 90 deg, turns in an area of sharp bathymetric changes that become sharper with deepening and large, complex marsh areas. These repeating tide results indicate that the model is capable of transporting salt up the estuary in a contrived case.

The overall result, then, is that the model predicts that the salinity of the system may decrease if deepened to about 13.4 m (44 ft). This decrease is likely the new result of two competing salinity transport mechanisms at work in the estuary. Deepening an estuary increases the tendency toward salinity stratification and results in increased salinity intrusion through density current flows. On the other hand, deepening may also increase the tide range, providing more mixing and, thus, a decrease in stratification and the associated density current related salinity intrusion. In the case of the Cape Fear River, increased channel depth increases the tide range, peaking in the Wilmington vicinity, but stratification below Wilmington remains the same. This indicates that the mixing mechanism is compensating for the stratification mechanism. Thus the stratification per unit depth is less in the deepening case, implying that less salt water is transported into

Table 8
Averaged Calculated Middepth Salinities from 385 Hour Time Series for Historical, Existing, and Proposed Deepening Conditions

Station	34 Flat, ppt	36 Flat, ppt	38 Flat, ppt	40 Flat, ppt	44 Flat, ppt
1.3	34.2	34.2	34.2	34.2	33.6
1.2a	34.3	34.2	34.3	34.2	33.7
1.2b	34.3	34.2	34.2	34.3	33.7
2	33.8	33.8	33.8	33.8	33.1
3	31.2	31.1	31.3	31.2	29.8
3.5	31.1	31.0	31.2	31.1	30.0
3.4	30.9	30.8	31.0	31.0	29.8
4	26.3	26.1	26.5	26.5	24.5
3.9a	26.0	25.9	26.3	26.4	24.6
3.9b	26.2	26.1	26.5	26.5	24.8
6A	16.5	16.5	17.3	17.7	15.9
5.9a	17.2	17.4	18.3	18.7	17.0
5.9b	18.2	18.2	19.0	19.3	17.5
NOAA	13.3	13.3	14.0	14.5	12.7
7	7.4	7.6	8.3	9.0	7.9
6.9a	7.5	7.7	8.4	9.0	7.9
6.9b	7.6	7.8	8.5	9.2	8.0
8	11.7	11.8	12.6	13.1	11.4
7.9a	11.8	11.9	12.7	13.5	12.0
7.9b	12.1	12.2	13.1	14.0	12.6

the estuary and resulting in lower salinities for the 13.4-m (44-ft) case. Such salinity decrease, attributable to enhanced connections between an estuary and the ocean caused by breaches in a dike, have been seen in other calculations of Galveston Bay (Berger 2000).

Tide Changes

Increased channel depth generally leads to increased tidal range. To determine the extent of any increase in high tide level in the Cape Fear River because of channel deepening, changes in high tide level between a 12.2-m- (40-ft-) deep channel and a 13.4-m- (44-ft-) deep channel with flat bottom topography were extracted for a 600 hr calculation. These changes in high tide level up the Cape Fear and the Northeast Cape Fear Rivers are shown in Figures 15, 16, and 17. Six hundred-hr average tide height differences, the average plus and minus one standard deviation, and the maximum and minimum high tide difference versus river mile are plotted. Tables 9, 10 and 11 contain the plotted values.

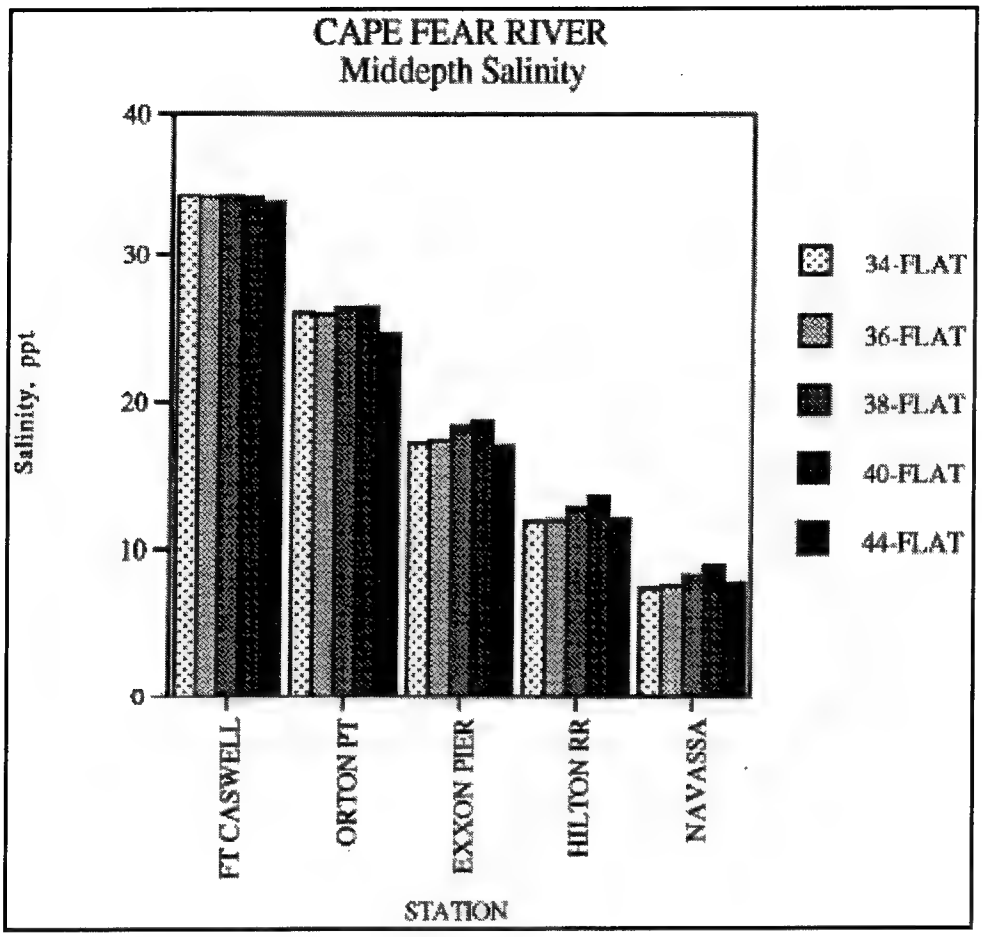

Figure 13. Salinity comparisons for historical and planned channel depths at selected locations

The tide differences are small at the entrance, but they steadily increase to an average of about 50 mm (2 in.) at Wilmington and then become smaller again above Wilmington. The maximum differences of about 90 mm (3.5 in.) are in the Wilmington vicinity. Nevertheless, only 4 to 6 percent of the high tide events (two or three) during the 600-hr, 48 tide, period are higher for the 13.4-m (44-ft) case that the highest tide level in the 11.6-m- (38-ft-) deep channel case. That is, for only 2.5 to 3.5 hr of the time (0.4 to 0.6 percent of the 600 hr) is the plan tide higher than the highest base condition tide. Since the highest tides occur less frequently than every 600 hr, these numbers are conservative.

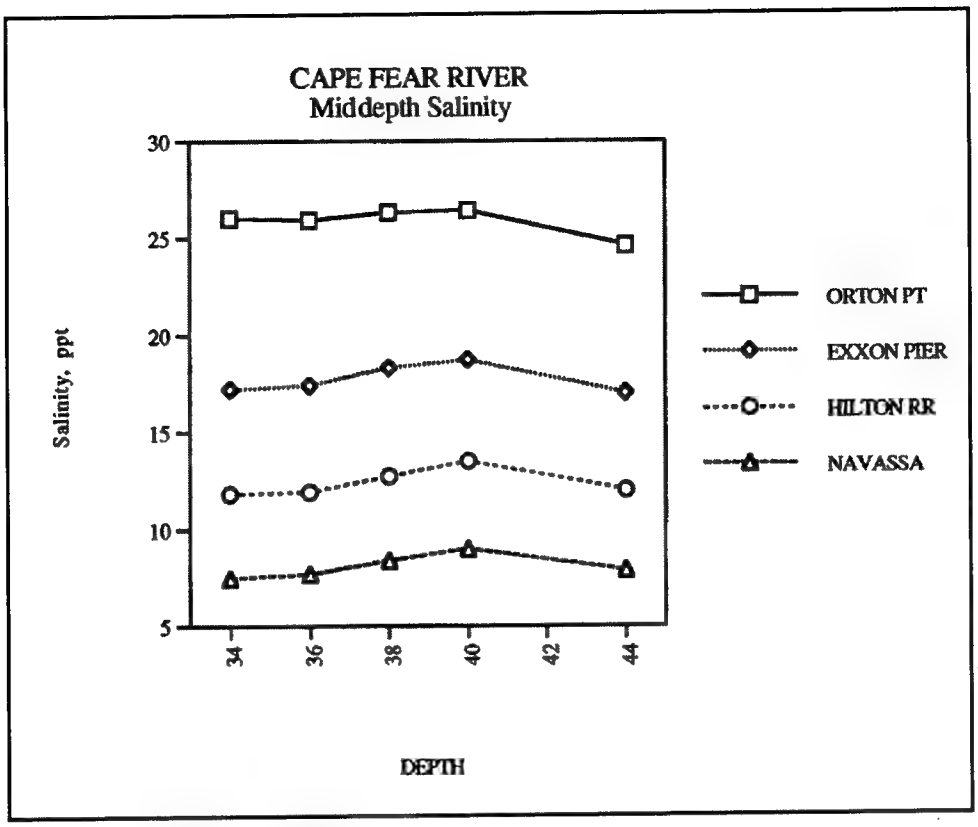

Figure 14. Salinity comparisons for historical and planned channel depths at selected locations

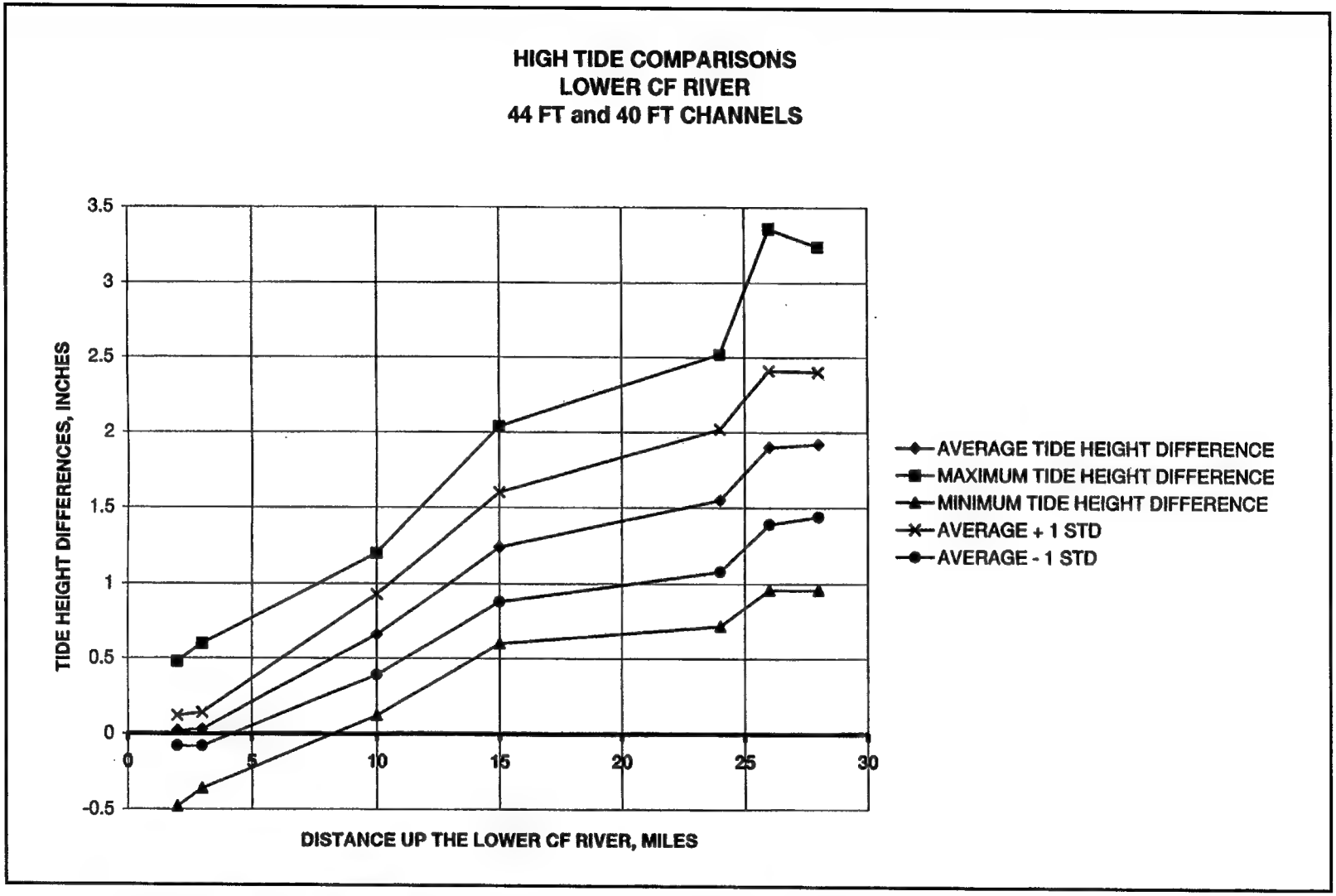

Figure 15. High tide differences between base and plan depth conditions from CFR entrance to Wilmington (To convert inches to meters, multiply by 0.0254. To convert feet to meters, multiply by 0.3048. To convert miles to kilometers, multiply by 1.852.)

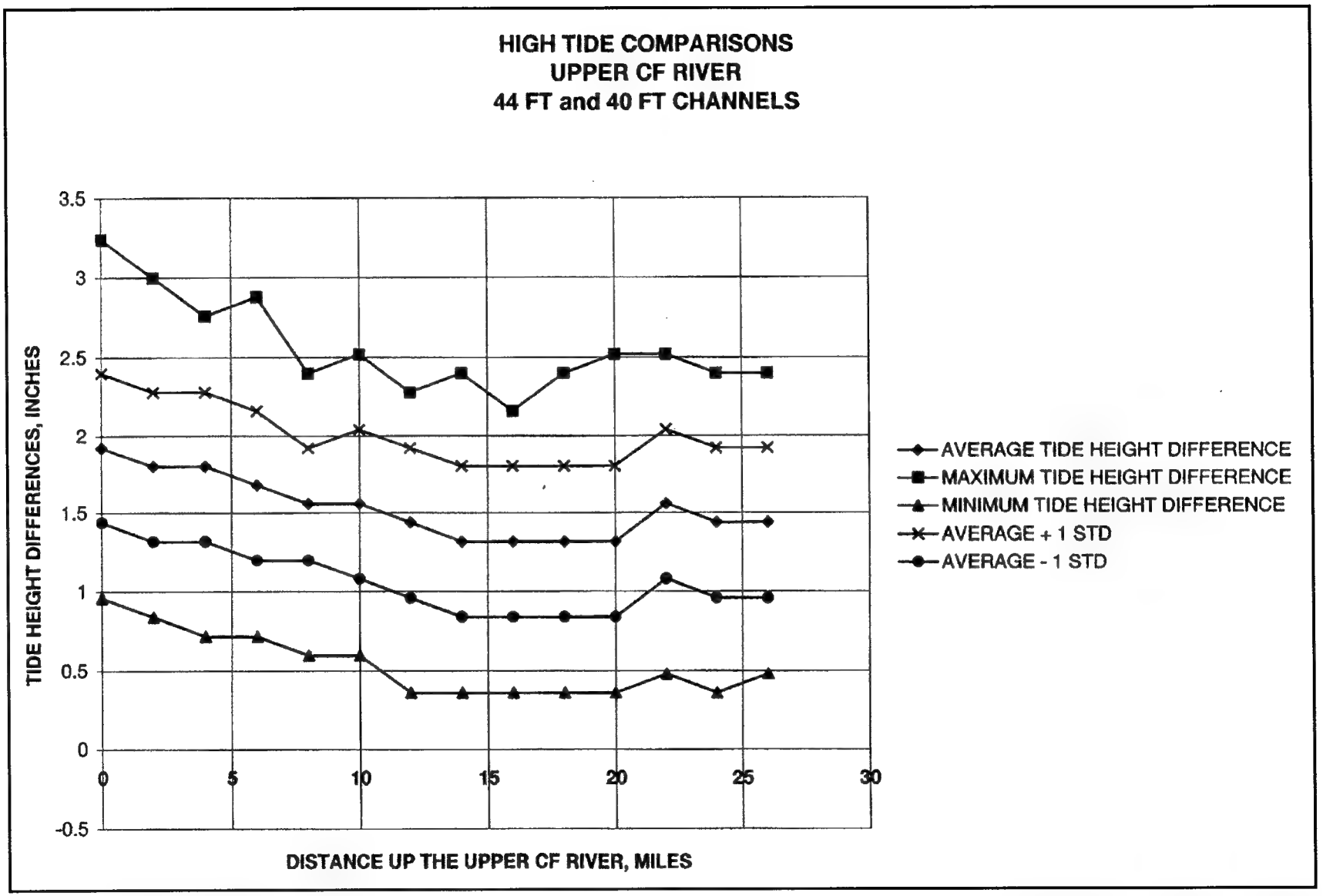

Figure 16. High tide differences between base and plan depth conditions from Wilmington up the CFR (To convert inches to meters, multiply by 0.0254. To convert feet to meters, multiply by 0.3048. To convert miles to kilometers, multiply by 1.852.)

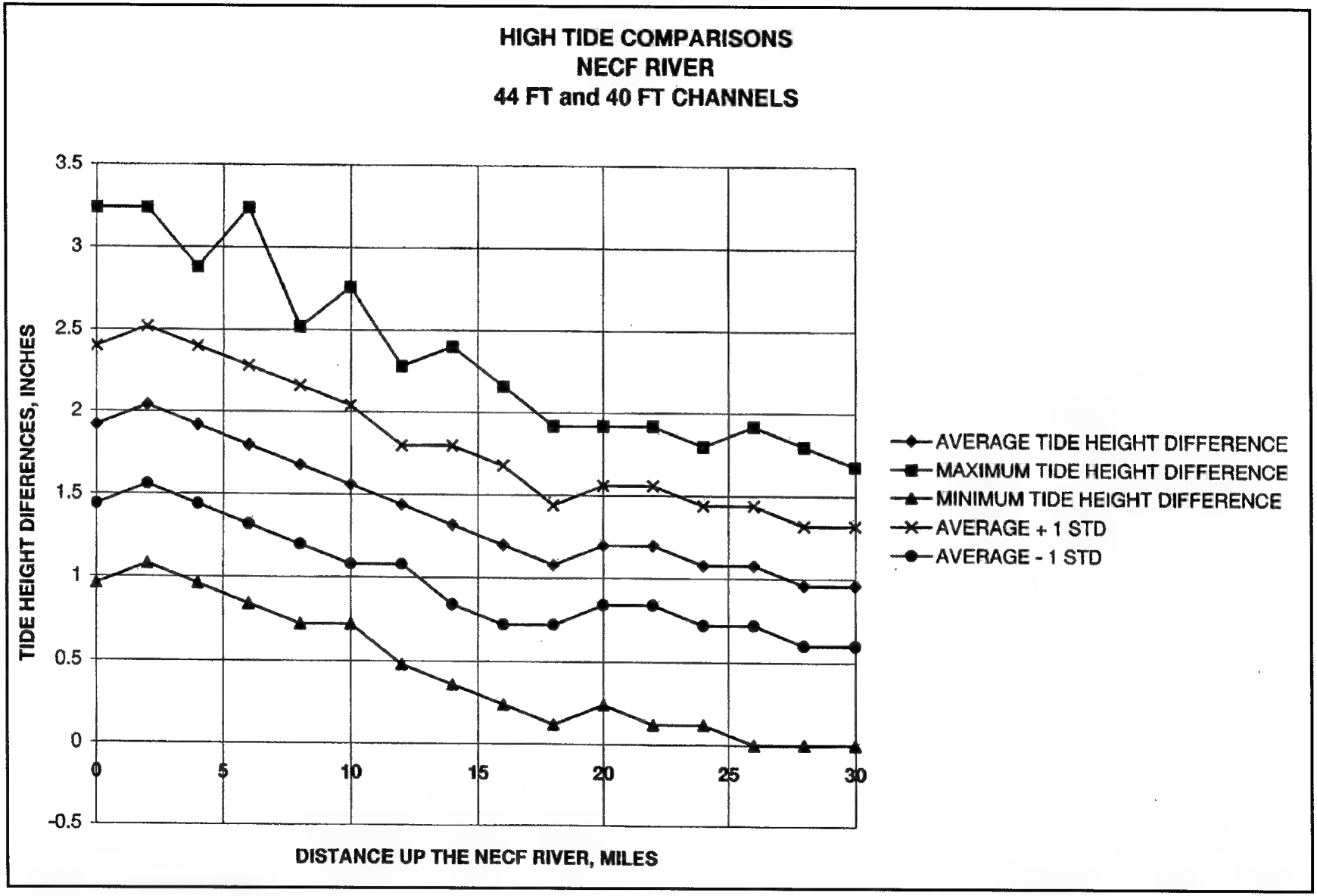

Figure 17. High tide differences between base and plan depth conditions from Wilmington up the NECFR (To convert inches to meters, multiply by 0.0254. To convert feet to meters, multiply by 0.3048. To convert miles to kilometers, multiply by 1.852.)

Table 9
Lower Cape Fear River High Tide Information as Used to Create Figure 15

River Mile	Average Inches[1]	Maximum Inches	Minimum Inches	Standard Deviation Inches	Average + Standard Deviation Inches	Average – Standard Deviation Inches
2	0.02	0.48	-0.48	0.10	0.12	-0.08
3	0.03	0.60	-0.36	0.11	0.14	-0.08
10	0.66	1.20	0.12	0.27	0.93	0.39
15	1.24	2.04	0.60	0.36	1.60	0.88
24	1.55	2.52	0.72	0.47	2.02	1.08
26	1.90	3.36	0.96	0.51	2.41	1.39
28	1.92	3.24	0.96	0.48	2.40	1.44

[1] High tide information is in inches. To convert inches to meters, multiply by 0.0254.

Table 10
Cape Fear River High Tide Information as Used to Create Figure 16

River Mile	Average Inches[1]	Maximum Inches	Minimum Inches	Standard Deviation Inches	Average + Standard Deviation Inches	Average – Standard Deviation Inches
0	1.92	3.24	0.96	0.48	2.40	1.44
2	1.80	3.00	0.84	0.48	2.28	1.32
4	1.80	2.76	0.72	0.48	2.28	1.32
6	1.68	2.88	0.72	0.48	2.16	1.20
8	1.56	2.40	0.60	0.36	1.92	1.20
10	1.56	2.52	0.60	0.48	2.04	1.08
12	1.44	2.28	0.36	0.48	1.92	0.96
14	1.32	2.40	0.36	0.48	1.80	0.84
16	1.32	2.16	0.36	0.48	1.80	0.84
18	1.32	2.40	0.36	0.48	1.80	0.84
20	1.32	2.52	0.36	0.48	1.80	0.84
22	1.56	2.52	0.48	0.48	2.04	1.08
24	1.44	2.40	0.36	0.48	1.92	0.96
26	1.44	2.40	0.48	0.48	1.92	0.96

[1] High tide information is in inches. To convert inches to meters, multiply by 0.0254.

Table 11
Northeast Cape Fear River High Tide Information as Used to Create Figure 17

River Mile	Average Inches[1]	Maximum Inches	Minimum Inches	Standard Deviation Inches	Average + Standard Deviation Inches	Average – Standard Deviation Inches
0	1.92	3.24	0.96	0.48	2.40	1.44
2	2.04	3.24	1.08	0.48	2.52	1.56
4	1.92	2.88	0.96	0.48	2.40	1.44
6	1.80	3.24	0.84	0.48	2.28	1.32
8	1.68	2.52	0.72	0.48	2.16	1.20
10	1.56	2.76	0.72	0.48	2.04	1.08
12	1.44	2.28	0.48	0.36	1.80	1.08
14	1.32	2.40	0.36	0.48	1.80	0.84
16	1.20	2.16	0.24	0.48	1.68	0.72
18	1.08	1.92	0.12	0.36	1.44	0.72
20	1.20	1.92	0.24	0.36	1.56	0.84
22	1.20	1.92	0.12	0.36	1.56	0.84
24	1.08	1.80	0.12	0.36	1.44	0.72
26	1.08	1.92	0.00	0.36	1.44	0.72
28	0.96	1.80	0.00	0.36	1.32	0.60
30	0.96	1.68	0.00	0.36	1.32	0.60

[1] High tide information is in inches. To convert inches to meters, multiply by 0.0254.

4 Summary and Conclusions

In this report the results of the development, verification, and use of a 3-D numerical model of the Cape Fear-Northeast Cape Fear River estuary system were presented. The model was developed using bathymetry and conditions of tide, wind, and freshwater inflow existing in the system in 1993. Verification of the model was completed with respect to tide, velocity, and salinity field data taken during 1993. Experiments performed using the model determined the impacts of channel deepening on salinity and tide height.

Verification consisted of qualitative and quantitative comparisons of calculations made for existing conditions with field data taken during the period for which calculations were made. Both the qualitative and quantitative comparisons showed the model adequately represents the estuary dynamics. Tides and velocities compared best, as is common in models of complex estuarine systems, but the salinity values compared well also, responding to both short-term and long-term tidal variations and the river hydrograph.

Experiments were conducted on various deepening scenarios, and included differing bottom topographies, inflows, and historical conditions. The results of the salinity calculations were that the system salinities increase with channel depth as the controlling depth increases from 10.4 m (34 ft) to 12.2 m (40 ft), but the salinities are predicted to fall as deepening increases to 13.4 m (44 ft). Additional experiments were performed to test this decrease in salinity result, and all tests with real tides showed the same effect. The results indicate that a complex process of tidal propagation changes and resultant changes in mixing lead to these counterintuitive results. These experiments are interpreted to indicate that there will be no increase in the salinity regime of the system with deepening to 13.4 m (44 ft).

The results of the tide height calculations indicate that the average maximum high tide in the Wilmington area will be increased by about 50 mm (2 in.). These calculations compared the high tide levels for 12.2-m- (40-ft-) deep and 13.4-m- (44-ft-) deep channels. Smaller average increases are predicted above and below Wilmington. The maximum increase in high tide level for a particular tide was about 90 mm (3.5 in.). Though the maximum high tide was on average higher for the 13.4-m- (44-ft-) deep channel, the higher tides calculated for this deeper channel rarely exceeded the highest tides occurring for the 12.2-m- (40-ft-) deep channel.

References

Benson, H. A., and Parman, J. W. (1995). "Field data collection report, Cape Fear River, Wilmington, North Carolina," Technical Report HL-95-4, U.S. Army Engineer Waterways Experiment Station, Vicksburg, MS.

Berger, R. C., McAdory, R. T., Hardy, C. J., and Campbell, L. (2000). "Texas City salinities," (in preparation) U.S. Army Engineer Research and Development Center, Vicksburg, MS.

Berger, R. C., McAdory, R. T., Martin, W. D,, and Schmidt, J. H. (1995a). "Houston-Galveston navigation channels, Texas project: Report 3, Three-dimensional hydrodynamic model verification," Technical Report HL-92-7, U.S. Army Engineer Waterways Experiment Station, Vicksburg, MS.

Berger, R. C., McAdory, R. T., Schmidt, J. H., and Martin, W. D. (1995b). "Houston-Galveston navigation channels, Texas project: Report 4, Three-dimensional numerical modeling of hydrodynamics and salinity," Technical Report HL-92-7, U.S. Army Engineer Waterways Experiment Station, Vicksburg, MS.

Fagerburg, T. L., Fisackerly, G. M., Parman, J. W., and Coleman, C. J. (1994). "Houston-Galveston navigation channels, Texas project: Report 1, Galveston Bay field investigation," Technical Report HL-92-7, U.S. Army Engineer Waterways Experiment Station, Vicksburg, MS.

Giese, G. L., Wilder, H. B., and Parker, Jr, G. G. (1985). "Hydrology of major estuaries and sounds of North Carolina," Paper 2221, U.S. Geological Survey, Alexandria, VA.

Henderson-Sellers, B. (1984). "A simple formula for vertical eddy diffusion coefficients under conditions of nonneutral stability," *Journal of Geophysical Research* 87(C8), 5860-5864.

Johnson, B. J., Kim, K. W., Heath, R. E., Hsieh, B. B., and Butler, H. L. (1993). "Validation of three-dimensional model of Cheasapeake Bay," *Journal of Hydraulic Engineering,* 119(1), 2-20.

King, I. P. (1982). "A finite element model for three-dimensional flow," Resource Management Associates, Lafayette, CA, for U.S. Army Engineer Waterways Experiment Station, Vicksburg, MS.

King, I. P. (1985). "Strategies for finite element modeling of three-dimensional hydrodynamic systems," *Advances in Water Resources, 8*, 69-76.

_____. (1993). "RMA-10, a finite element model for three-dimensional density stratified flow," Department of Civil and Environmental Engineering, University of California, Davis.

Krone, R. B. (1962). "Flume studies of the transport of sediment in estuarial shoaling processed, final report," Hydraulic Engineering Laboratory and Sanitary Engineering Research Laboratory, University of California, Berkeley.

Mellor, G. L., and Yamada, T. (1982). "Development of a turbulence closure model for geophysical fluid problems," *Reviews of Geophysics and Space Physics* 20(4), 851-875.

National Ocean Service. (1991). "Tide tables 1992," National Oceanic and Atmospheric Administration, Riverdale, MD.

_____. (1993). TIDES.

Parthenaides, E. (1962). "A study of erosion and deposition of cohesive soils in salt water," Ph.D. thesis, University of California, Berkeley.

Pritchard, D. W. (1982). "A summary concerning the newly adopted practical salinity scale, 1978, and the international equation of state of seawater, 1980," Marine Sciences Research Center, State University of New York, Stony Brook, New York.

Stelling, G. S., and van Kester, J. A. T. M. (1993). "Horizontal gradients in sigma transformed bathymetries with steep bottom slopes," *Hydraulic Engineering '93*, Proceedings of the 1993 Conference, ASCE, 2123-2134.

U.S. Army Engineer District, Wilmington. (1960). "Study of shoaling, Cape Fear River and Sunny Point Army Terminal," Wilmington, NC.

_____. (1992). "Reconnaissance report on improvement of navigation, Cape Fear - Northeast Cape Fear Rivers comprehensive study, Wilmington, North Carolina, Volume III - Feasibility study cost-sharing agreement," Wilmington, NC.

_____. (1993). "1993 survey," Wilmington, NC.

U.S. Geological Survey. (1998). "United States NWIS-W data retrieval." *http://h2o-nwis.er.usgs.gov/nwis-w/US/*

Welch, J. M., and Parker, B. B. (1979). "Circulation and hydrodynamics of the lower Cape Fear River, North Carolina," NOAA Technical Report NOS 80, Office of Oceanography, Rockville, MD.

Willmott, C. J., Ackleson, S. G., Davis, R. E., Feddema, J. J., Klinck, K. M., Legates, D. R., O'Donnell, J., and Rowe, C. M. (1985). "Statistics for the evaluation and comparison of model," *Journal of Geophysical Research* 90(C5), 8995-9005.

Willmott, C. J. (1982). "Some comments on the evaluation of model performance," Bulletin, American Meteorological Society 63(11), 1309-1313.

Wu, J. (1980). "Wind-stress coefficients over sea surface near neutral conditions-a revisit," *Journal of Physical Oceanography* 10(5), 727-740.

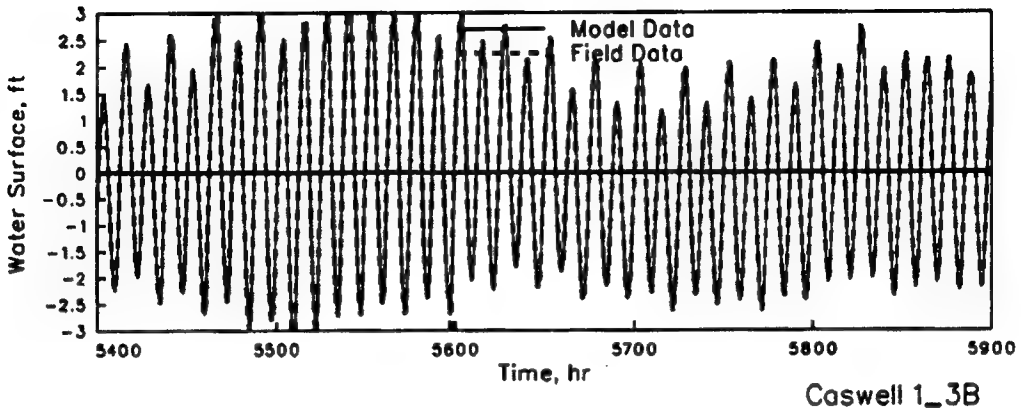

Caswell 1_3B

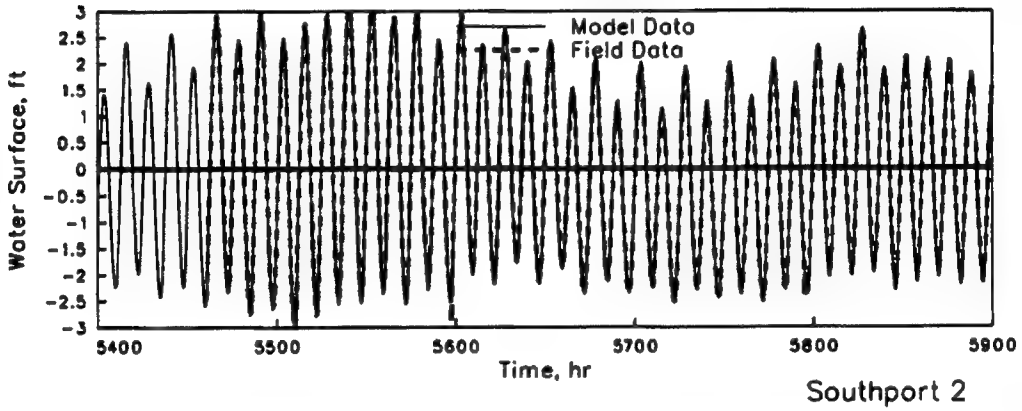

Southport 2

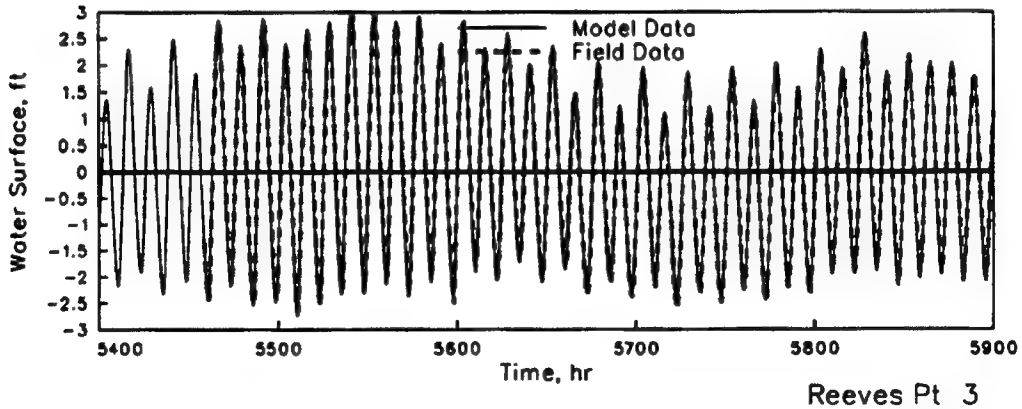

Reeves Pt 3

WATER SURFACE ELEVATIONS
MODEL VERIFICATION
STATIONS 1_3B, 2, AND 3
JULIAN HOURS 5400-5900
(To convert water surface to meters multiply by 0.3048)

Plate 1

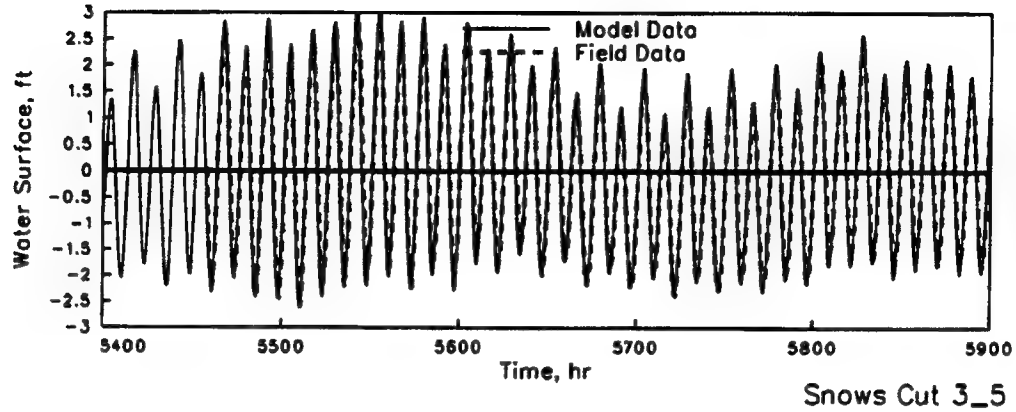

Snows Cut 3_5

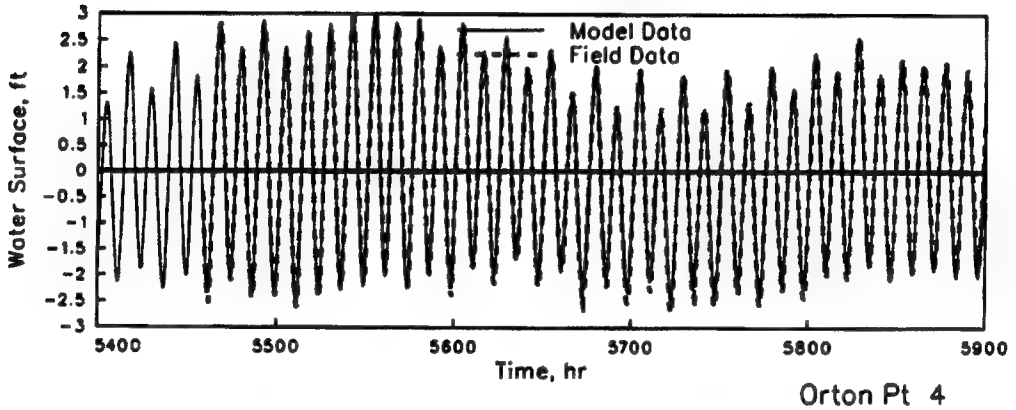

Orton Pt 4

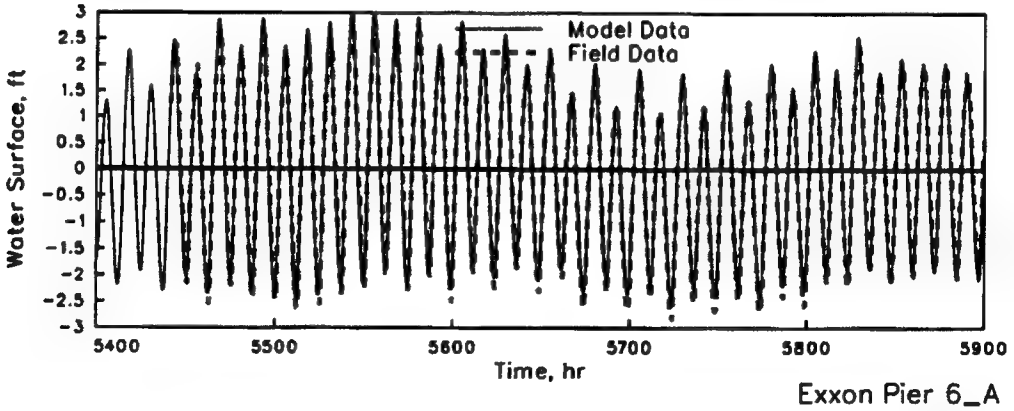

Exxon Pier 6_A

WATER SURFACE ELEVATIONS
MODEL VERIFICATION
STATIONS 3_5, 4, AND 6_A
JULIAN HOURS 5400-5900

Plate 2

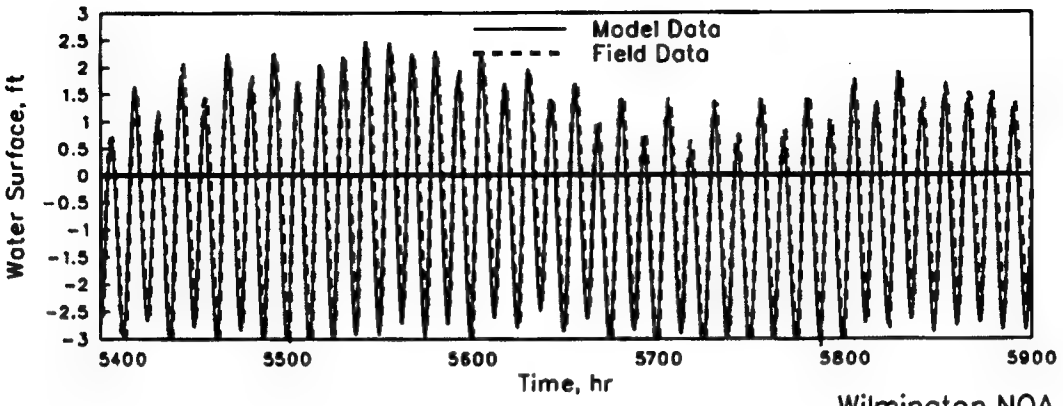

Wilmington NOA

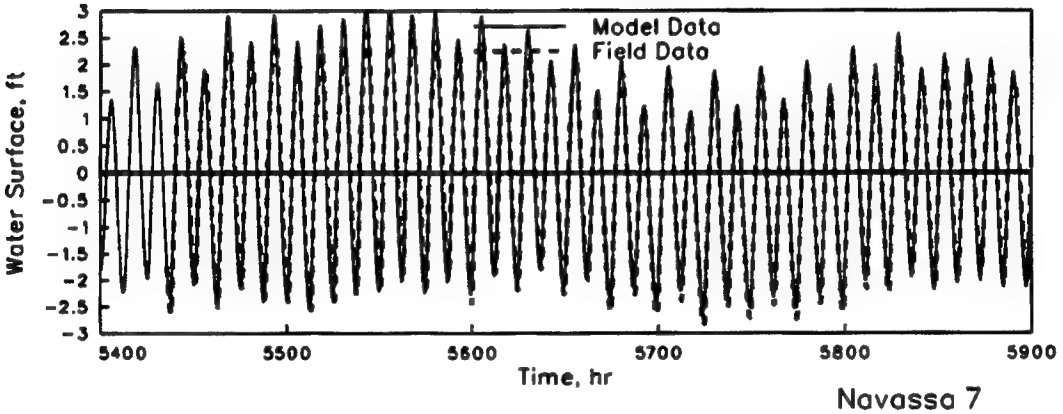

Navassa 7

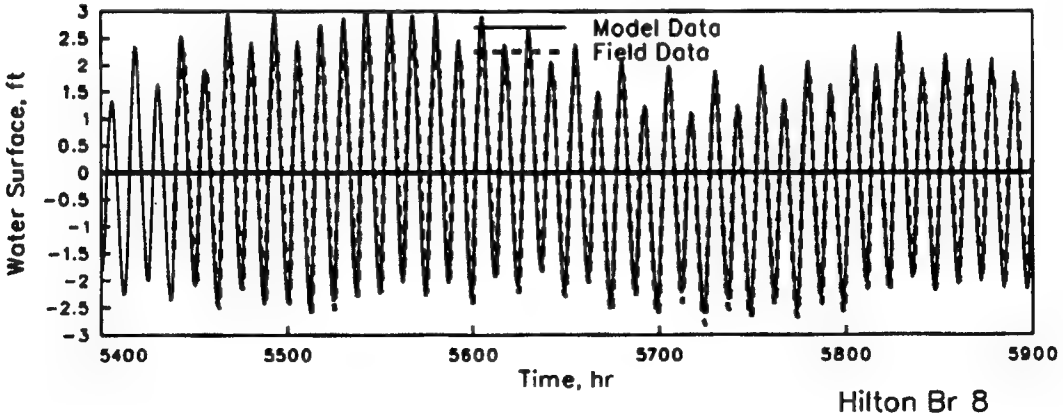

Hilton Br 8

WATER SURFACE ELEVATIONS
MODEL VERIFICATION
STATIONS NOAA, 7, AND 8
JULIAN HOURS 5400-5900

Plate 3

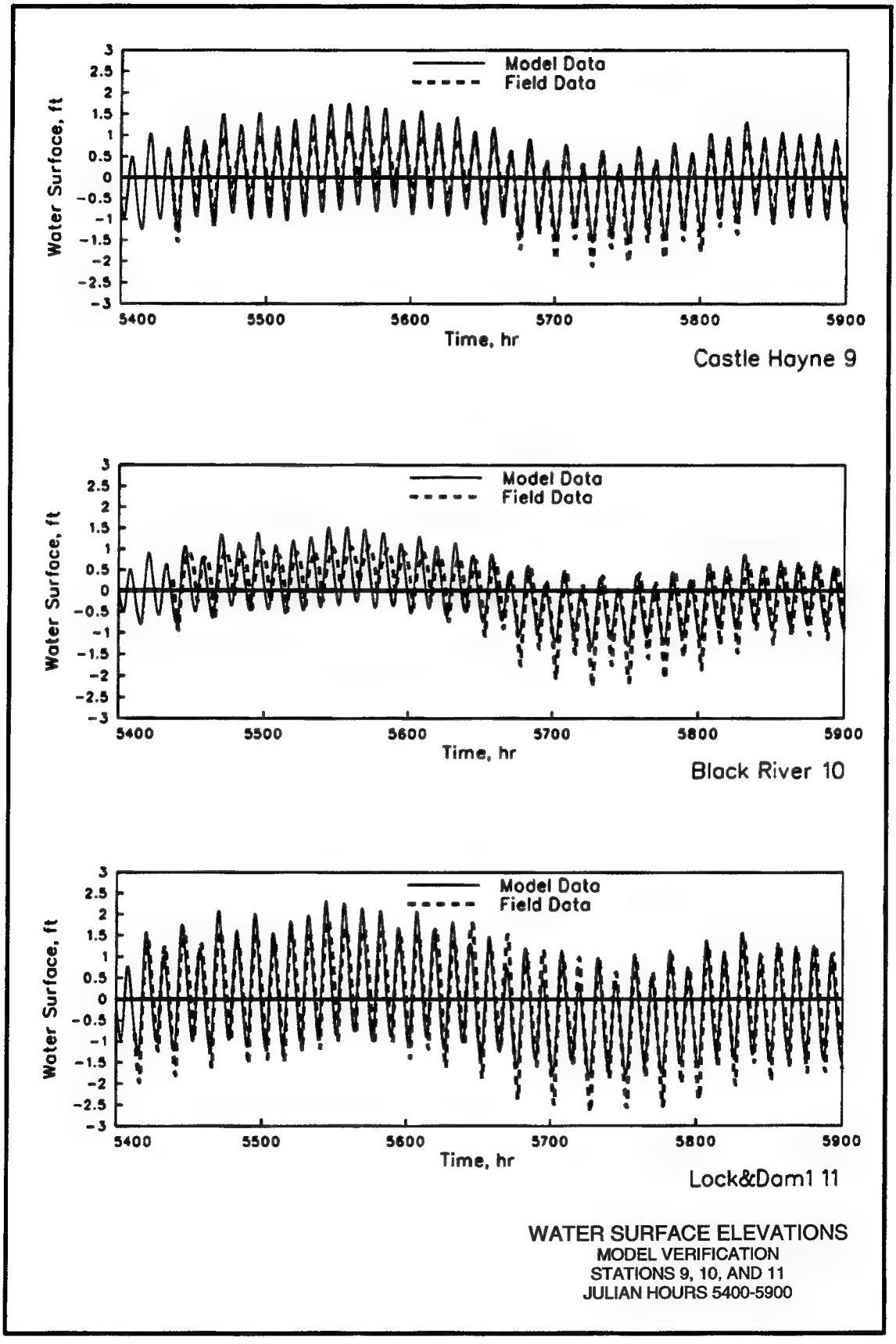

WATER SURFACE ELEVATIONS
MODEL VERIFICATION
STATIONS 9, 10, AND 11
JULIAN HOURS 5400-5900

Plate 4

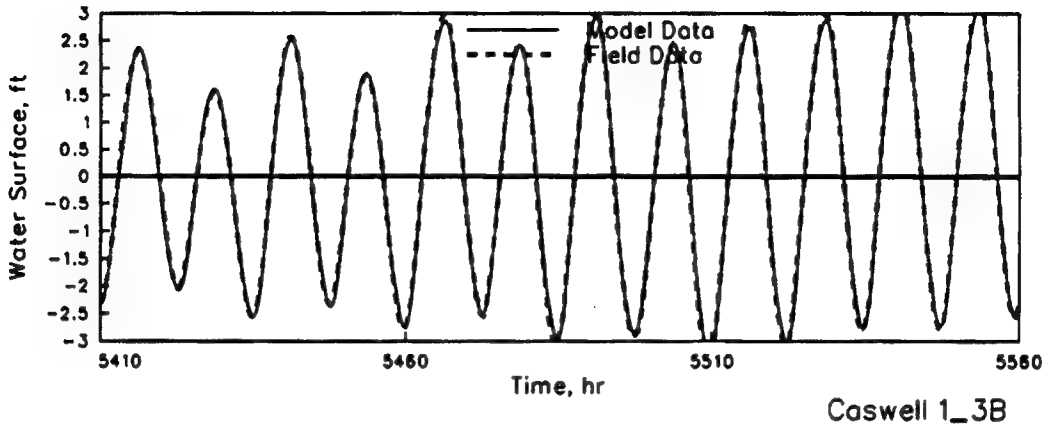

Caswell 1_3B

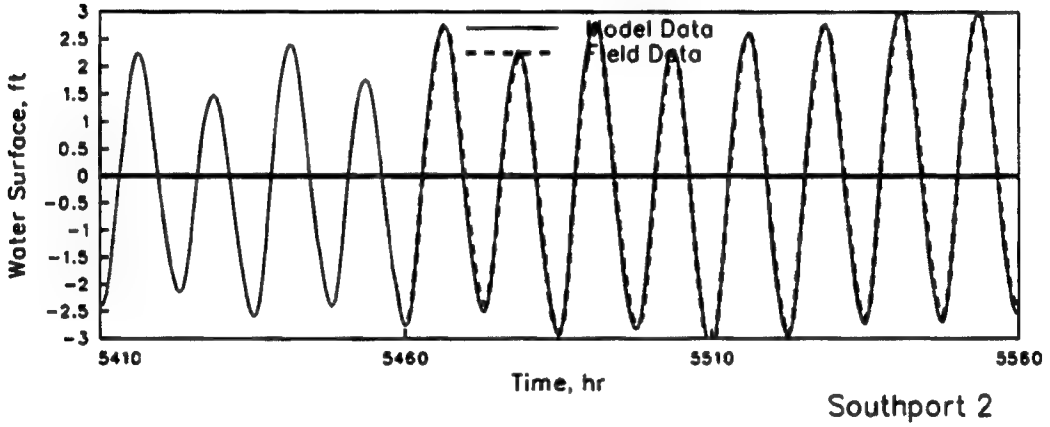

Southport 2

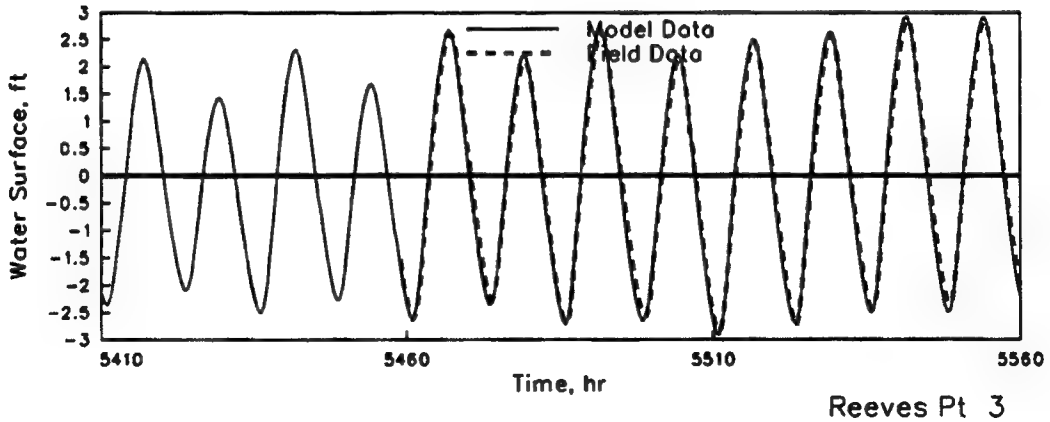

Reeves Pt 3

WATER SURFACE ELEVATIONS
MODEL VERIFICATION
STATIONS 1_3B, 2, AND 3
JULIAN HOURS 5410-5560

Plate 5

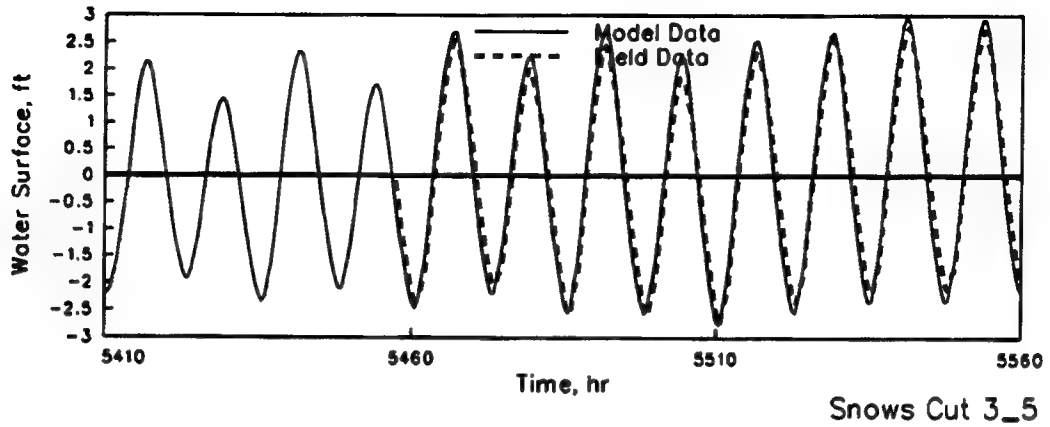

Snows Cut 3_5

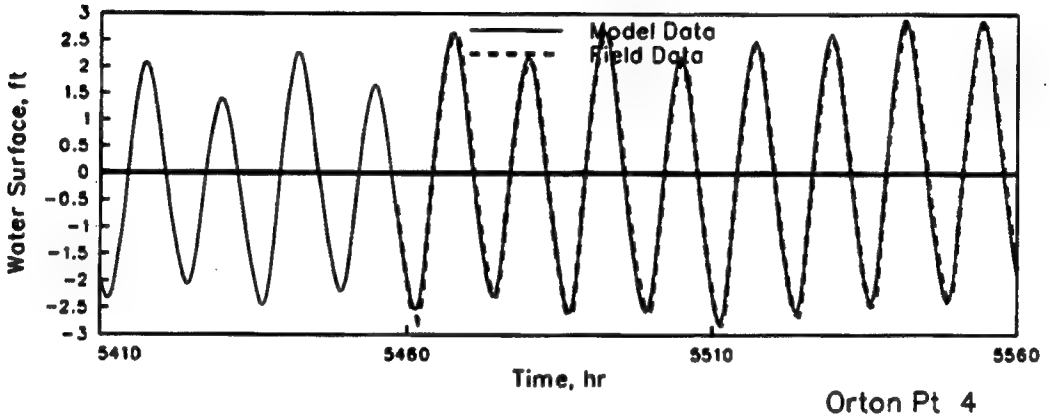

Orton Pt 4

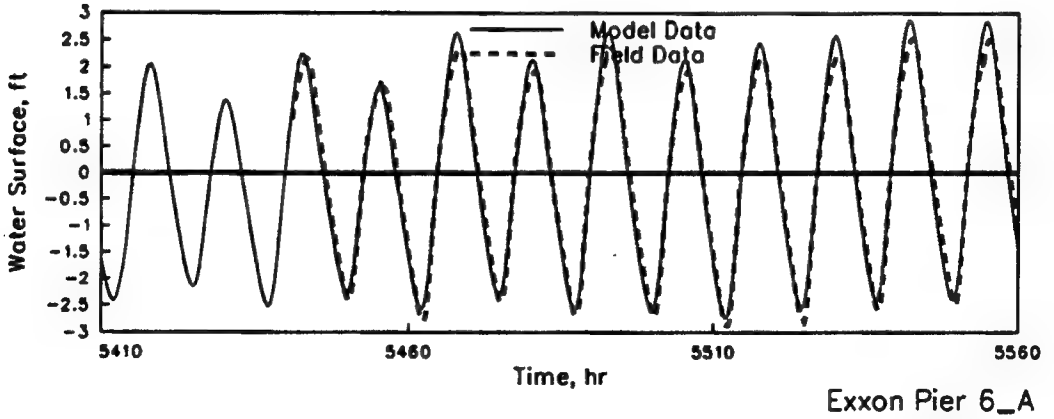

Exxon Pier 6_A

WATER SURFACE ELEVATIONS
MODEL VERIFICATION
STATIONS 3_5, 4, AND 6_A
JULIAN HOURS 5410-5560

Plate 6

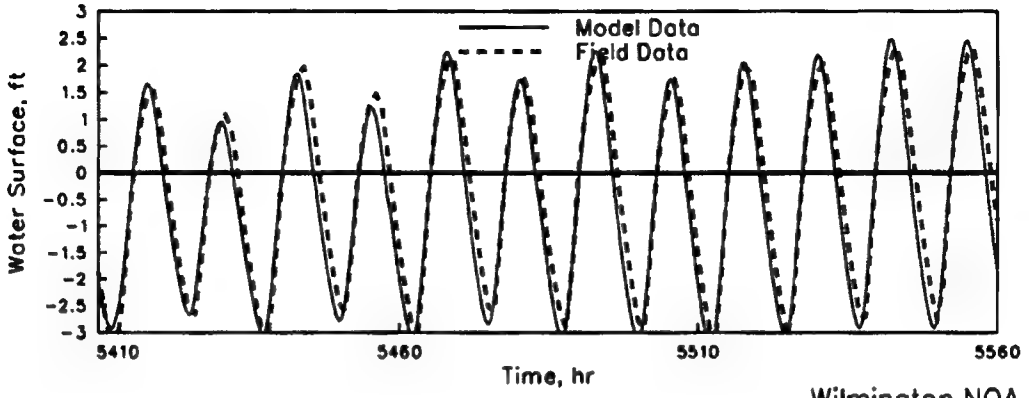

Wilmington NOA

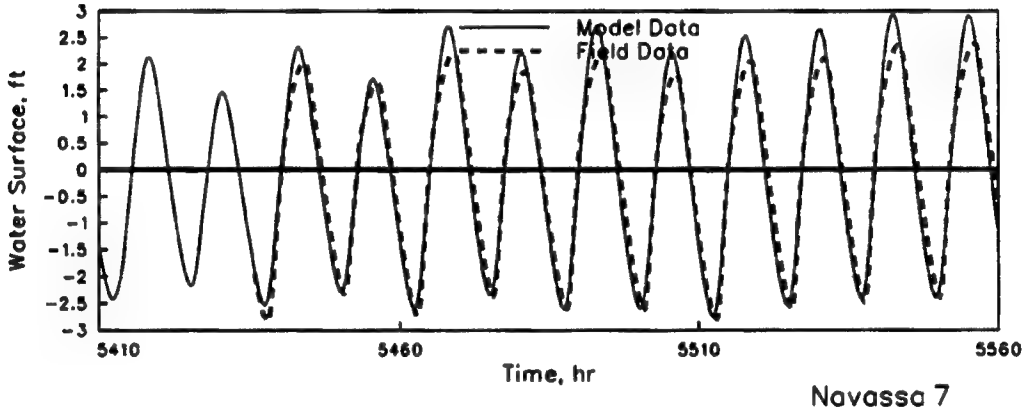

Navassa 7

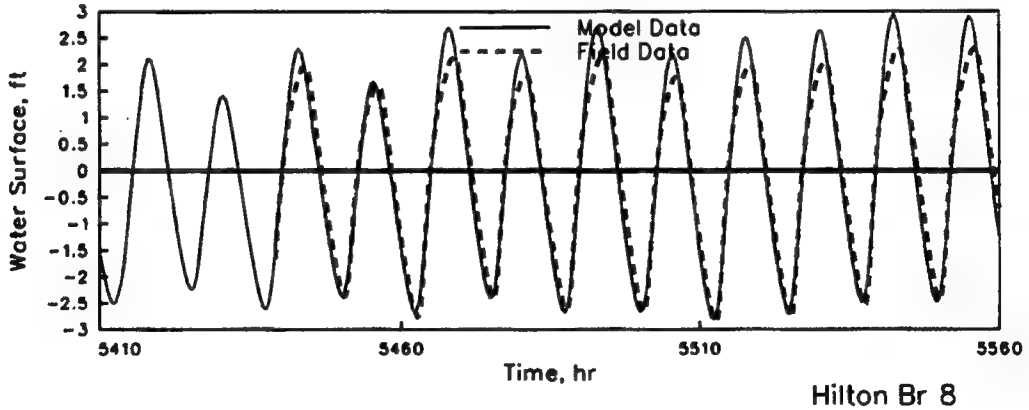

Hilton Br 8

WATER SURFACE ELEVATIONS
MODEL VERIFICATION
STATIONS NOAA, 7, AND 8
JULIAN HOURS 5410-5560

Plate 7

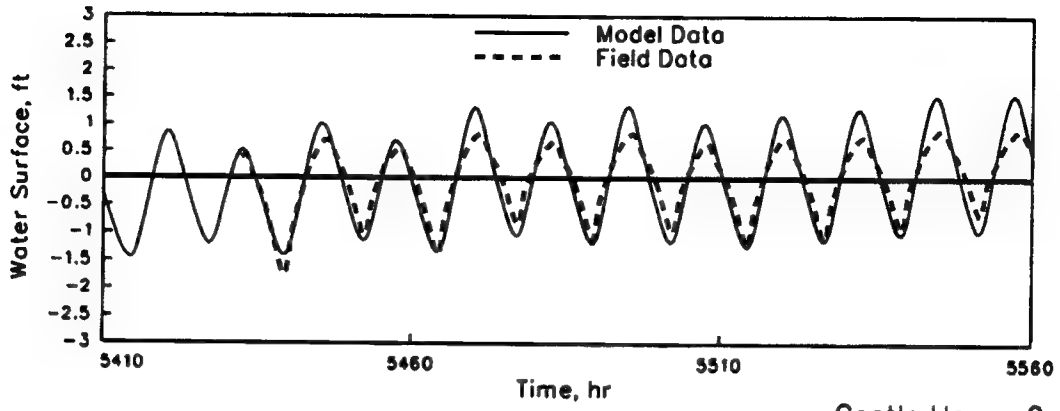

Castle Hayne 9

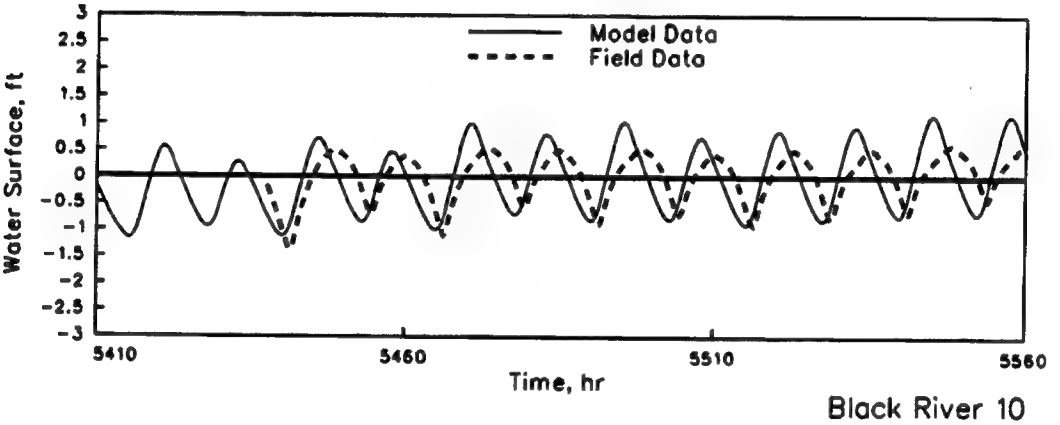

Black River 10

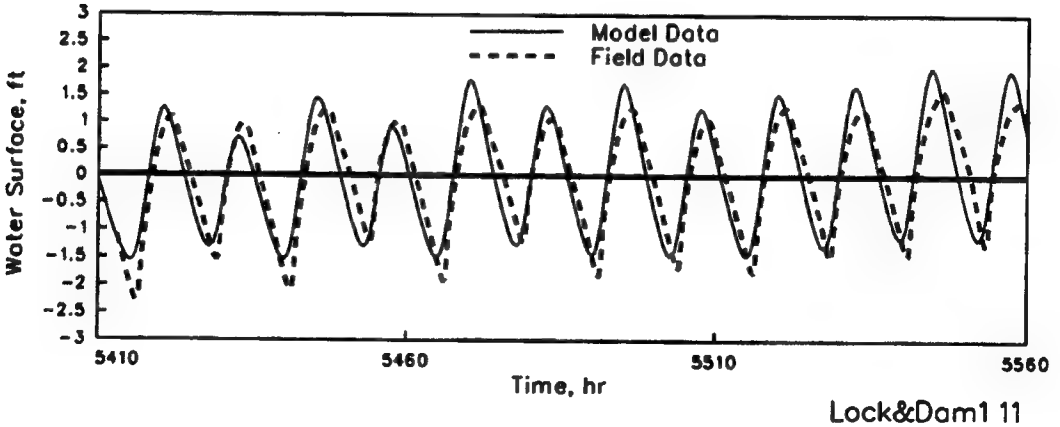

Lock&Dam1 11

WATER SURFACE ELEVATIONS
MODEL VERIFICATION
STATIONS 9, 10, AND 11
JULIAN HOURS 5410-5560

Plate 8

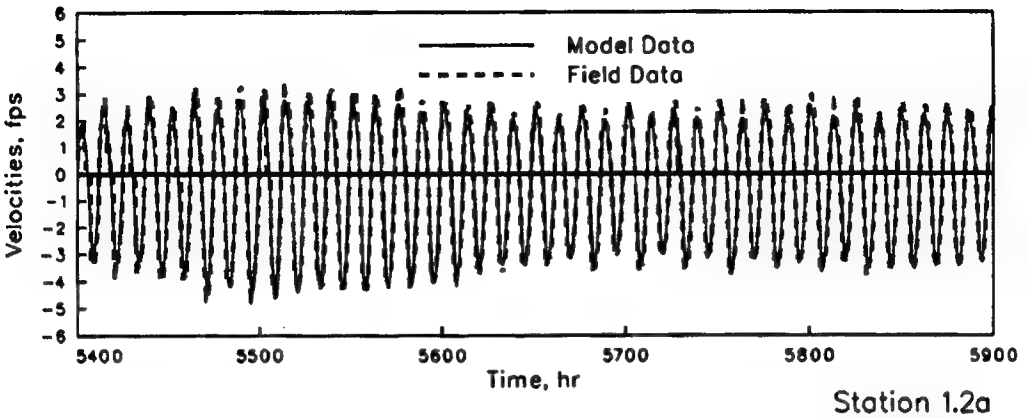

Station 1.2a
Caswell mid

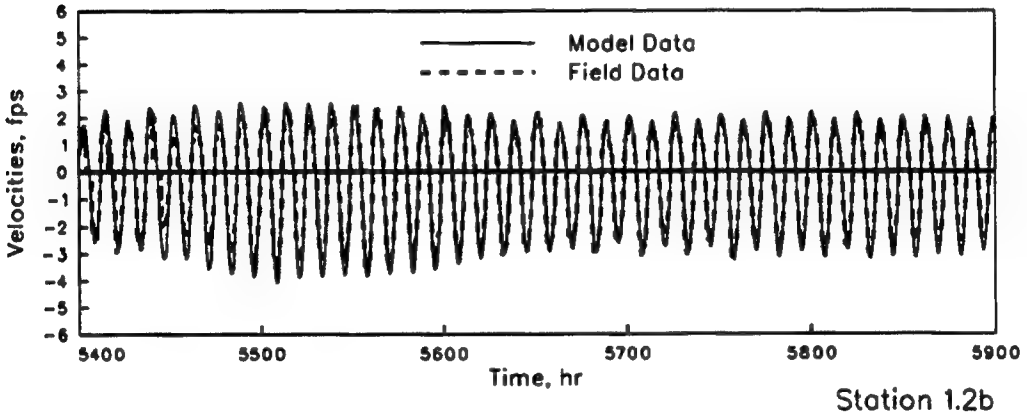

Station 1.2b
Caswell bot

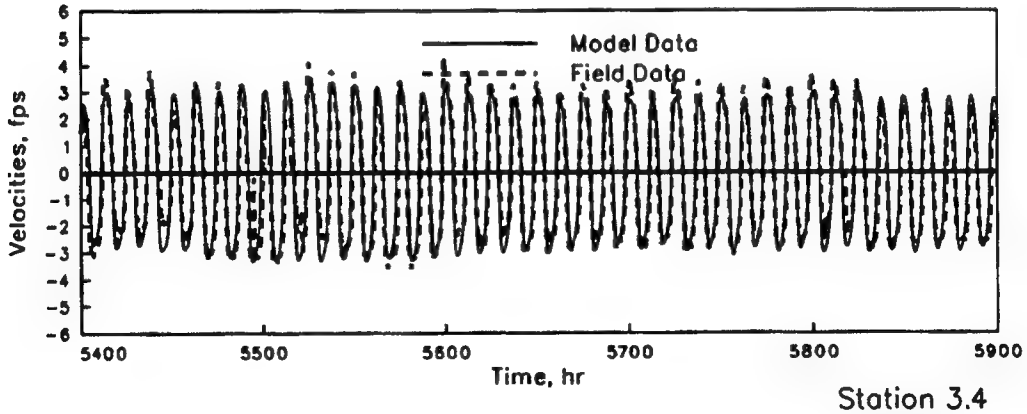

Station 3.4
Snow's Cut

CAPE FEAR VELOCITIES
MODEL VERIFICATION
STATIONS 1.2a, 1.2b, AND 3.4
JULIAN HOURS 5400-5900
(To convert velocities to meters/sec multiply by 0.3048)

Plate 9

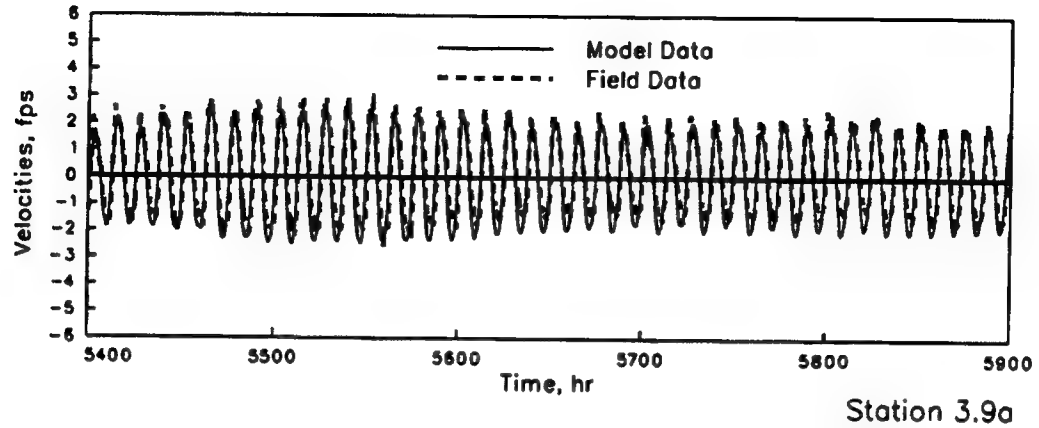

Station 3.9a
Orton mid

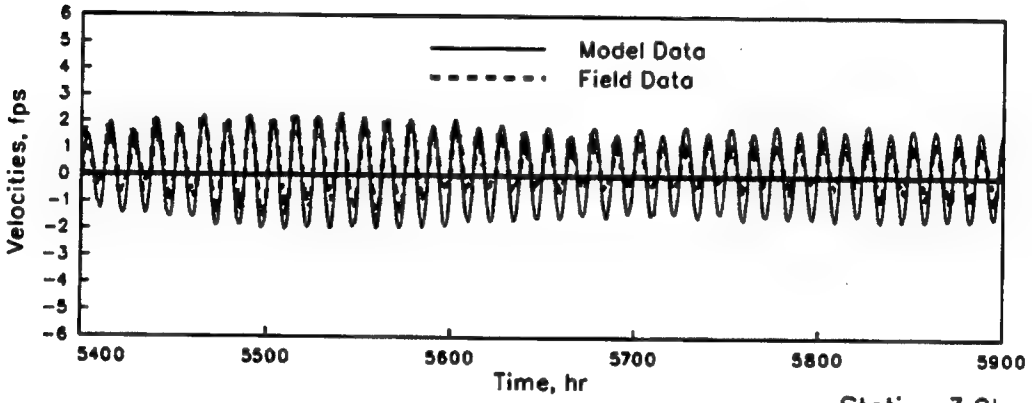

Station 3.9b
Orton bot

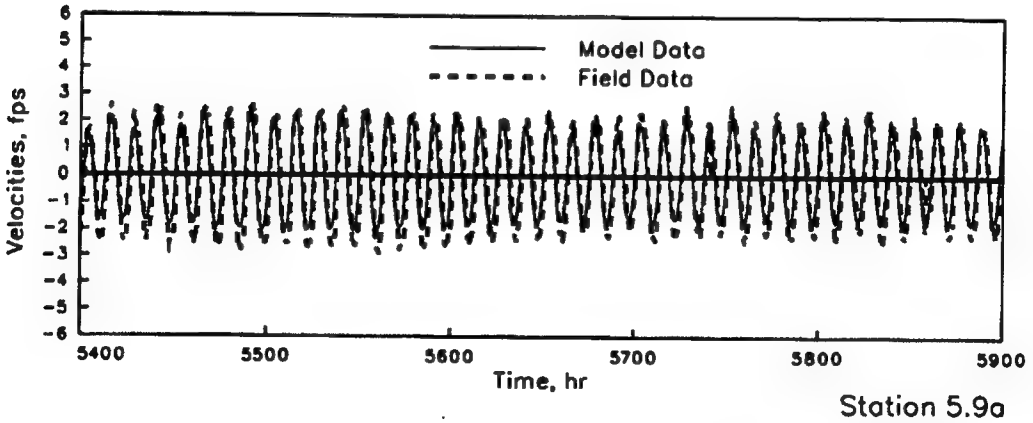

Station 5.9a
Exxon mid

CAPE FEAR VELOCITIES
MODEL VERIFICATION
STATIONS 3.9a, 3.9b, AND 5.9a
JULIAN HOURS 5400-5900

Plate 10

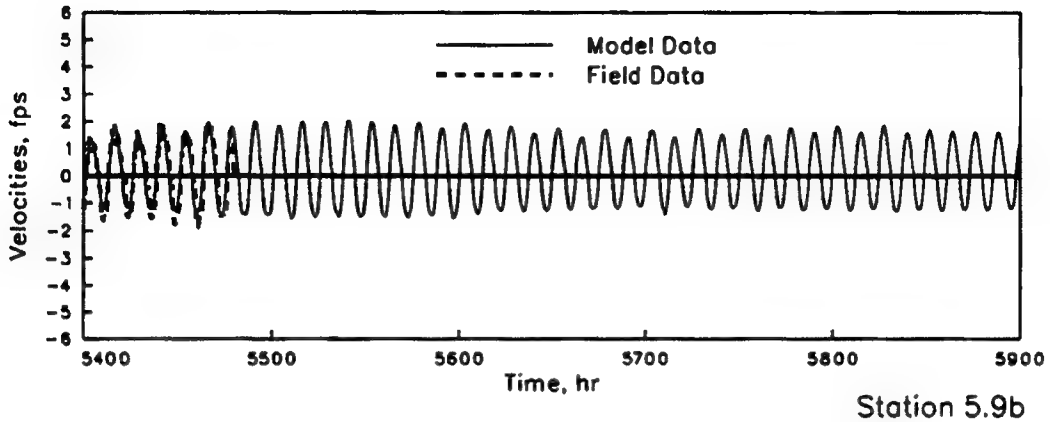

Station 5.9b
Exxon bot

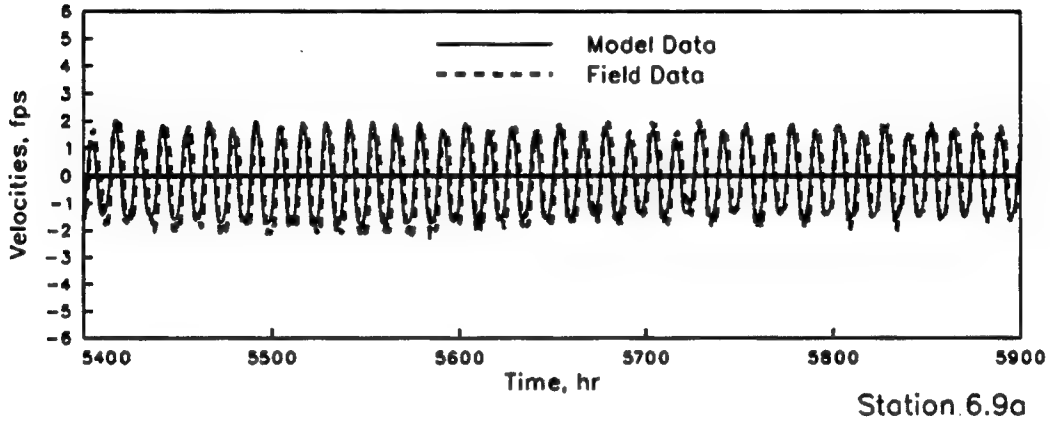

Station 6.9a
Navassa mid

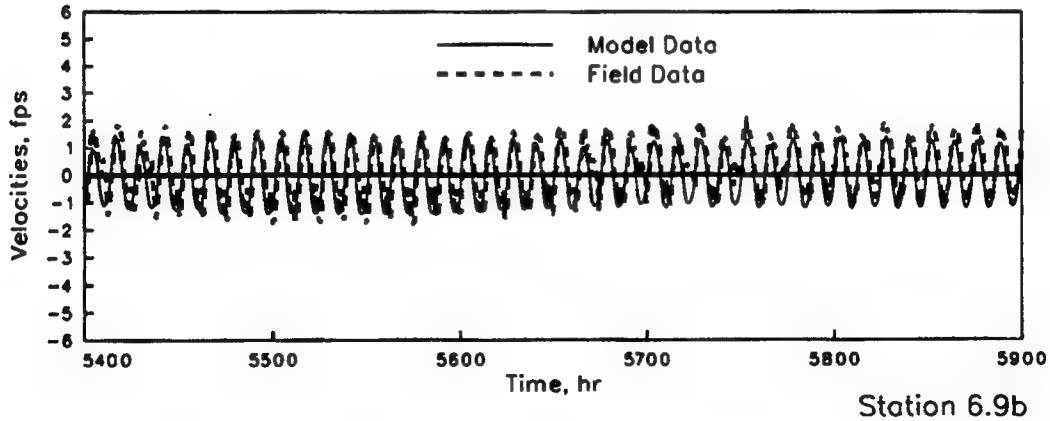

Station 6.9b
Navassa top

CAPE FEAR VELOCITIES
MODEL VERIFICATION
STATIONS 5.9b, 6.9a, AND 6.9b
JULIAN HOURS 5400-5900

Plate 11

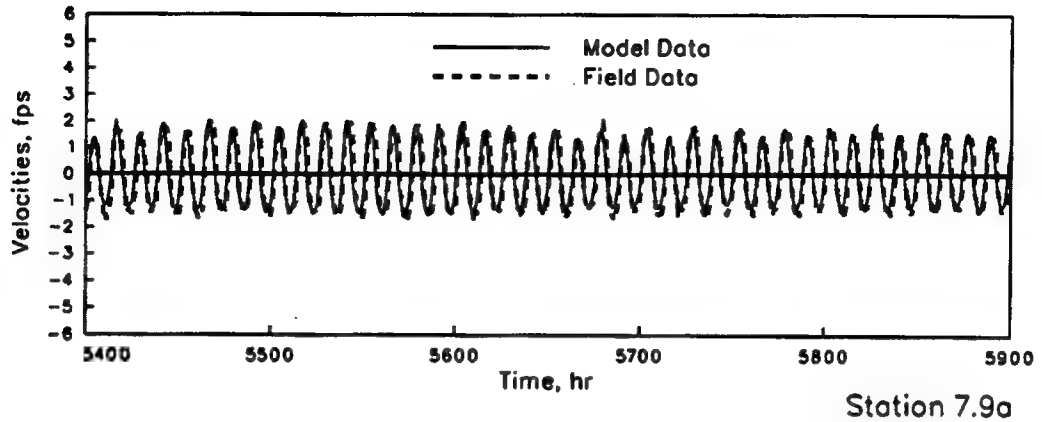

Station 7.9a
Hilton mid

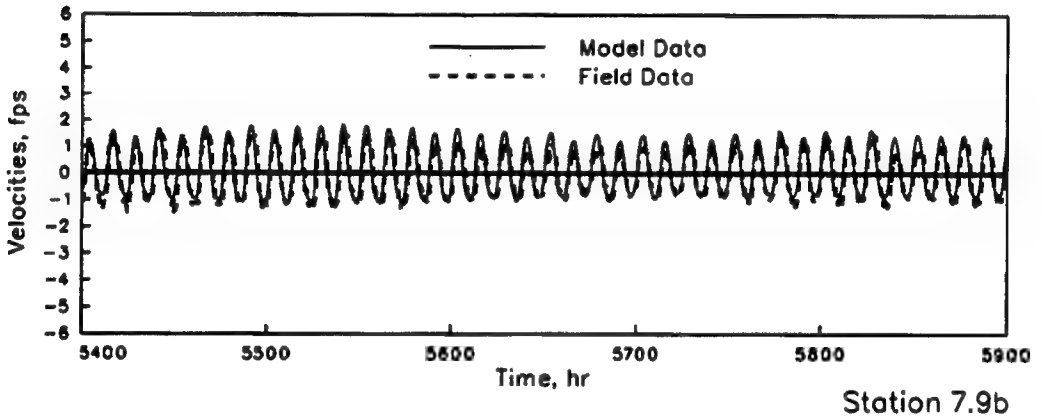

Station 7.9b
Hilton bot

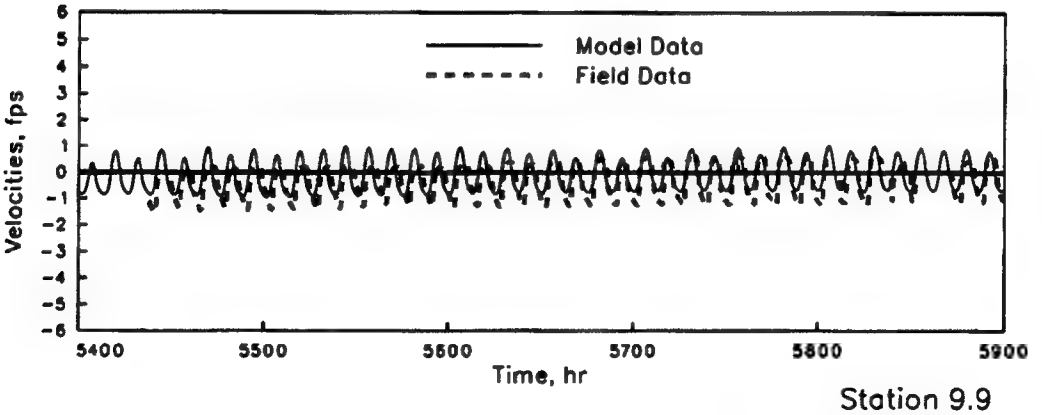

Station 9.9
Black River

CAPE FEAR VELOCITIES
MODEL VERIFICATION
STATIONS 7.9a, 7.9b, AND 9.9
JULIAN HOURS 5400-5900

Plate 12

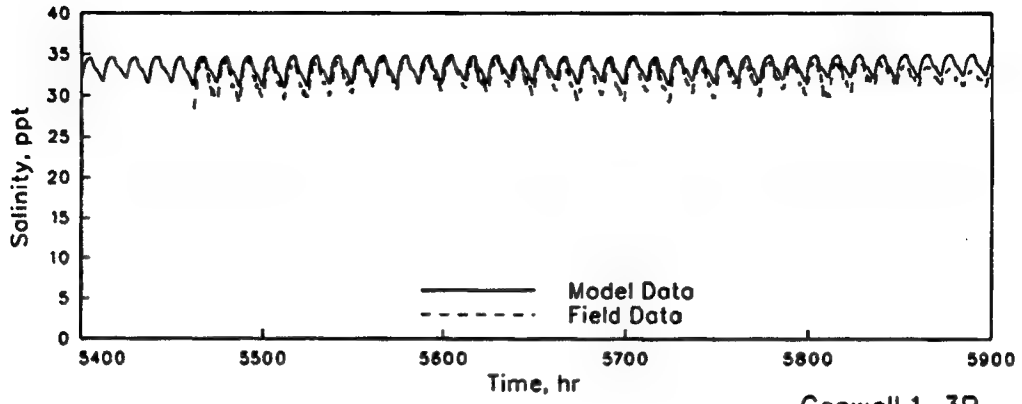

Caswell 1_3B

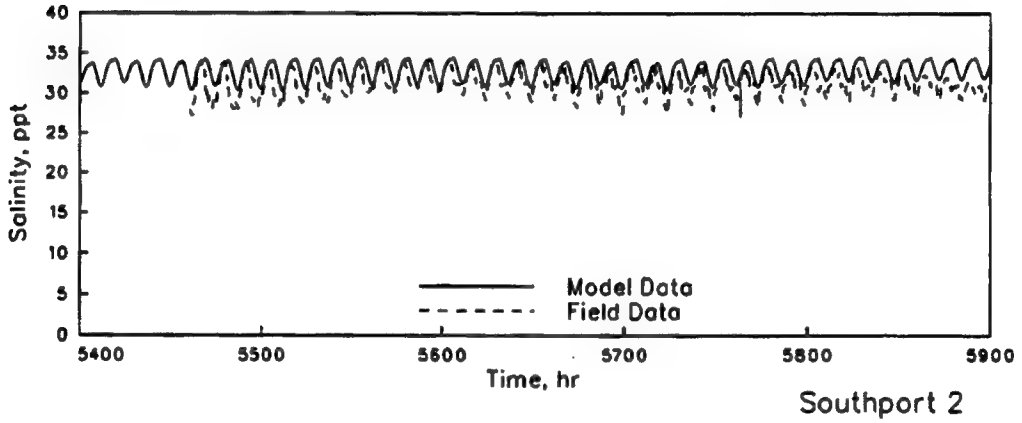

Southport 2

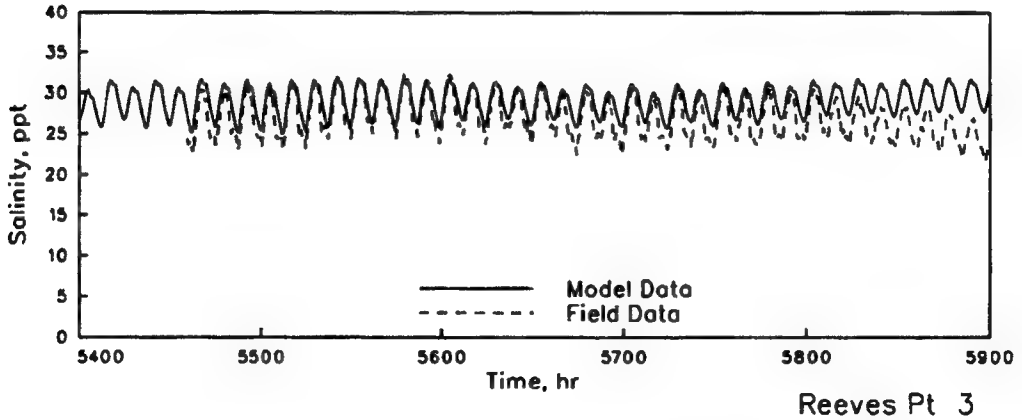

Reeves Pt 3

CAPE FEAR SALINITIES
MODEL VERIFICATION
STATIONS 1_3B, 2, AND 3
JULIAN HOURS 5400-5900

Plate 13

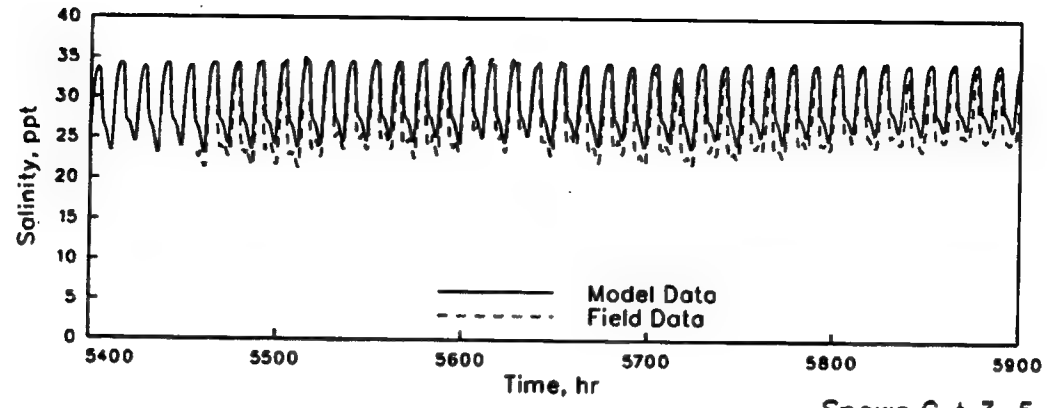

Snows Cut 3_5

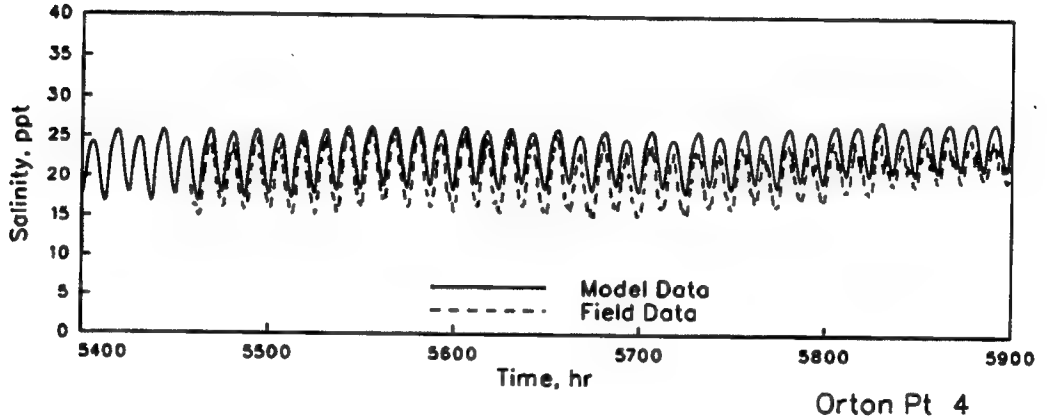

Orton Pt 4

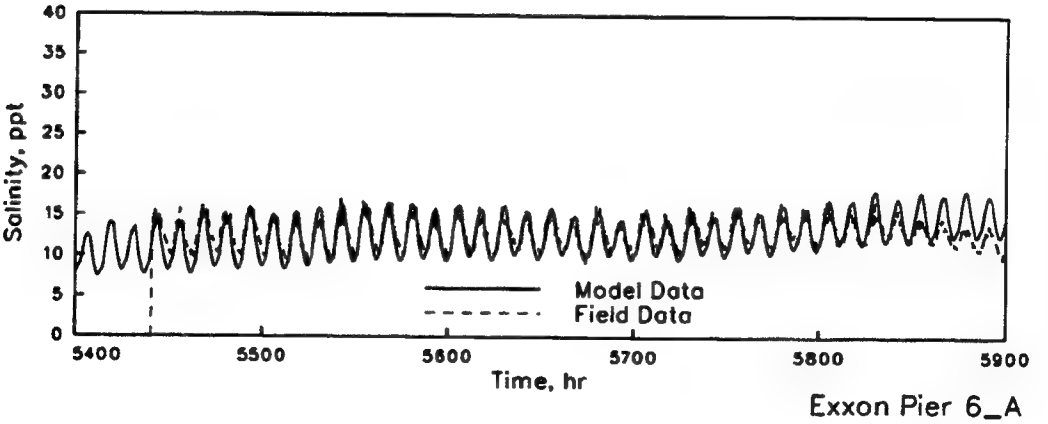

Exxon Pier 6_A

CAPE FEAR SALINITIES
MODEL VERIFICATION
STATIONS 3_5, 4, AND 6_A
JULIAN HOURS 5400-5900

Plate 14

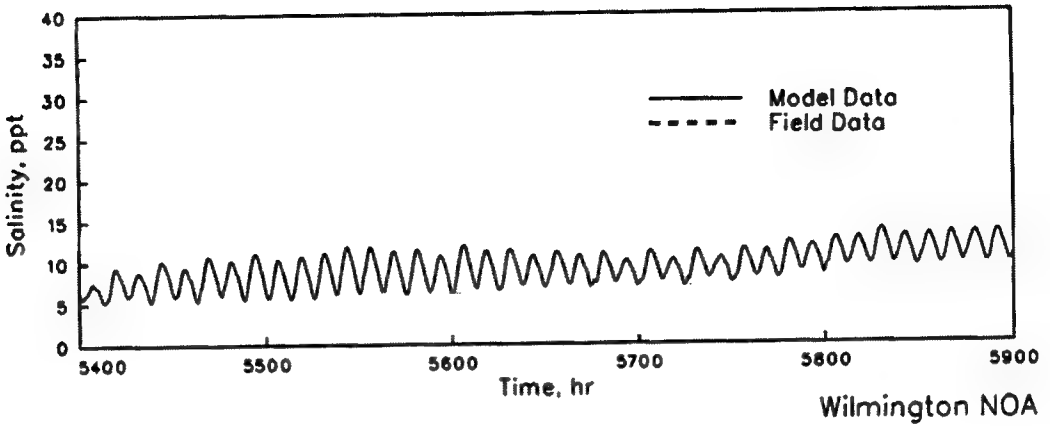

Wilmington NOA

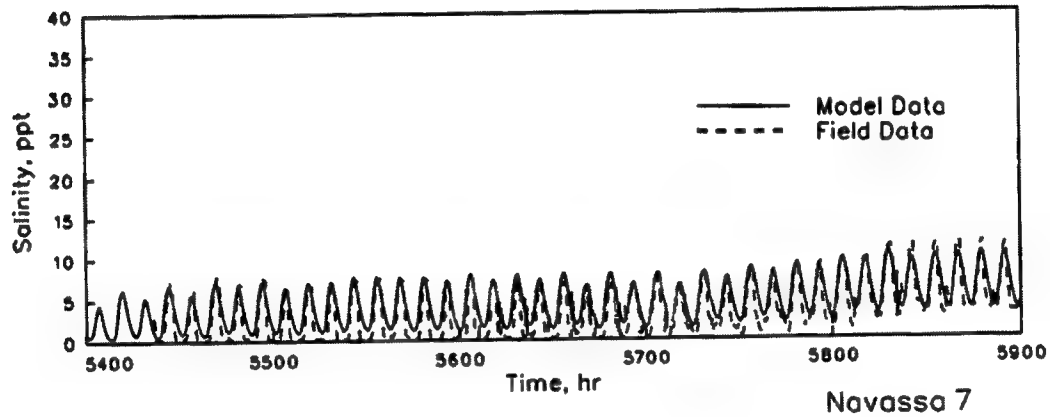

Navassa 7

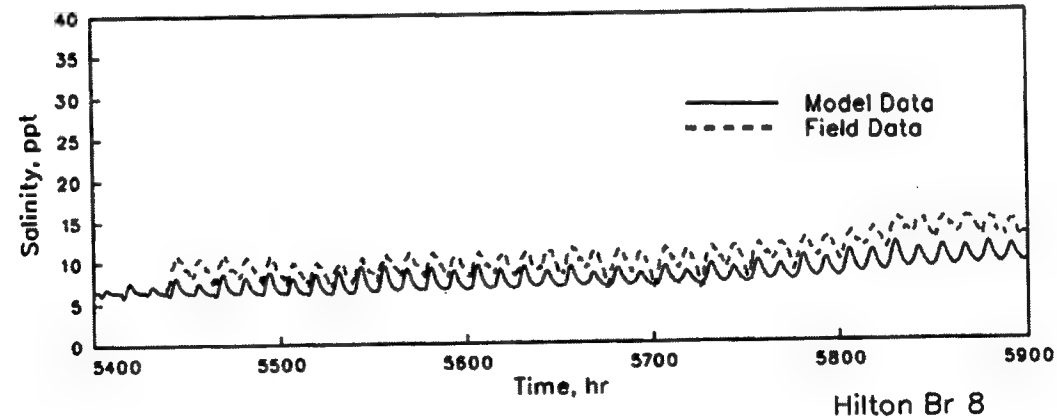

Hilton Br 8

CAPE FEAR SALINITIES
MODEL VERIFICATION
STATIONS NOAA, 7, AND 8
JULIAN HOURS 5400-5900

Plate 15

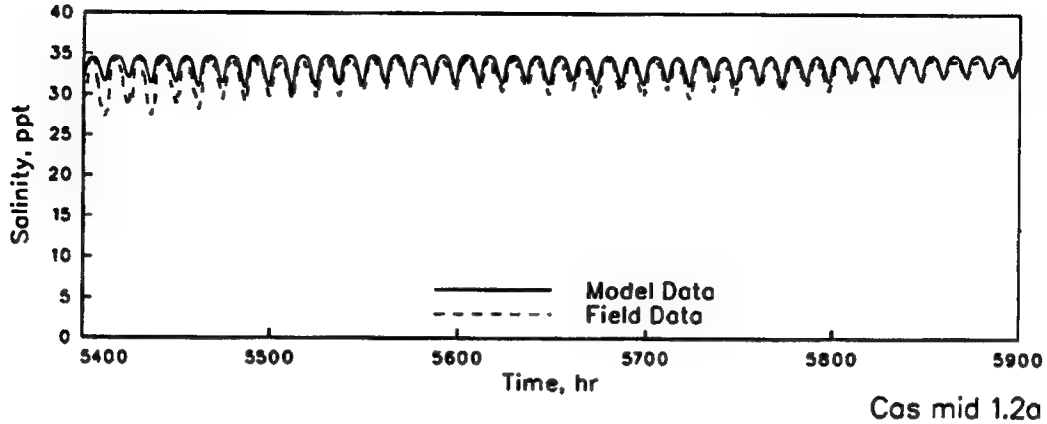

Cas mid 1.2a

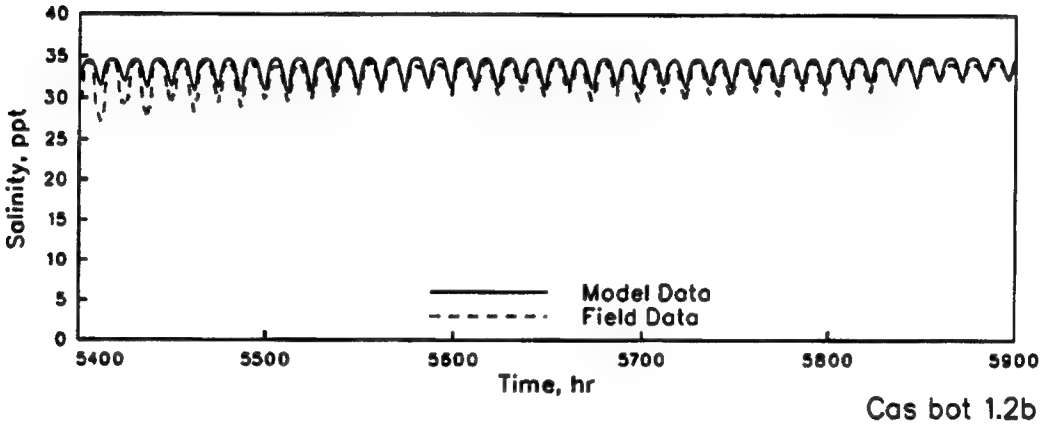

Cas bot 1.2b

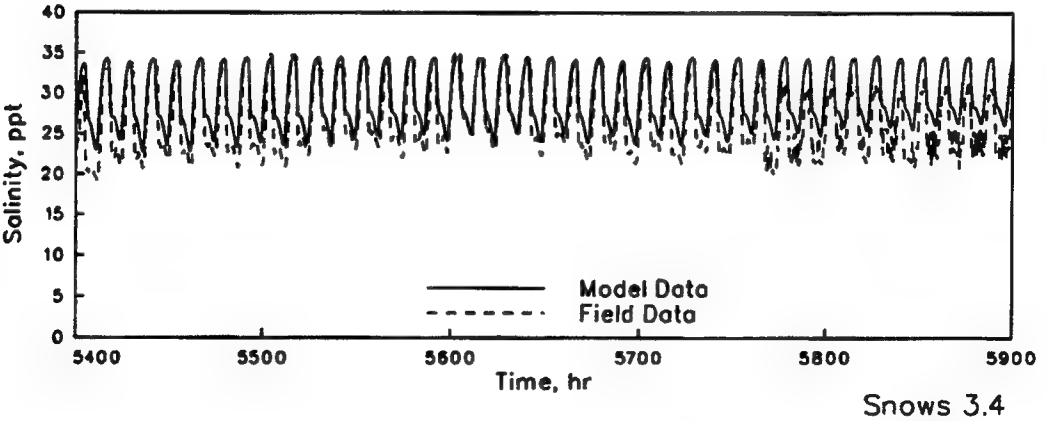

Snows 3.4

CAPE FEAR SALINITIES
MODEL VERIFICATION
STATIONS 1.2a, 1.2b, AND 3.4
JULIAN HOURS 5400-5900

Plate 16

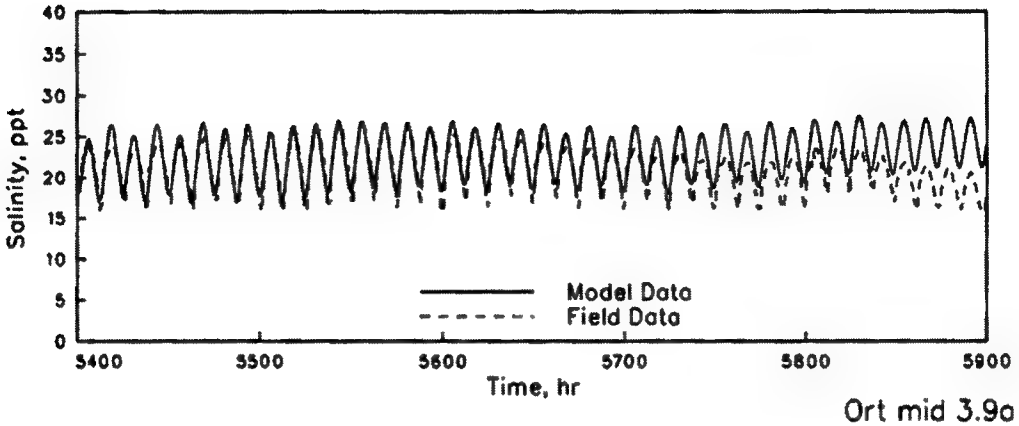

Ort mid 3.9a

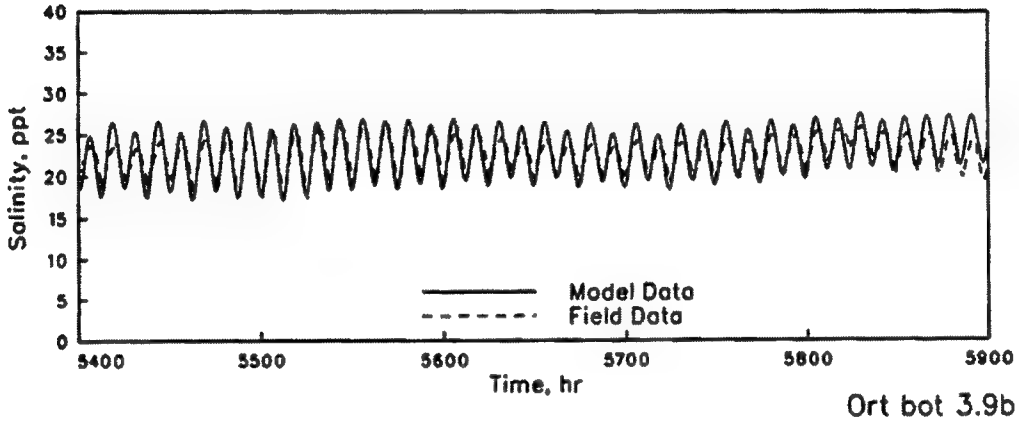

Ort bot 3.9b

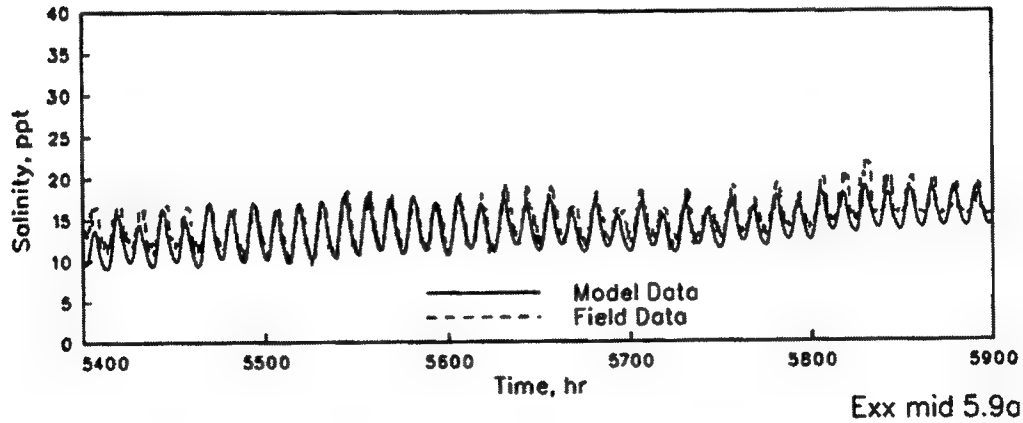

Exx mid 5.9a

CAPE FEAR SALINITIES
MODEL VERIFICATION
STATIONS 3.9a, 3.9b, AND 5.9a
JULIAN HOURS 5400-5900

Plate 17

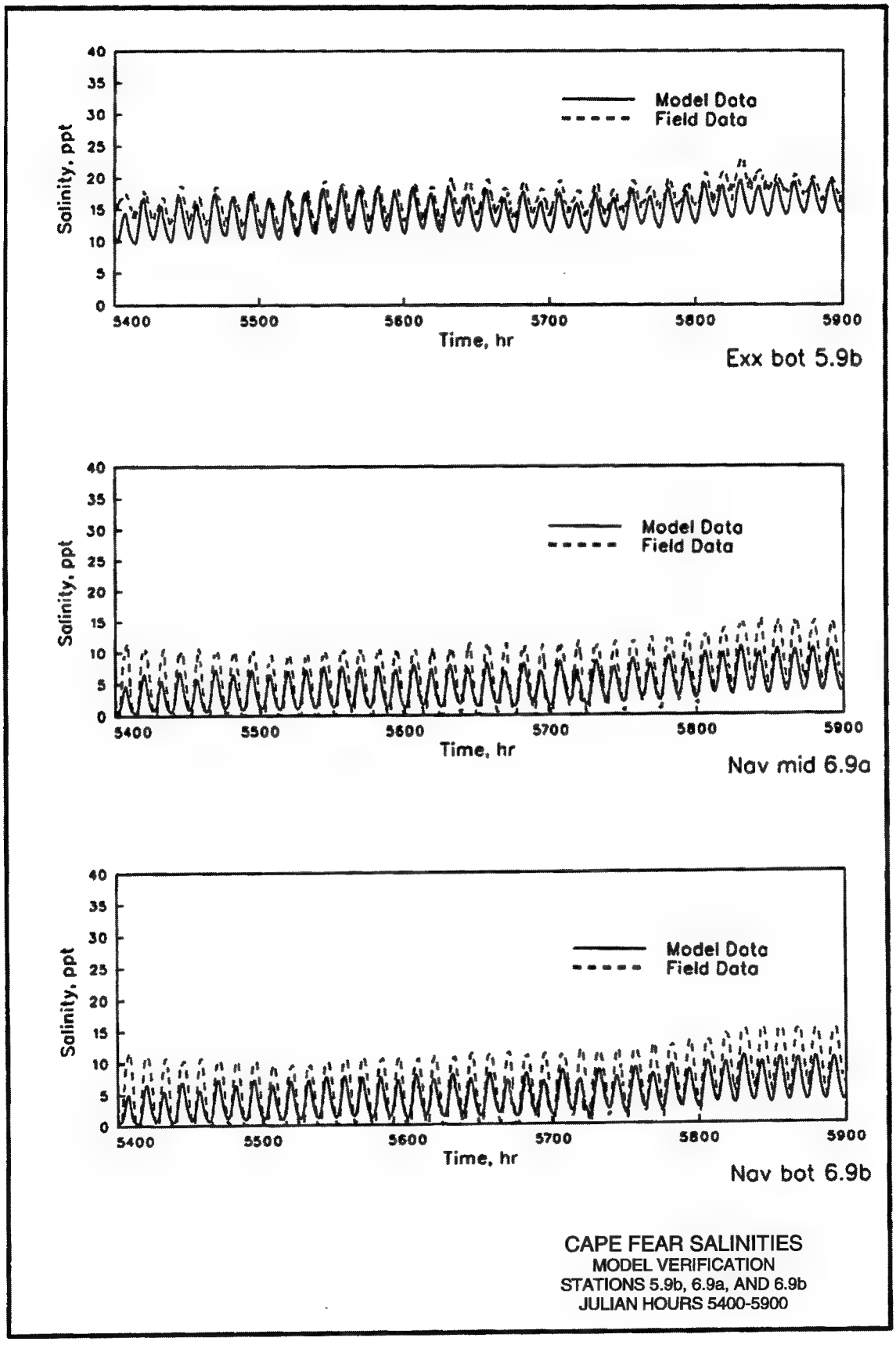
Salinity, ppt
Time, hr
Model Data
Field Data
Exx bot 5.9b
Nav mid 6.9a
Nav bot 6.9b
CAPE FEAR SALINITIES
MODEL VERIFICATION
STATIONS 5.9b, 6.9a, AND 6.9b
JULIAN HOURS 5400-5900

Plate 18

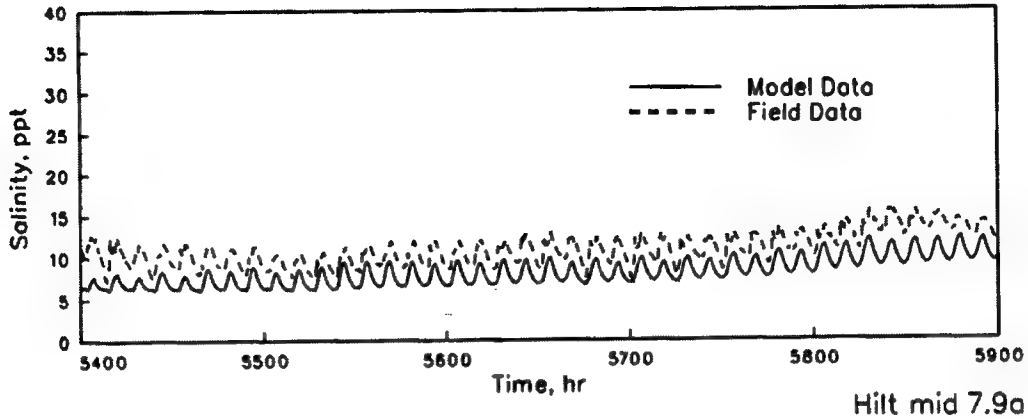

Hilt mid 7.9a

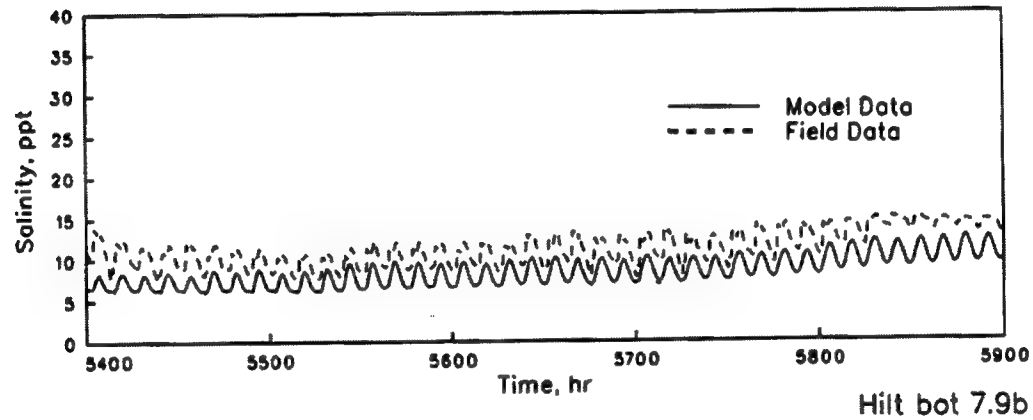

Hilt bot 7.9b

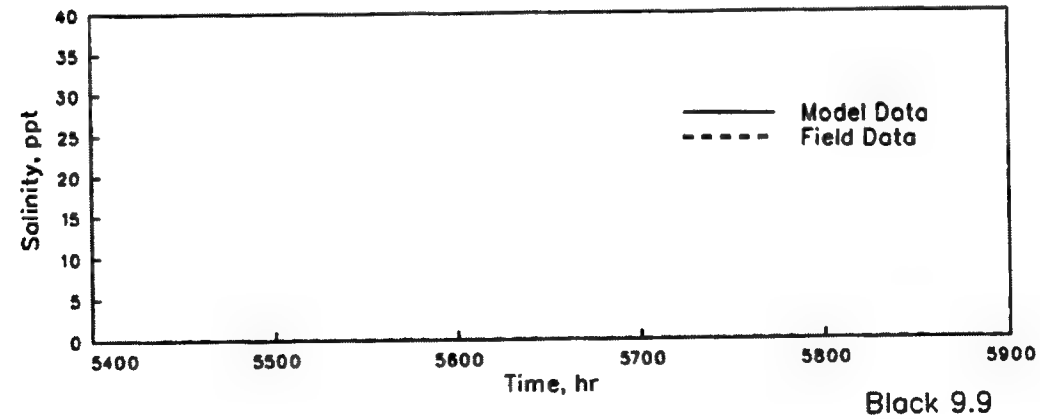

Black 9.9

CAPE FEAR SALINITIES
MODEL VERIFICATION
STATIONS 7.9a, 7.9b, AND 9.9
JULIAN HOURS 5400-5900

Plate 19

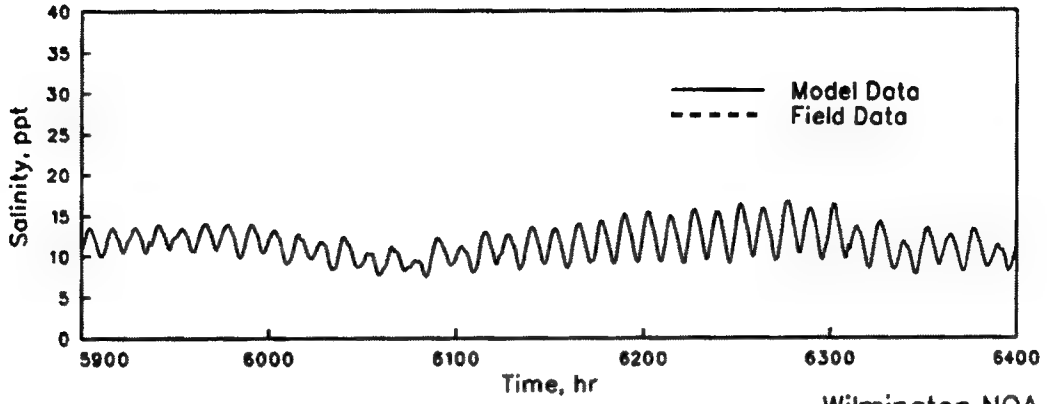

Wilmington NOA

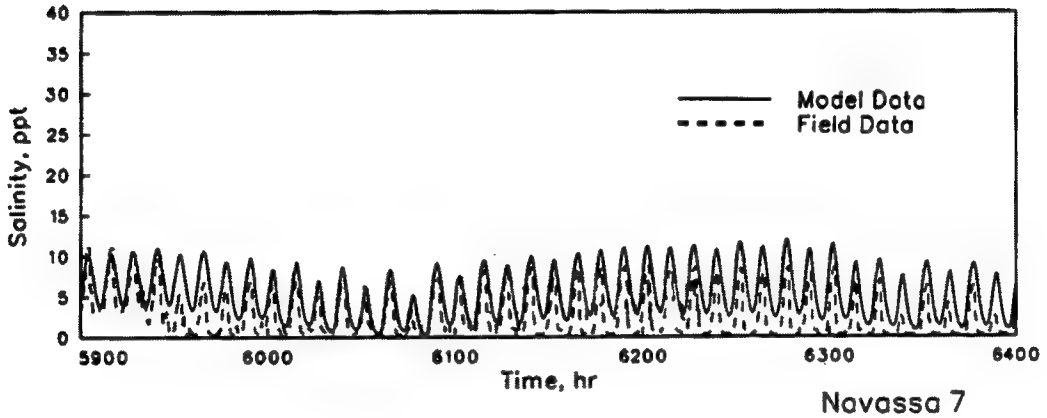

Navassa 7

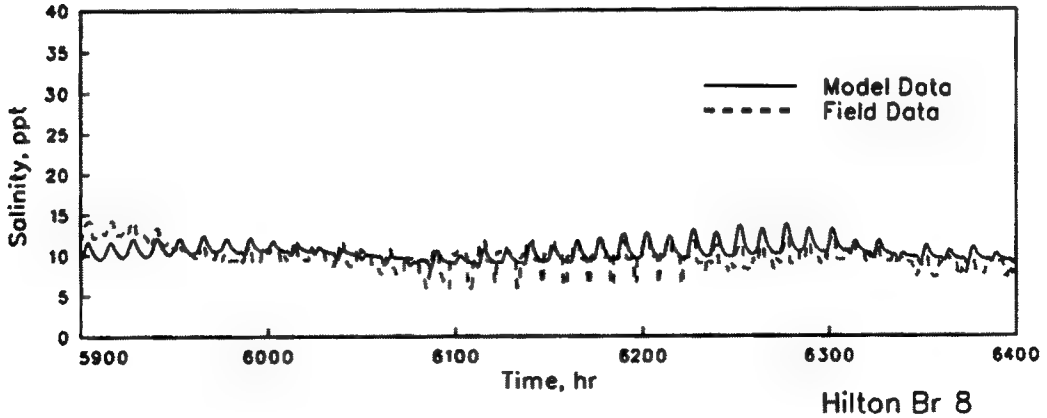

Hilton Br 8

CAPE FEAR SALINITIES
MODEL VERIFICATION
STATIONS NOAA, 7, AND 8
JULIAN HOURS 5900-6400

Plate 20

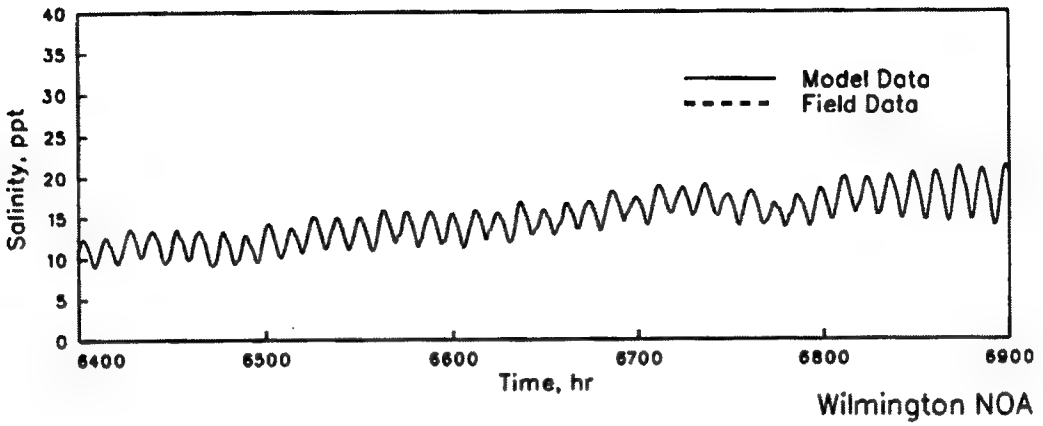

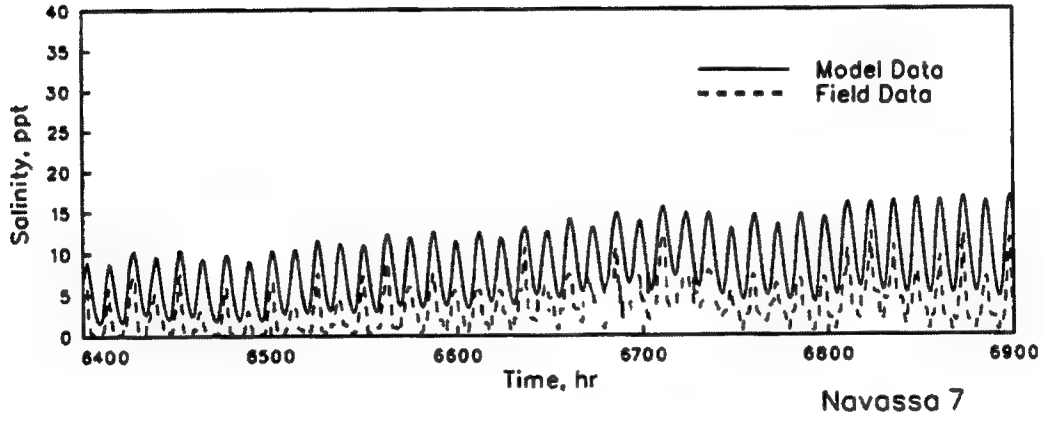

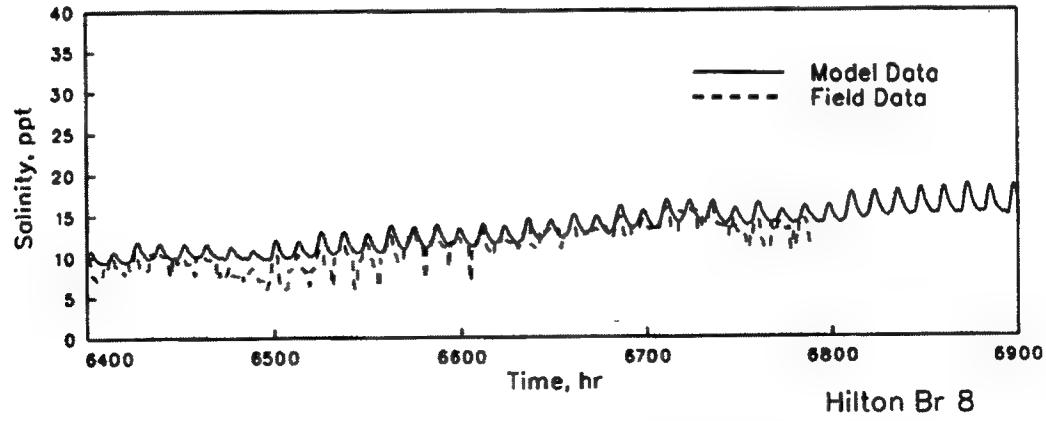

CAPE FEAR SALINITIES
MODEL VERIFICATION
STATIONS NOAA, 7, AND 8
JULIAN HOURS 6400-6900

Plate 21

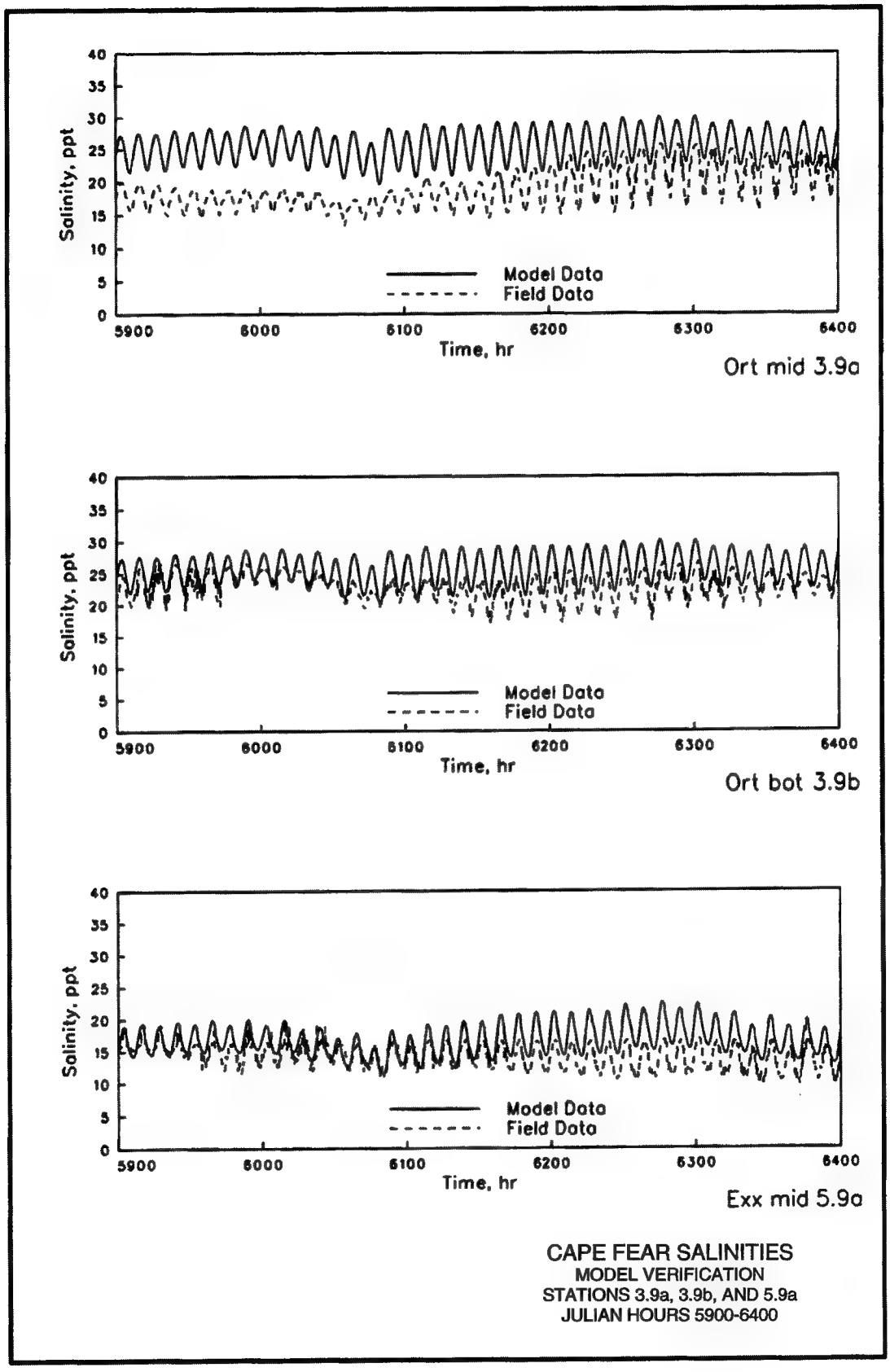
Salinity, ppt
40
35
30
25
20
15
10
5
0
5900
6000
6100
6200
6300
6400
Time, hr
Model Data
Field Data
Ort mid 3.9a
Salinity, ppt
Time, hr
Model Data
Field Data
Ort bot 3.9b
Salinity, ppt
Time, hr
Model Data
Field Data
Exx mid 5.9a
CAPE FEAR SALINITIES
MODEL VERIFICATION
STATIONS 3.9a, 3.9b, AND 5.9a
JULIAN HOURS 5900-6400

Plate 22

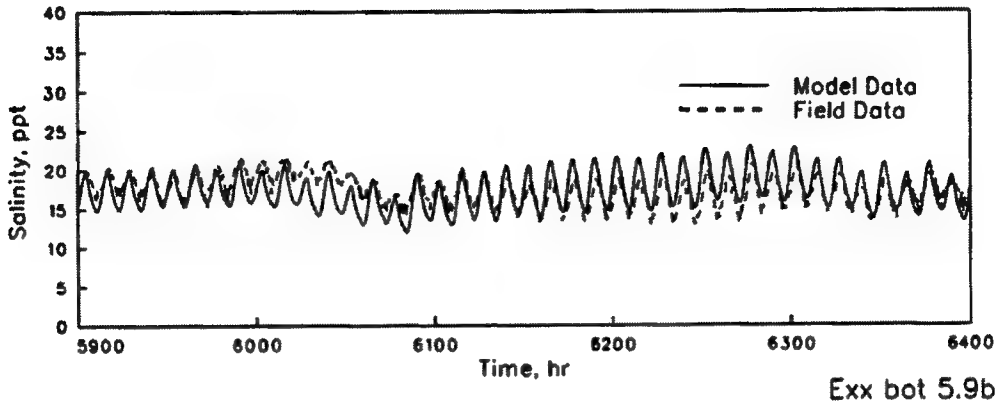

Exx bot 5.9b

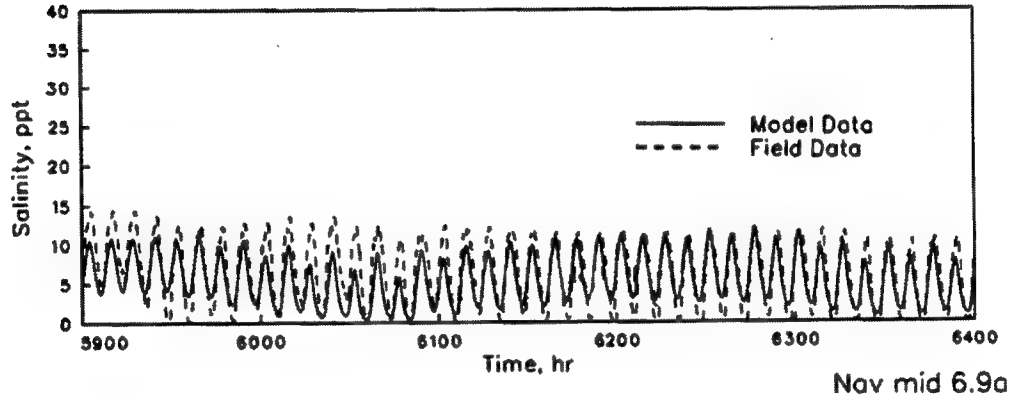

Nav mid 6.9a

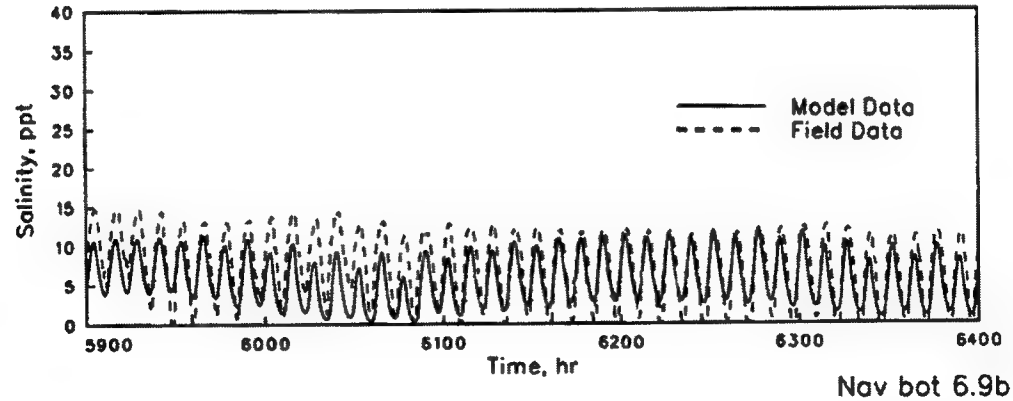

Nav bot 6.9b

CAPE FEAR SALINITIES
MODEL VERIFICATION
STATIONS 5.9b, 6.9a, AND 6.9b
JULIAN HOURS 5900-6400

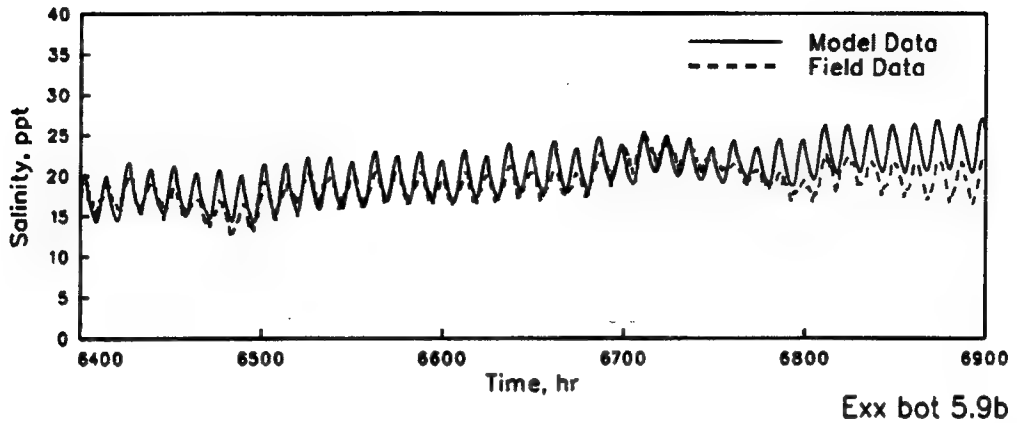

Exx bot 5.9b

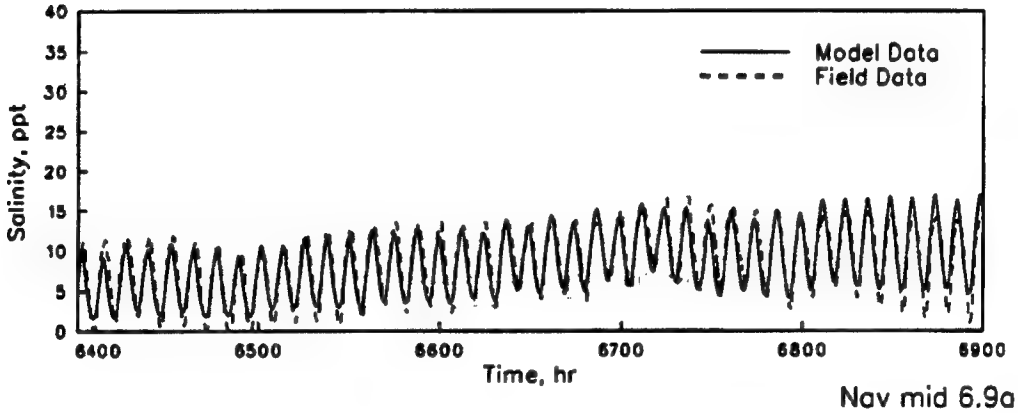

Nav mid 6.9a

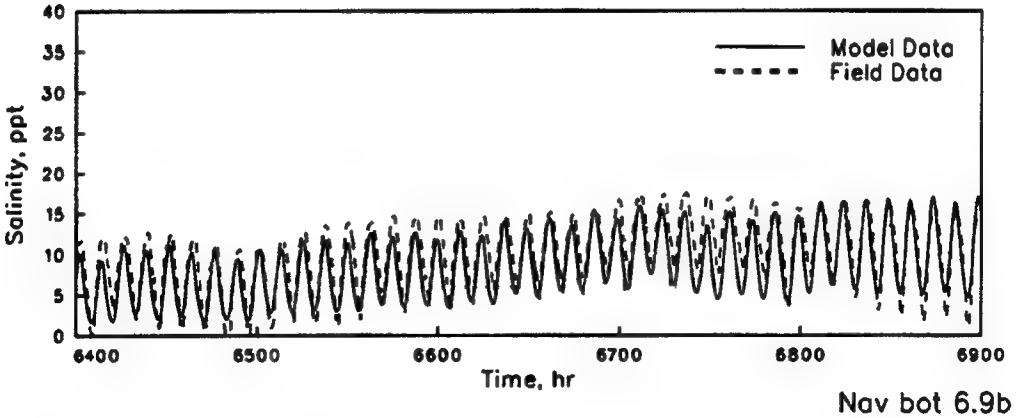

Nav bot 6.9b

CAPE FEAR SALINITIES
MODEL VERIFICATION
STATIONS 5.9b, 6.9a, AND 6.9b
JULIAN HOURS 6400-6900

Plate 24

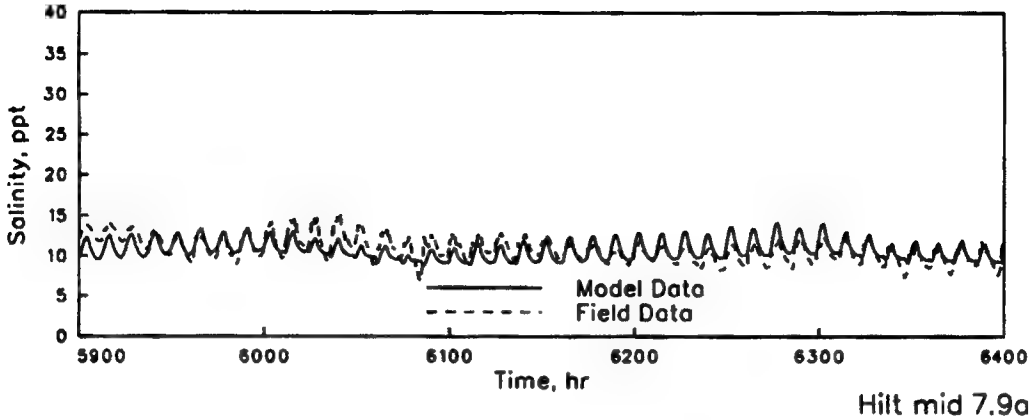

Hilt mid 7.9a

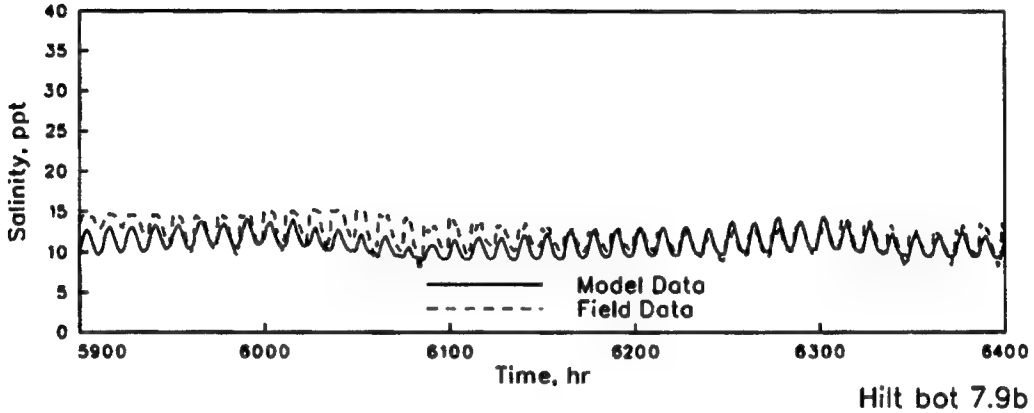

Hilt bot 7.9b

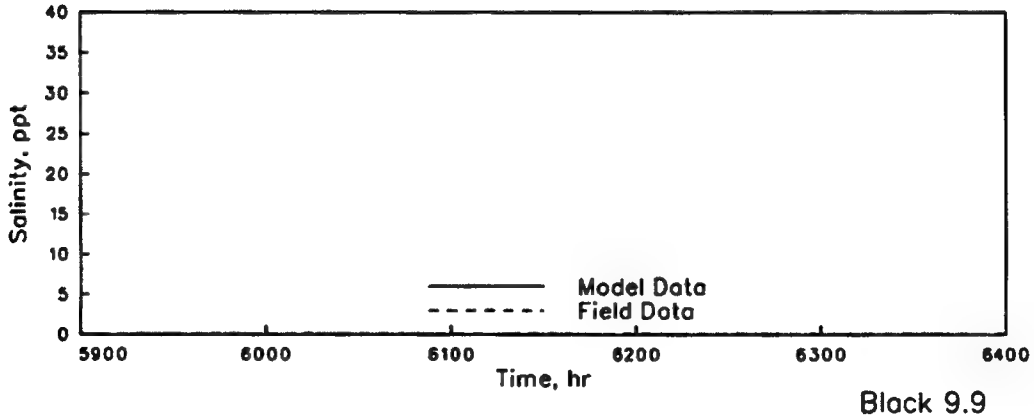

Black 9.9

CAPE FEAR SALINITIES
MODEL VERIFICATION
STATIONS 7.9a, 7.9b, AND 9.9
JULIAN HOURS 5900-6400

Plate 25

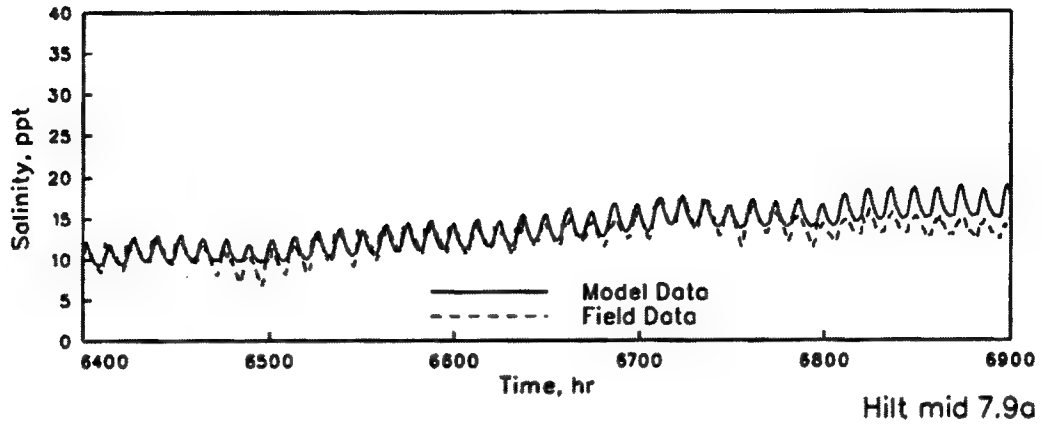

Hilt mid 7.9a

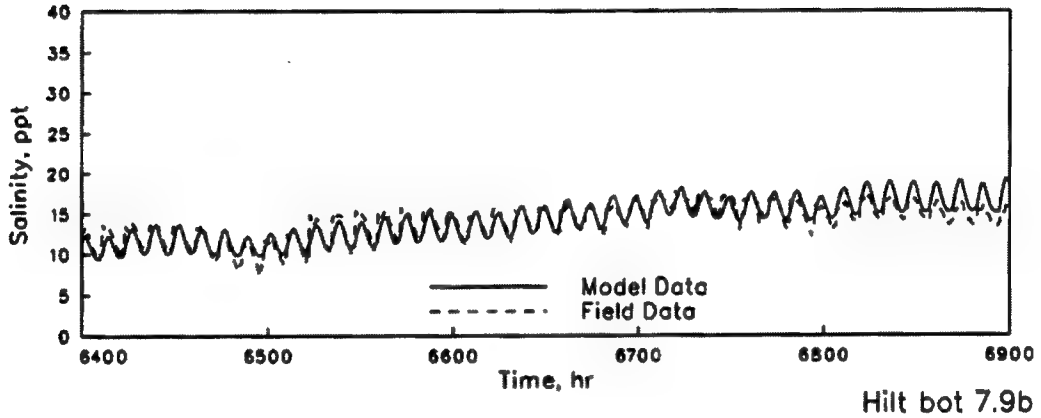

Hilt bot 7.9b

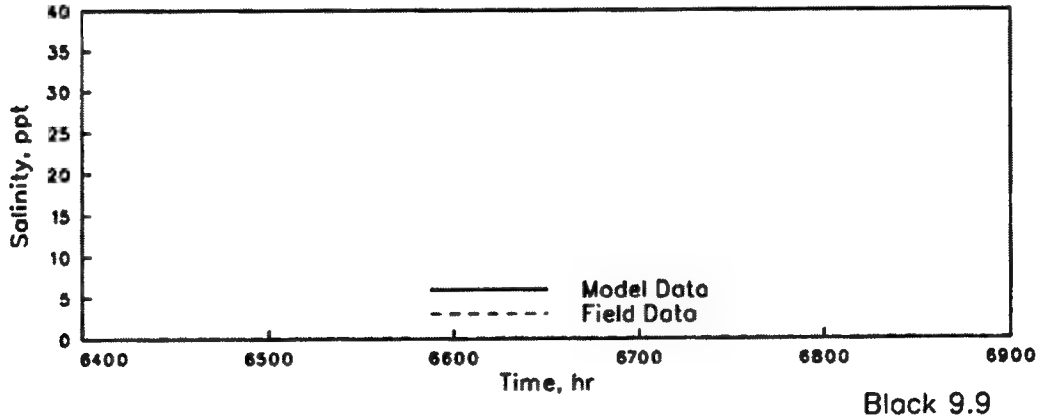

Black 9.9

CAPE FEAR SALINITIES
MODEL VERIFICATION
STATIONS 7.9a, 7.9b, AND 9.9
JULIAN HOURS 6400-6900

Plate 26

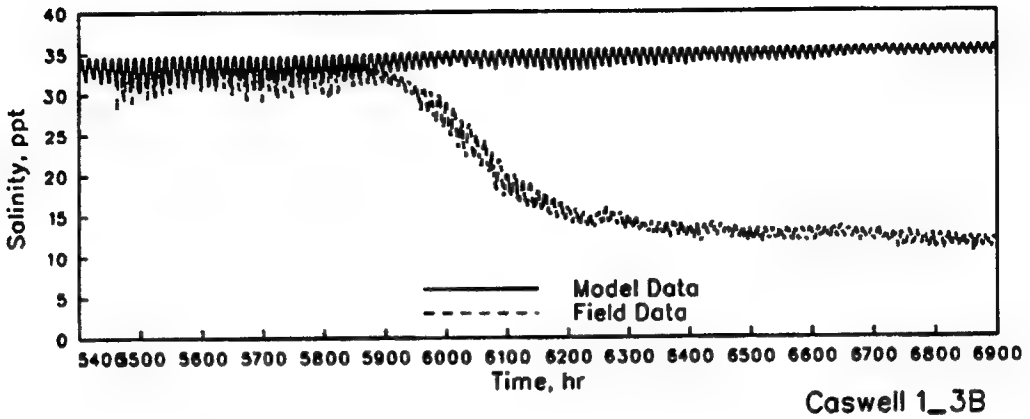

Caswell 1_3B

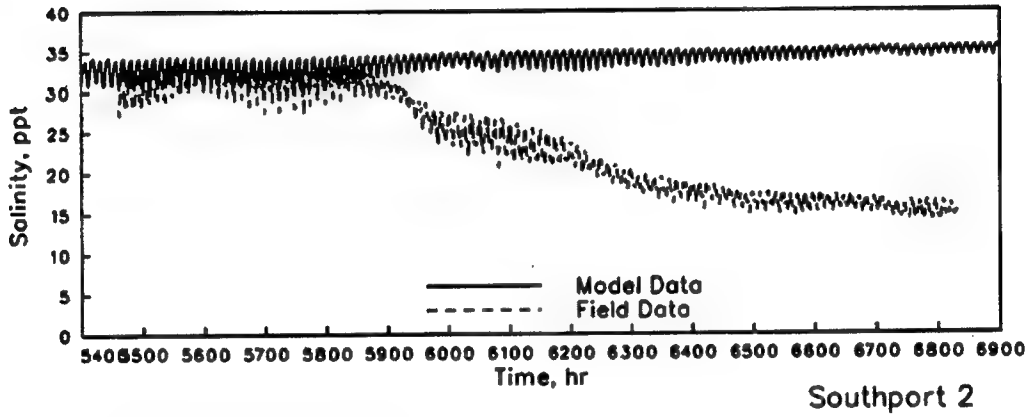

Southport 2

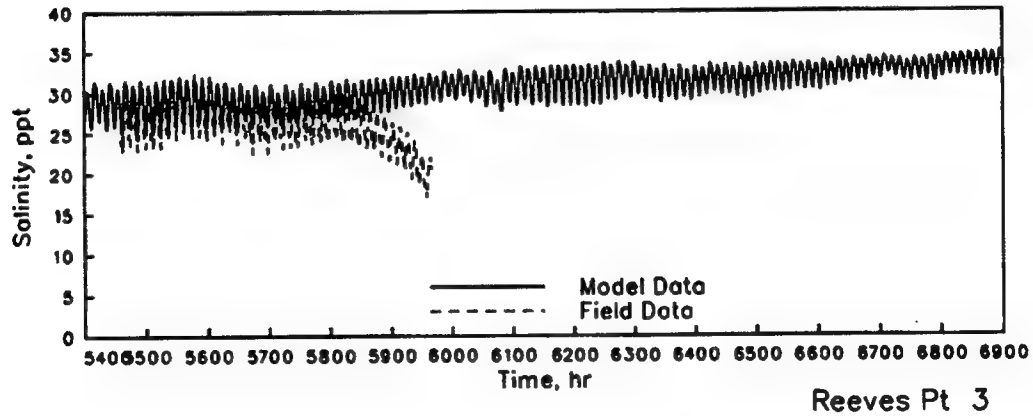

Reeves Pt 3

CAPE FEAR SALINITIES
MODEL VERIFICATION
STATIONS 1_3B, 2, AND 3
JULIAN HOURS 5400-6900

Plate 27

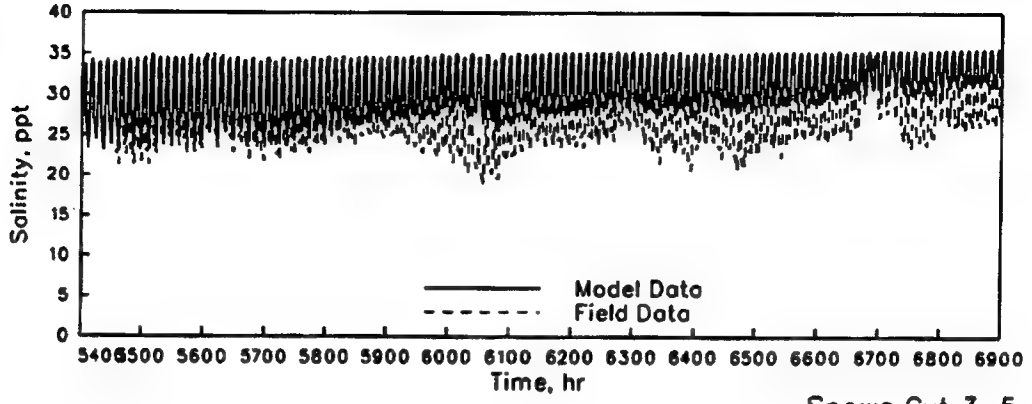

Snows Cut 3_5

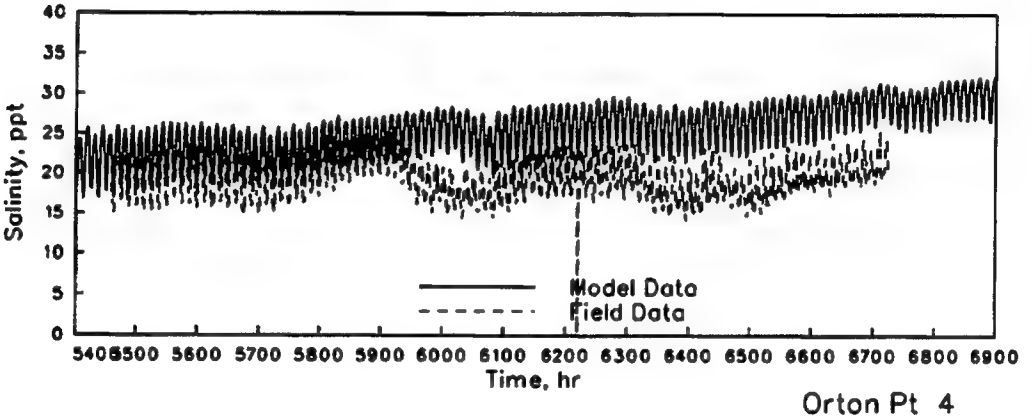

Orton Pt 4

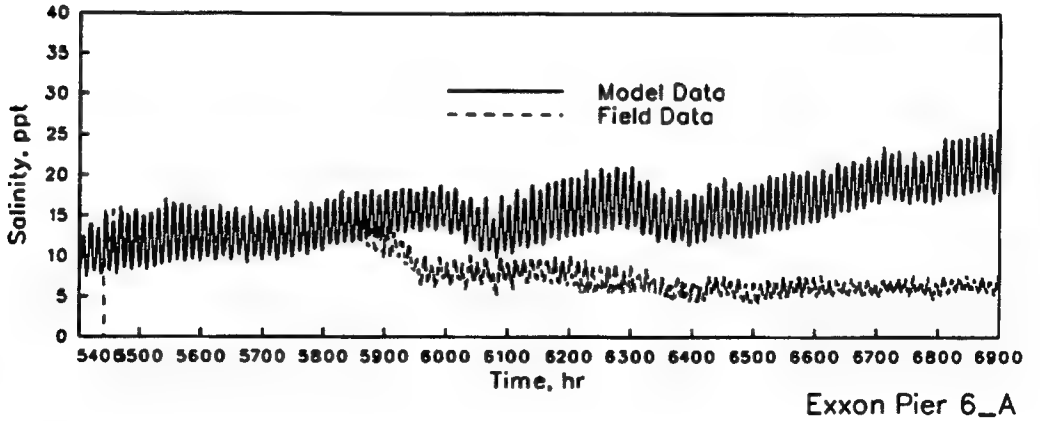

Exxon Pier 6_A

CAPE FEAR SALINITIES
MODEL VERIFICATION
STATIONS 3_5, 4, AND 6_A
JULIAN HOURS 6400-6900

Plate 28

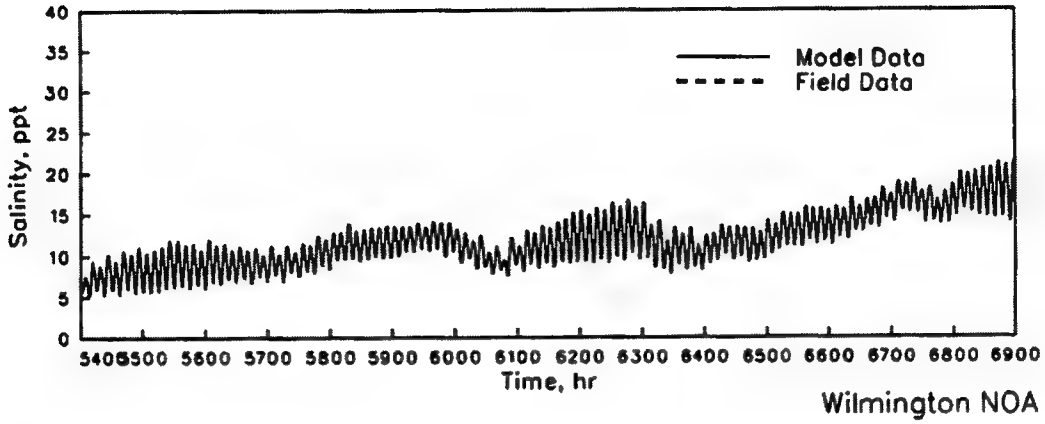

Wilmington NOA

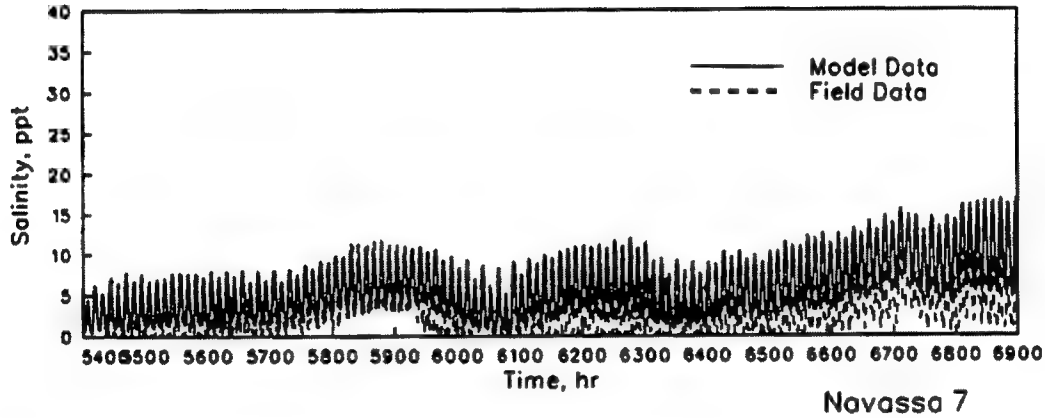

Navassa 7

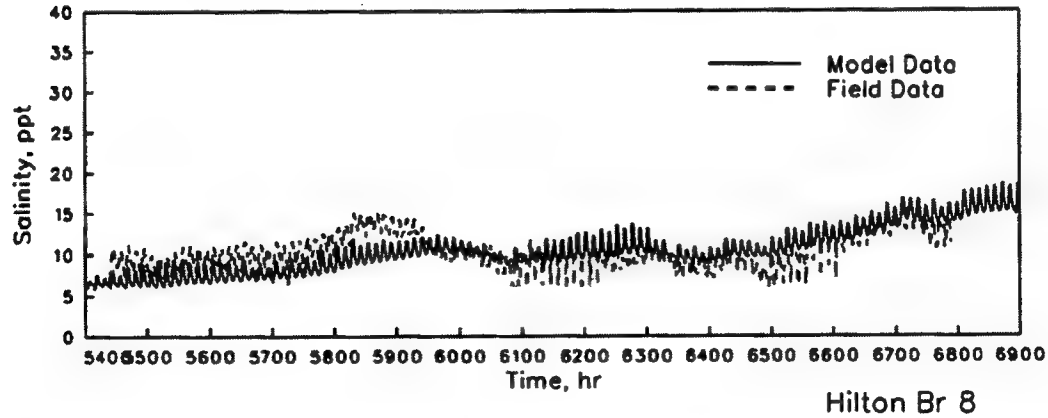

Hilton Br 8

CAPE FEAR SALINITIES
MODEL VERIFICATION
STATIONS NOAA, 7, AND 8
JULIAN HOURS 5400-6900

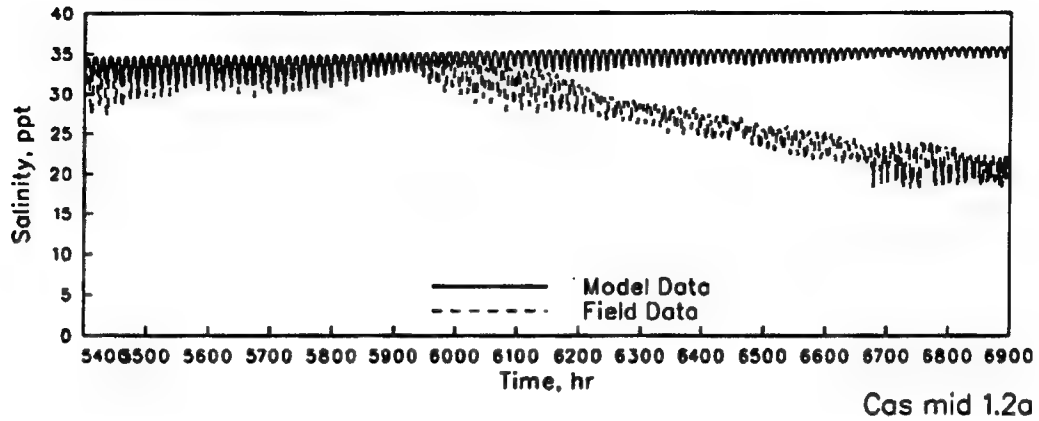

Cas mid 1.2a

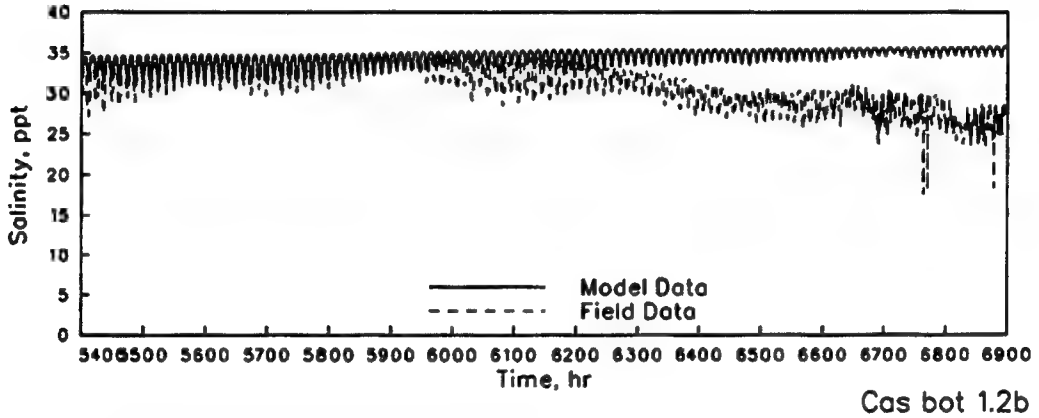

Cas bot 1.2b

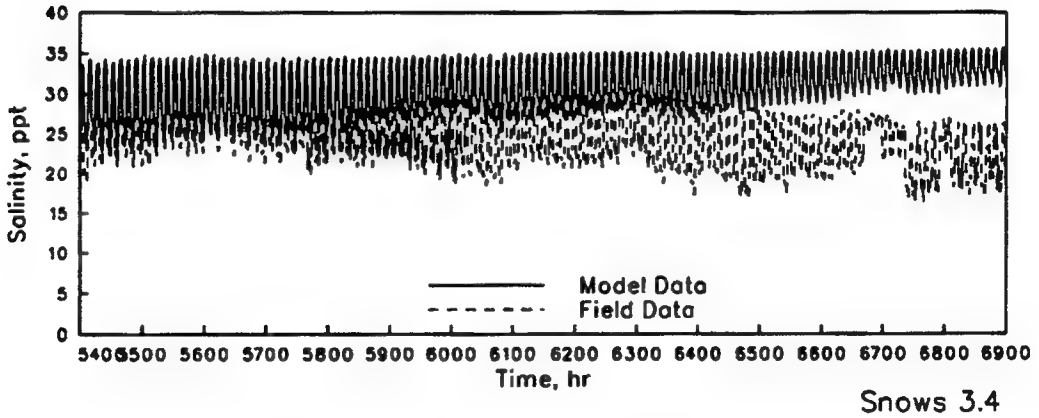

Snows 3.4

CAPE FEAR SALINITIES
MODEL VERIFICATION
STATIONS 1.2a, 1.2b AND 3.4
JULIAN HOURS 5400-6900

Plate 30

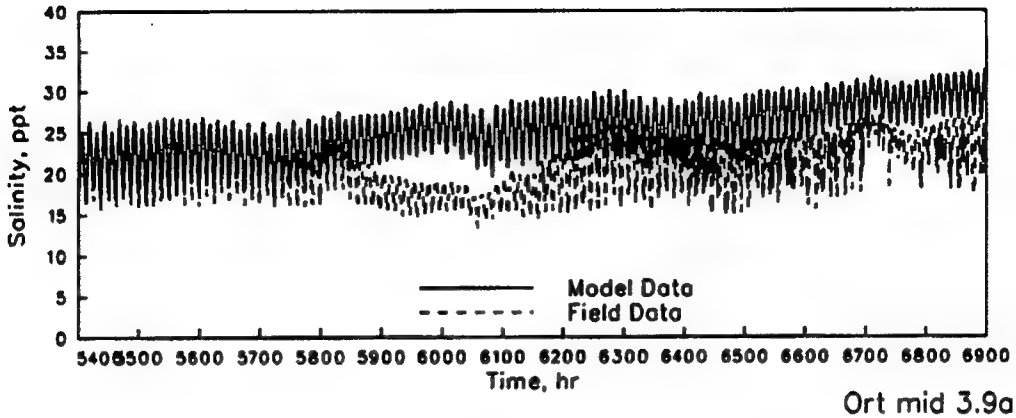

Ort mid 3.9a

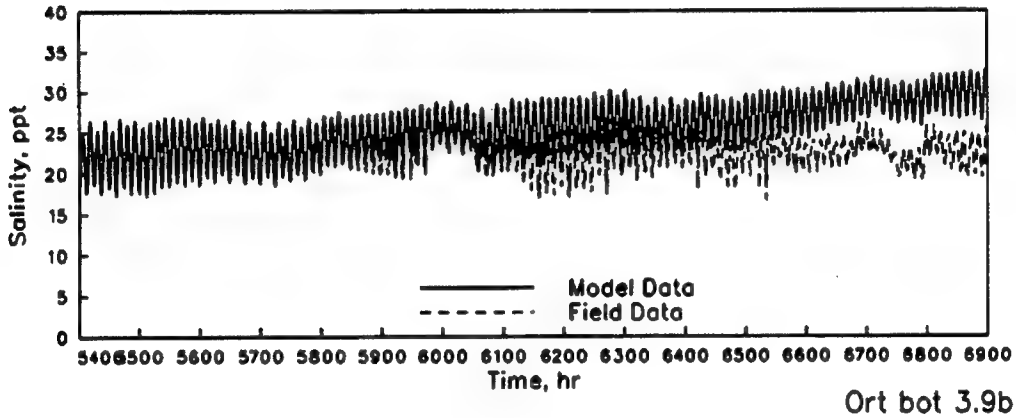

Ort bot 3.9b

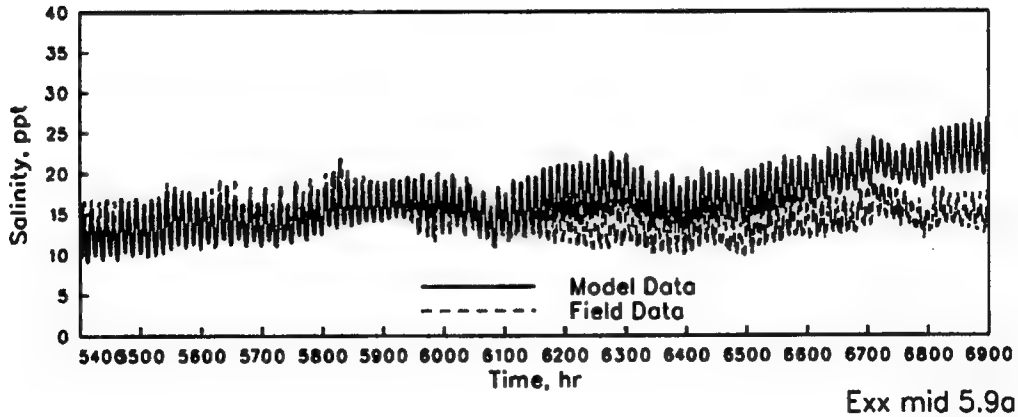

Exx mid 5.9a

CAPE FEAR SALINITIES
MODEL VERIFICATION
STATIONS 3.9a, 3.9b AND 5.9a
JULIAN HOURS 5400-6900

Plate 31

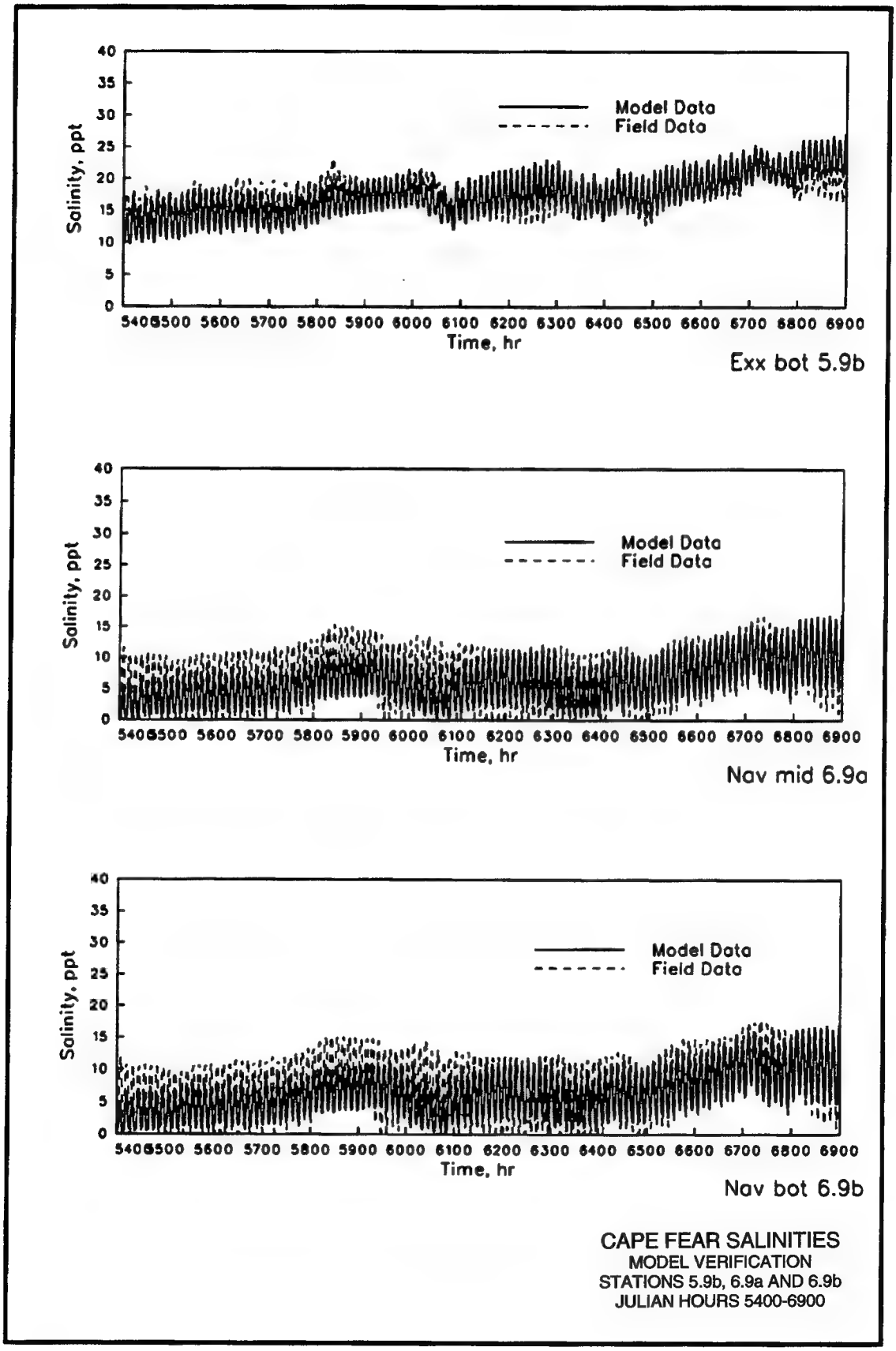
Salinity, ppt
Time, hr
Model Data
Field Data
0 5 10 15 20 25 30 35 40
5400 5500 5600 5700 5800 5900 6000 6100 6200 6300 6400 6500 6600 6700 6800 6900
Exx bot 5.9b
Nav mid 6.9a
Nav bot 6.9b
CAPE FEAR SALINITIES
MODEL VERIFICATION
STATIONS 5.9b, 6.9a AND 6.9b
JULIAN HOURS 5400-6900

Plate 32

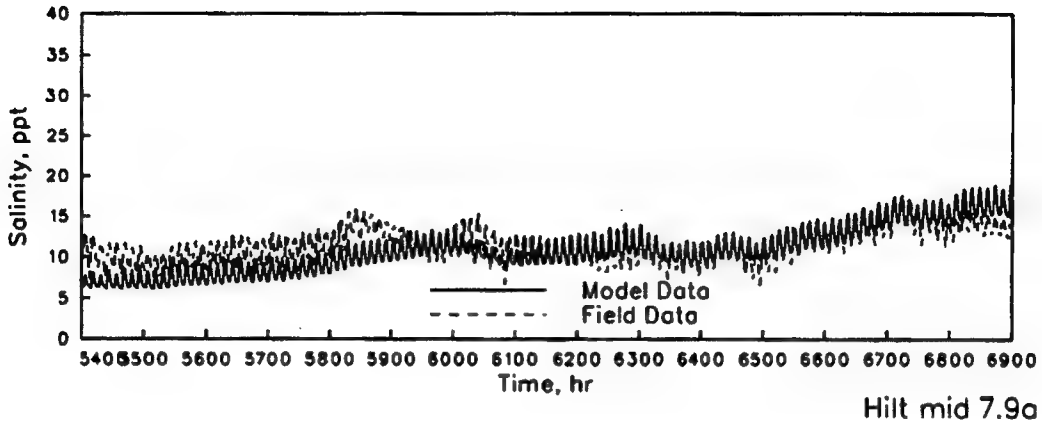

Hilt mid 7.9a

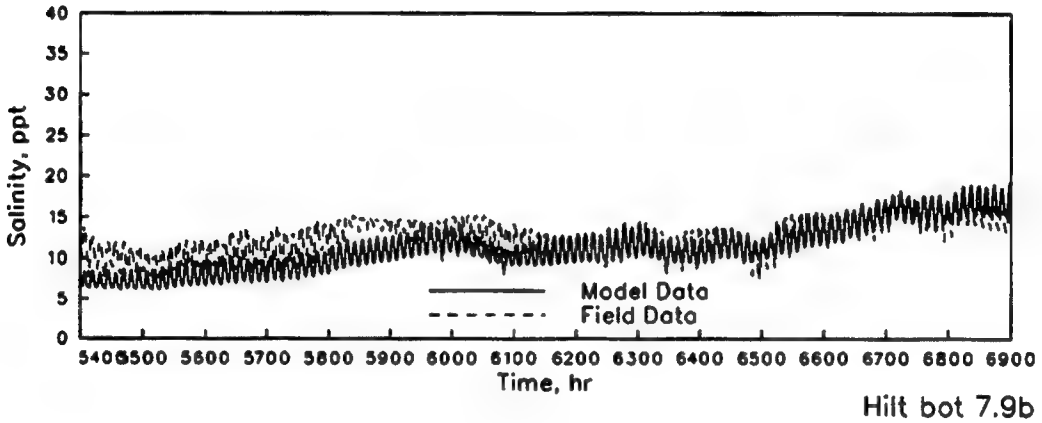

Hilt bot 7.9b

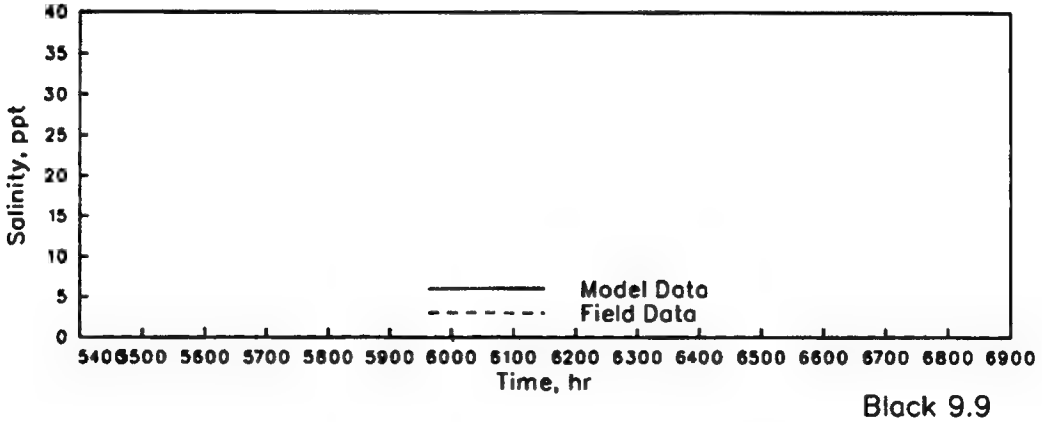

Black 9.9

CAPE FEAR SALINITIES
MODEL VERIFICATION
STATIONS 7.9a, 7.9b AND 9.9
JULIAN HOURS 5400-6900

Plate 33

Appendix A
Finite Elements Approach to Modeling Hydrodynamics and Sediment Transport Using RMA10-WES

Introduction

A model of a particular estuary, river or reservoir is composed of several parts. There is the geometric description which not only includes the X, Y, and Z locations of points chosen, but also the delineation of bed cover such as grasses, sands, etc. There is also the specification of boundary conditions including all of the forcing mechanisms, tides, wind, inflow, and any constituents. The third part is numerical code. This code has at its core, the basic laws of physics, in particular the relationship between force and acceleration. A consistent model code is a faithful representation of these equations, for sufficient resolution. Since these equations are universal, the range of applicability of the code is limited by the additional empirical relationships to describe turbulent processes, bed roughness, equations of state, and wind stress, and by any simplifying assumptions made in the equations.

There is some degree of uncertainty associated with the geometric description, the boundary conditions and in the numerical code. Often the error indicated by these uncertainties is highest for the specification of the boundary conditions, followed by the geometric description, with the numerical code providing the least of the error. The precise values of inflow and wind fields, particularly in estuarine models, are usually fairly crude. The inflows, for example, are determined by gauges far upstream from the estuary. They leave out large ungauged downstream areas. Also, at the gauge the relationship between gauge elevation and discharge is far from perfect. This relationship changes over time and flow conditions.

These errors can be minimized by careful model verification. Also, modelers can use sound testing procedures to eliminate much of the error from the decision process. These techniques include plans to base comparisons and sensitivity analysis.

In this appendix, one hydrodynamic code is described, RMA10-WES. The Galerkin-based finite element model RMA10-WES is a U.S. Army Engineer Waterways Experiment Station (presently Engineer Research and Development Center) adaptation of the RMA-10 code developed by King (1993).[1] This code computes time-varying open-channel flow and salinity/temperature transport in one, two, and three dimensions. It invokes the hydrostatic pressure and mild slope assumption. Vertical turbulence is supplied using a Mellor-Yamada Level II (Mellor and Yamada 1982) $k-\ell$ approach modified for stratification by the method of Henderson-Sellers (1984). The salinity/density relationship is based upon Pritchard (1982). The RMA2 code is a predecessor to RMA10-WES, but is limited to at most two-dimensional cases. The formulation is similar to RMA10-WES and so the only descriptions reported herein will be those of RMA10-WES.

Model Description

The full three-dimensional equations are reduced to a set of two momentum equations, an integrated continuity equation, a convection-diffusion equation, and an equation of state. The simplification is a result of the hydrostatic pressure approximation.

$$\rho\frac{Du}{Dt} - \nabla\cdot\sigma x + \frac{\partial P}{\partial x} - \Gamma x = 0 \tag{1}$$

$$\rho\frac{Dv}{Dt} - \nabla\cdot\sigma y + \frac{\partial P}{\partial y} - \Gamma y = 0 \tag{2}$$

$$\frac{\partial h}{\partial t} + u\zeta\frac{\partial\zeta}{\partial x} - u_a\frac{\partial a}{\partial x} + v\zeta\frac{\partial\zeta}{\partial y} - va\frac{\partial a}{\partial y} + \int_a^{\zeta}\left(\frac{\partial u}{\partial x} + \frac{\partial v}{\partial y}\right)dz = 0 \tag{3}$$

$$\frac{Ds}{Dt} - \frac{\partial}{\partial x}\left(D_x\frac{\partial s}{\partial x}\right) - \frac{\partial}{\partial y}\left(D_y\frac{\partial s}{\partial y}\right) - \frac{\partial}{\partial z}\left(D_z\frac{\partial s}{\partial z}\right) = 0 \tag{4}$$

$$\rho = F(s) \tag{5}$$

[1] References cited in this appendix are listed in the References at the end of the main text.

Elevation-related terms are defined in Figure 1.

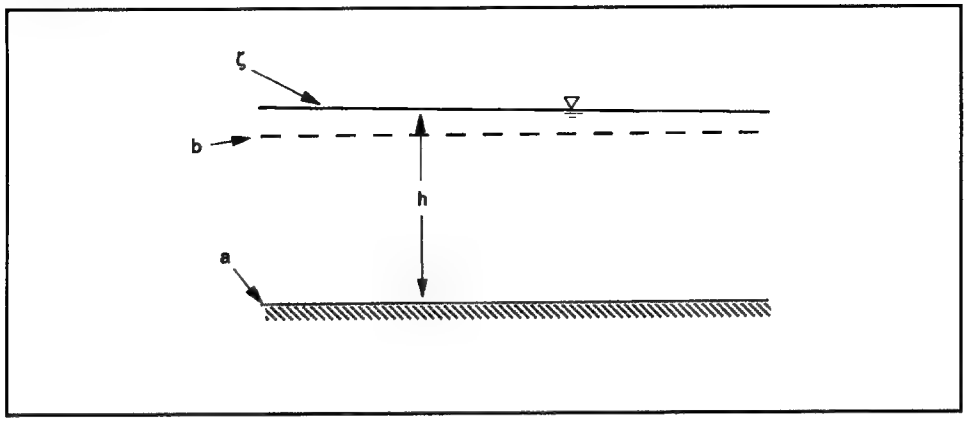

Figure 1. Definitions for elevation terms

where

$$\sigma_x = \begin{Bmatrix} E_{xx}\dfrac{\partial u}{\partial x} \\ E_{xy}\dfrac{\partial u}{\partial y} \\ E_{xz}\dfrac{\partial u}{\partial z} \end{Bmatrix}; \quad \sigma_y = \begin{Bmatrix} E_{yx}\dfrac{\partial v}{\partial x} \\ E_{yy}\dfrac{\partial v}{\partial y} \\ E_{yz}\dfrac{\partial v}{\partial z} \end{Bmatrix}$$

and

ρ = density

u,v,w = x,y,z velocity components

t = time

P = pressure

$$\Gamma_x = \rho\Omega v - \frac{\rho g u_a (u_a^2 + v_a^2)^{1/2}}{C^2} + \psi W^2 \cos(\Theta)$$

$$\Gamma_y = \rho\Omega u - \frac{\rho g v_a (u_a^2 + v_a^2)^{1/2}}{C^2} + \psi W^2 \sin(\Theta)$$

$\Omega = 2\omega\sin(\phi)$

ω = rate of angular rotation of the earth

ϕ = local latitude

g = gravitational acceleration

C = Chezy or Manning friction formulation

ψ = a coefficient from Wu (1980)

W = wind speed

Θ = wind direction counterclockwise from easterly

h = depth

u_ζ, v_ζ = x,y velocity components at the water surface

ζ = water surface elevation

u_a, v_a = x,y velocity

a = bed elevation

s = salinity

D_x, D_y, D_z = diffusion coefficient for salt

E = eddy viscosity components

The continuity equation

$$\frac{\partial u}{\partial x} + \frac{\partial v}{\partial y} + \frac{\partial w}{\partial z} = 0 \tag{6}$$

is solved as a second part of each solution step. Equation 6 is converted to an appropriate boundary value problem through differentiation with respect to z. After rearrangement it takes the form:

$$\frac{\partial^2 w}{\partial z^2} = - \frac{\partial}{\partial z}\left(\frac{\partial u}{\partial x} + \frac{\partial v}{\partial y}\right) \tag{7}$$

subject to boundary conditions specified for the water surface and the bed.

$$w_\zeta = u_\zeta \frac{\partial \zeta}{\partial x} + V_\zeta \frac{\partial \zeta}{\partial y} + \frac{\partial h}{\partial t} \quad \textit{at the water surface} \tag{8}$$

and

$$w_a = u_a \frac{\partial a}{\partial x} + V_a \frac{\partial a}{\partial y} \quad at\ the\ bed \tag{9}$$

Note that in these equations the values of u and v will be known at all locations from the previous part of the solution step. Values of w in this solution are used in the next iteration for u, v, h, and s.

The geometric system varies with time; i.e., the water depth h varies during the simulation. To develop an Eulerian form for the solution, it is desirable to transform this system to one that can be described with a constant geometric structure. Early development of the model (King 1982) used a σ - transformation in which the bed and the water surface are transformed to constants. In a later analysis of this method, King (1985) pointed out that at locations where a sharp break in bottom profile occurs, the transformation is not unique and momentum in the component directions may not be correctly preserved. An alternative transformation that preserves the bottom profile as defined, but transforms the water surface to a constant elevation is now used (z^{∇} transformation).

This transformation is defined by:

$$x^{\nabla} = x \tag{10}$$

$$y^{\nabla} = y \tag{11}$$

$$z^{\nabla} = a + (z - a)\frac{(b - a)}{h} \tag{12}$$

where b is the fixed vertical location to which the water surface will be transformed. Equations 1-6 and 7-9 then incorporate the transformation (10-12).

Another advantage of this transformation is that it produces z^{∇} = constant lines that are close to horizontal, i.e., z = constant lines. This results in less fictitious density-driven currents near bed profile breaks (Stelling and van Kester 1993). Since stratification-related phenomena are usually nearly horizontal, it is important that the transformation leave constant surfaces that are nearly horizontal. Considering the pressure gradient (due to the density gradient) in this transformation produces:

$$\frac{\partial P}{\partial x} = \frac{\partial P}{\partial x^{\nabla}} + \frac{\partial P}{\partial z^{\nabla}} \frac{\partial z^{\nabla}}{\partial x} \tag{13}$$

In a strongly stratified stagnant system this pressure gradient should be 0. However, note that Equation 13 in the transformed system is dependent upon two terms (each of which could be large) to cancel each other. This could cause artificial currents due to truncation and roundoff error. A transformation in which, $\partial z^{\sigma}/\partial x \approx 0$, i.e., $z^{\sigma} \approx z$, will reduce this problem. Figure 2 shows an example for a case similar to the Cape Fear project in which a 12.19-m- (40-ft-) deep channel passes through an 2.43-m- (8-ft-) deep bay. Here b is chosen to be an elevation of 0 and ζ is 0.60 m (2 ft). Near the break in the bed profile $\partial z^{\nabla}/\partial x$ is fairly small, or z^{∇} surfaces are nearly horizontal. Contrast this with the σ transformation in Figure 3. The σ = constant surfaces are far from horizontal along the channel side slopes. The truncation and roundoff errors tend to drive fictitious currents that cause the denser salt water to leave the channel. The z^{∇} transformation results in

$$\frac{\partial z^{\nabla}}{\partial x} = O(\zeta - b) \tag{14}$$

whereas the σ transformation is

$$\frac{\partial \sigma}{\partial x} = O(h) \tag{15}$$

which is much larger.

The Galerkin finite element approximation of Equations 1-4 and 7 uses a quadratic approximation for u,v,w, and s and linear for h and P. The nonlinearity is addressed by Newton-Raphson iteration at each time-step. Generally the iteration process is split into calculation of Equations 1-3, then 7, followed by 4. This sequence is repeated until sufficient convergence is reached.

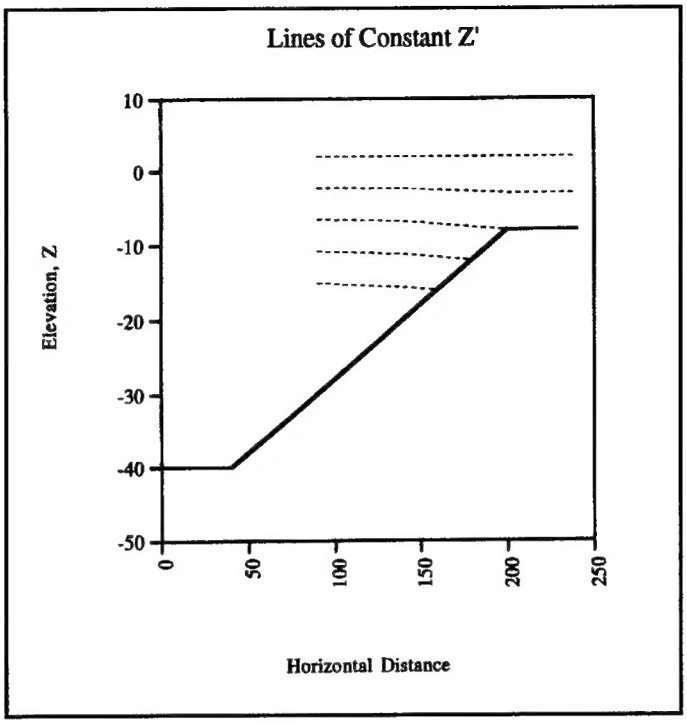

Figure 2. Lines of constant z^{∇} near a significant grade change

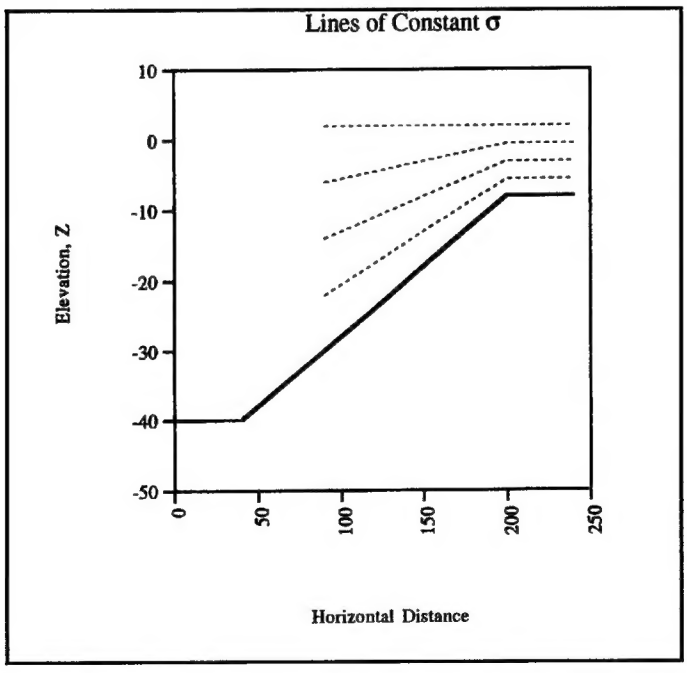

Figure 3. Lines of constant σ near a significant grade change

Sediment Transport

RMA2 is an ancestor of the RMA10-WES code and is similar in approach. That code was 2-D and 1-D. It did not directly handle sediment transport. Instead, it supplied the currents and water surface elevations to drive a separate sediment transport code, STUDH or SED2D. These sediment transport codes include both cohesive and non-cohesive sediment and the bed interaction algorithms. By separating the hydrodynamics and sediment transport into two codes, the sedimentation process could not directly influence the hydrodynamics. In the development of RMA10-WES, we have included the sediment transport in the hydrodynamic code. At present only cohesive sediments are programmed.

For cohesive sediment the erosion and deposition is described by time rates that are dependent upon the bed shear stress. In RMA10-WES the deposition rate is described by Krone (1962).

$$S = -V_s C(1-\frac{\tau}{\tau_d}) \text{for } C \le C_c$$
$$S = -V_k C^{5/3}(1-\frac{\tau}{\tau_d}) \text{for } C \ge C_c \qquad (16)$$

where

τ = bed shear stress

τ_d = critical shear stress for deposition

V_s = settling velocity

C = the concentration near the bed

C_c = critical concentration, 300 *mg/l*

V_k = the hindered settling velocity, $v_s/C_c^{4/3}$

The erosion rate is given by Partheniades (1962).

$$S = P(\frac{\tau}{\tau_e} - 1) \qquad (17)$$

where

P = erosion rate constant

τ_e = the critical shear stress for particle erosion.

The bed algorithm is maintained as a set of fluctuation layers, each with assigned properties. The concentration of the sediment is approximated quadratically over each element in the grid.

REPORT DOCUMENTATION PAGE

Form Approved
OMB No. 0704-0188

1. AGENCY USE ONLY *(Leave blank)*	2. REPORT DATE	3. REPORT TYPE AND DATES COVERED
	August 2000	Final report

4. TITLE AND SUBTITLE
Cape Fear-Northeast Cape Fear River, North Carolina; Numerical Model Study

5. FUNDING NUMBERS

6. AUTHOR(S)
Robert T. McAdory, Jr.

7. PERFORMING ORGANIZATION NAME(S) AND ADDRESS(ES)
U.S. Army Engineer Research and Development Center
Coastal and Hydraulics Laboratory
3909 Halls Ferry Road, Vicksburg, MS 39180-6199

8. PERFORMING ORGANIZATION REPORT NUMBER
ERDC/CHL TR-00-18

9. SPONSORING/MONITORING AGENCY NAME(S) AND ADDRESS(ES)
U.S. Army Engineer District, Wilmington
P.O. Box 1890
Wilmington, NC 28402-1890

10. SPONSORING/MONITORING AGENCY REPORT NUMBER

11. SUPPLEMENTARY NOTES

12a. DISTRIBUTION/AVAILABILITY STATEMENT
Approved for public release; distribution is unlimited

12b. DISTRIBUTION CODE

13. ABSTRACT *(Maximum 200 words)*

A three-dimensional hydrodynamic and salinity numerical model of the Cape Fear River Estuary, NC, was developed, verified, and used in an experimental program. The purpose of the model was to determine salinity and water level changes in the estuary that may result from a planned deepening of the Wilmington Harbor channel. The model included a discretized representation, or numerical grid, of the system, boundary condition forcings, and the RMA10-WES (TABS-MS) finite element code. Verification was realized by comparisons of model results to approximately 8 weeks of prototype data for tides, velocities, and salinities. The experimental program consisted of calculating salinity and water level results for differing proposed channel depths and comparing these values to the base, or existing, conditions. The results indicate that deepening beyond 12.2 m (40 ft) resulted in average maximum tide height increases of 50 m (2 in.) and small decreases in salinity in the Wilmington vicinity.

14. SUBJECT TERMS
Black River
Cape Fear River
Channel deepening
Northeast Cape Fear River
Salinity intrusion
Tide amplification

15. NUMBER OF PAGES
93

16. PRICE CODE

17. SECURITY CLASSIFICATION OF REPORT	18. SECURITY CLASSIFICATION OF THIS PAGE	19. SECURITY CLASSIFICATION OF ABSTRACT	20. LIMITATION OF ABSTRACT
UNCLASSIFIED	UNCLASSIFIED		